DEVELOPMENT OF GROUND MOTION ATTENUATION

RELATIONSHIPS FOR SOUTHERN ITALY

BASED ON ATTENUATION MODELS

AND STOCHASTIC

SIMULATIONS

Sebastiano D'Amico, Dottore in Fisica

An Abstract Presented to the Graduate Faculty of
Saint Louis University in Partial Fulfillment
of the Requirements for the Degree of
Doctor of Philosophy

2010

Abstract

The evaluation of the expected peak ground motion caused by an earthquake is an important problem in earthquake seismology. It is particularly important for regions where strong-motion data are lacking. With the approach presented in this study of using data from small earthquakes, it is possible to extrapolate the peak motion parameters beyond the magnitude range of the weak-motion data set on which they are calculated. To provide a description of the high frequency attenuation and ground motion parameters in southern Italy we used seismic recordings coming from two different projects: the SAPTEX (Southern Apennines Tomography Experiment) and the CAT/SCAN (Calabria Apennine Tyrrhenian – Subduction Collision Accretion Network). We used about 10,000 records with magnitudes between M=2.5 and M=4.7. Using regression model with the large number of weak-motion data, the regional propagation and the absolute source scaling were determined. To properly calibrate the source scaling it was necessary to compute moment magnitudes of several events in the data set. We computed the moment tensor solutions using the "Cut And Paste" and the SLUMT methods. Both methods determine the source depth, moment magnitude and focal mechanisms using a grid search technique. The methods provide quality solutions in the area in a magnitude range (2.5-4.5) that has been too small to be included in the Italian national earthquake catalogues. The derived database of focal mechanisms allowed us to better detail the transitional area in the Messina Strait between the extensional domain related to subduction trench retreat (southern Calabria) and the compressional one associated with continental collision (central-western Sicily).

Stochastic simulations are generated for finite-fault ruptures using the derived propagation parameters to predict the absolute peaks of the ground acceleration for

several faults, magnitude, and distance range, as well as beyond the magnitude range of the weak-motion data set on which the input parameters are calculated. Finally we derived a functional form for a predictive relationship valid in the study area.

DEVELOPMENT OF GROUND MOTION ATTENUATION

RELATIONSHIPS FOR SOUTHERN ITALY

BASED ON ATTENUATION MODELS

AND STOCHASTIC

SIMULATIONS

Sebastiano D'Amico, Dottore in Fisica

A Dissertation Presented to the Graduate Faculty of
of Saint Louis University in Partial Fulfillment
of the Requirements for the Degree of
Doctor of Philosophy

2010

COMMITTEE IN CHARGE OF CANDIDACY

Professor Robert B. Herrmann
Chairperson and Advisor

Associate Professor Keith D. Koper

Associate Professor Lupei Zhu

Acknowledgments

Table of Contents

List of Tables

List of Figures

CHAPTER 1: Iintroduction

The assessment of seismic hazard is probably the most important contribution of seismology to society. The prediction of the earthquake ground motion has always been of primary interest for seismologists and structural engineers. Large earthquakes that have occurred in recent years in densely populated areas of the world (Izmit, Turkey, 17 August 1999; Duzce, Turkey, 12 November 1999; Chi-Chi, Taiwan 20 September 1999, Bhuj, India, 26 January 2001; Sumatra, Indonesia 26 December 2004; Wenchuan, China, May 12, 2008; L'Aquila, Italy, April 6, 2009) dramatically highlight the inadequacy of a massive portion of the buildings erected in and around the epicentral areas. The Izmit event was particularly destructive because a large number of buildings were unable to withstand even moderate levels of ground shaking, demonstrating poor construction criteria and, more generally, the inadequacy of the application of building codes for the region. Another example is the L'Aquila earthquake (April, 06, 2009; Mw=6.3) in which 300 persons were killed and over 65,000 were left homeless (Akinci and Malagnini, 2009). It was the deadliest Italian earthquake since the 1980, Irpinia earthquake, and initial estimates place the total economic loss at over several billion Euros. Many studies are already carried out describing the rupture process and the characteristics of local site effects (Cirella et al., 2009; D'Amico et al., 2010a; Atzori et al., 2009, Akinci et al., 2009) for this earthquake. It has been observed that many houses were unable to withstand to the ground shaking.

Building earthquake-resistant structures and retrofitting old buildings on a national scale may be extremely costly and may represent an economic challenge even for developed western countries. Planning and design should be based on available national hazard maps, which, in turn, must be produced after a careful calibration of

ground motion predictive relationships for the region (Kramer, 1996). Updating existing hazard maps represents one of the highest priorities for seismologists who contribute by refining the ground motion scaling relations and reducing the related uncertainties.

The quantitative estimate of the ground motion is obtained through the use of the so-called attenuation relationships (see Kramer, 1996), which allow the estimation of specific ground-motion parameter as a function of magnitude, distance from the source, and frequency. These relationships should be calibrated in the region of interest.

Often these attenuation relationships are usually obtained byregressing a large number of strong-motion data (Campbell and Bozorgnia, 1994; Boore et al., 1993; Ambraseys et al., 1996; Ambraseys and Simpson, 1996; Sabetta and Pugliese, 1987; 1996). For the Italian region the most used attenuation relationships are those obtained by Sabetta and Pugliese (1987, 1996). They were the first to present the result of regression of strong motion data to define the attenuation of the peak horizontal acceleration (PHA) and peak horizontal velocities (PHV), and up to date they are the only available for the whole country. The database used by Sabetta and Pugliese (1987) contained waveforms generated by a quite small number of events in different tectonic and geological environments. To obtain their equations Sabetta and Pugliese (1987) used the largest of the two peaks on the horizontal time histories together with the local earthquake magnitude. Sabetta and Pugliese (1996) developed empirical predictive relationships for the vertical and the horizontal components of the response spectra. Sabetta and Pugliese (1987) used 190 horizontal components from 17 earthquakes recorded in Italy since 1976 ($4.6 < M < 6.8$) while Sabetta and Pugliese (1996) used 95 accelerograms among the same data set. A multiple regression was carried out in the 1996 article for 14 different response spectra frequencies in the range 0.25–25 Hz. It has

been shown that these attenuation relationships do not reproduce the ground motion in the proper way (Malagnini et al. 2002; Morasca et al. 2006; Scognamiglio et al. 2005). This is probably due to the fact that Sabetta and Pugliese (1987, 1996) attenuation relationships are calibrated just using few earthquakes occurred in different tectonic and geological environments. Furthermore they are calibrated in a limited magnitude range and they should be used just up to magnitude 6.8. The southern Italy region have experienced several earthquake in past having magnitude even greater than 7. For these reasons the Sabetta and Pugliese (1987, 1996) attenuation relationships are not suitable for predicting the ground motion in the southern Italy. It is also a key point to evaluate the regional features of the investigated area for having a model that can be used to reproduce realistic scenarios based on the complete knowledge of the area (e.g. attenuation property of the crust, site effects and source characteristics).

The attenuation properties of the crust can be evaluated using the background seismicity as suggested by Chouet et al. (1978) and later demonstrated by Raoof et al. (1999) and Malagnini et al (2000a, 2007). In other words, it is possible to develop regionally-calibrated special attenuation relationships even where strong-motion data are not available. One of the purposes of this work is to describe quantitatively the regional attenuation and source characteristics for constraining the amplitude of strong motion expected from future earthquake in the area. In this work we use the background seismicity to perform our analysis (details in Malagnini et. 2000a, 2007). For each seismogram the logarithm of its peak value is written as the sum of an excitation term relative to an arbitrary reference distance, a site term, and a propagation term.

As discussed later we derive the crustal attenuation parameters and factors related to the source scaling from the results of the regression. Modeling is also carried

out through the use of Random Vibration theory (RVT) (Cartwright and Louguent-Higgins, 1956) to obtain estimates of the peak ground motion parameters in the time domain. From these we can construct predictive relationships as a function of distance from the earthquake and earthquake source size. These kinds of studies are usually calibrated on "rock-site". However, from an engineering point of view, it is necessary also consider the characteristic of a specific site (Rapolla et al. 2008). In fact, these are very important and can affect a lot of structures. The effect of amplification at a site, due to the surface geology and subsurface structure, should be considered in ground motion evaluation at the site. To estimate the site amplification different methods are proposed (King and Tucker, 1984; Malagnini et al. 2004, 2007; Stiedl et al., 1996; Moya et al., 2000). Amplification and deamplification due to surface geology of a particular site is a quite complex phenomenon which also depends on the frequency and the level of the ground motion. However in this study we will refer to the NEHRP classification (BSSC, 1994) in order to consider different site conditions.

The methodology used in here for determining the attenuation properties has been successfully applied in different part of the world: California (Raoof et al. 1999; Malagnini et al. 2007), northwestern United States (Herrmann and Dutt, 1999; Jeon and Herrmann 2004), central United States (Herrmann and Malagnini, 1996), Mexico (Ortega et al., 2003), Greece and Crete (Pino et al., 2001), Italy (Malagnini et al., 2000a,c: 2002; Morasca et al. 2006; Scognamiglio et al. 2005), Central Europe (Malagnini et al, 2000b, Bay et al. 2003), Turkey (Akinci et al., 2001, 2006), India (Bodin et al., 2004). The approach has been applied in different parts of Italy but, due to the "poor" distribution of seismic stations in Southern Italy, the area has not yet been studied from this point of view. Fortunately, the deployment of a large number of

temporary seismic stations in the area provides a good data set for performing the necessary analysis to find a suitable attenuation relationship for Southern Italy. Using the source and attenuation parameters estimated in this study, stochastic simulations (Motezidian and Atkinson, 2005; Assatourians and Atkinson, 2007; Boore, 2010) and characteristic of the mapped fault, it will be possible to predict the expected ground shaking such as Peak Ground Acceleration (PGA) and Peak Ground Velocity (PGV). The source terms are calibrated using the magnitude calibrated through waveform modeling of the largest events (D'Amico et al. 2010b, 2010c). Finally a functional form for a predictive relationship in the study area will be also derived. This approach allows us to extrapolate predictions to magnitudes larger than those sampled in the data set. This is really important because one can make predictions for regions where strong-motion data are lacking or where even data for moderate earthquakes are not available (D'Amico et al. 2010d). To test the possibility of making ground motion predictions for magnitudes larger than those sampled in the original data set we performed those studies also for Taiwan (D'Amico et al. 2010d). In fact, in this area there are a large number of data recorded from earthquakes up to magnitude 7.6. The results (D'Amico et al., 2010d) obtained in the study clearly highlight the applicability of the approach.

The model obtained for southern Italy can later be used for upgrading the most recent hazard map of Italy and for engineering designs as well. The results obtained in this study are also useful to implement tools like *ShakeMap®* (Wald et al. 2005) which use this kind of information to generate a rapid estimate of shaking. *ShakeMap®* is a tool used to portray the extent of potentially damaging shaking following an earthquake. It can be used for emergency response, loss estimation, and public information.

ShakeMap® was first developed for earthquakes in southern California. Istituto Nazionale di Geofisica e Vulcanologia (INGV) runs this tool for Mediterranean earthquakes and in particular for the Italian region. Shake maps show the distribution of ground shaking in the region, information that can be really critical for emergency management decision making. In fact, it is the distribution of peak ground motion and intensity rather than the magnitude that provides useful information about areas prone to damage. Having this information in real time will result in lives saved and reduction in property damage. After a damaging earthquake, emergency responders must quickly find answers to important questions such as the location of the most serious damage, and specifying the resources that must be mobilized. Usually government response organizations answer these questions after a preliminary survey of the damaged area. This reconnaissance can require several hours or sometimes some days to be completed. As a result, decisions regarding search and rescue, medical emergency response, care and shelter for the injured and displaced persons, and other critical response must often be made while information is still incomplete. In this context a rapid and automatic estimate of earthquake effects for the affected area is really important, that is why attenuation relationships play a key and really important role in improving these tools.

In the present thesis the first chapter presents a brief introduction on the problem discussed in this work and the motivation. The second and third chapters provide moment tensor solutions in the Calabrian-Peloritan area. The moment tensors were computed by applying waveform inversion to small and moderate magnitude earthquakes. The obtained focal mechanisms also furnish new knowledge about low-magnitude earthquake mechanics that will be useful for improved understanding of the local geodynamics. The fourth chapter briefly presents the methodology described by

Raoof et al. (1999) and used here for determining the attenuation properties of southern Italy. Chapter five describes the approach used to obtain the estimation of the ground motion parameters (such as PGA) and the derived predictive ground motion relationship for central and southern Italy obtained by performing the regression of the Peak Ground Acceleration data.

CHAPTER 2: Testing the Stability of Focal Mechanism Solutions for Small and Moderate Earthquakes in the Calabrian-Peloritan Arc Region (Southern Italy)

Introduction

During the last two decades the use of waveforms recorded at local-to-regional distances has increased considerably. Waveform modeling has been used to estimate faulting parameters of small to moderate size earthquakes (D'Amico et al., 2008, 2010b, 2010c; Mancilla et al. 2002; Tan et al. 2006; Zhu et al. 2006). Waveform modeling also has implications for seismic verification efforts and provides useful information for understanding the tectonic features of many regions where only small events are available to provide information on regional deformation.

Southern Italy is one of the most seismically active areas of the Italian peninsula and is characterized by a low-to-moderate activity at present. According to the existing seismic instrumental catalogues ["Catalogo della Sismicita Italiana" (CSI, Working Group 2001), "Bollettino Sismico Italiano" (http://bollettinosismico.rm.ingv.it/), ISIDE (http://iside.rm.ingv.it) and the catalogue of the regional seismic network of Calabria University] the area has experienced just a few events with magnitude above 5 in the last thirty years. However, based on the historical record, the area has suffered intensity X or higher at several times in the past centuries (for example in 1638, 1659, 1783, 1870, 1905, 1908) (Boschi et al., 2000; CPTI, Working Group 2004) and is known to be an area of high seismic hazard (http://zonesismiche.mi.ingv.it; "Mappa di pericolosità sismica del territorio nazionale"). Modeling regional seismograms for constraining moment tensors is widely accepted and largely documented by extensive literature.

Modeling regional waveforms provides a good constraint in determining accurately the source mechanism and depth. Langston (1981) showed that it is possible to use the relative amplitude of P, SH, and SV waveforms to discriminate among fault types. Many attempts for modeling regional seismograms have been done in the last decades by using the body (Fan and Wallace, 1991 and Dreger and Helmberger , 1993) and surface waves at different periods (Thio and Kanamori, 1995; Romanowicz et al., 1993; Ritsema and Lay, 1993; Herrmann, 2008). However, the use of the surface waves only requires a good azimuthal coverage around the source, which makes the application less effective in cases where only a few stations are available. The Cut and Paste (CAP) method (Zhu and Helmberger, 1996, Tan et al. 2006) can be considered as a step forward since by using this method, it is possible to separate the entire records into body and surface waves and model them with different time shifts. In doing so this method desensitizes the timing between the principal crustal arrivals. Therefore accurate source estimates can be achieved with use of imperfect Green's functions.

The ultimate goal of this chapter is to test the possibility of estimating faulting parameters of low and moderate magnitude events in the Calabrian-Peloritan arc region. We test the applicability of the CAP (Zhu and Helmberger, 1996; Tan et al. 2006) and SLUMT (Herrmann, 2008) methods in order to implement the procedure for a compilation of a moment tensor catalogue for the area with a magnitude threshold as low as possible. This is important to improve the knowledge of the regional stress field and for understanding the tectonic features of the area. To illustrate the results of the methods we present as examples the moment tensor solutions obtained for three small earthquakes. For several larger earthquakes, we compare our solutions to those available in the RCMT (Regional Centroid Moment Tensor, Pondrelli et al. 2006;

http://mednet.rm.ingv.it/quick_rcmt.php), TDMT (Time Domain Moment Tensor; http://earthquake.rm.ingv.it/tdmt.php; Scognamiglio et al. 2009) catalogues, and those computed by Li et al. (2007). It is important to remark that, for this region, just a small number of moment tensor solutions have been reported. Our results provide a key element, still incomplete but useful, to constrain the regional tectonic processes in the Calabrian arc especially considering that the solutions estimated from P-onset polarities are often poorly constrained in this magnitude range.

Green's functions evaluation

The Green's functions were computed using a 1-D velocity model with the frequency-wave number method described by Zhu and Rivera (2002) and stored in a separate library in order to reduce the computational time. They represent the basic functions for all the double-couple mechanisms. To properly take into account the lithospheric heterogeneities of the study region we used the most detailed 3-D velocity models available for the region (Barberi et al., 2004 and Neri et al., 2010) to derive a specific 1-D velocity model for each target area. To compute such 1-D model, we define a set of earthquakes and stations covering the target area and we have computed the theoretical travel times using the 3-D velocity model. Such travel times are then used to build a plot of travel time versus epicentral distance on which we introduce proper best fit curves (1st order polynomials). Finally, the 1-D velocity model can be estimated from the best fit curves by using the theoretical travel-time curves in layered media. This kind of approach permits us to obtain, for a specific set of ray-paths, a 1-D velocity model "equivalent" to the 3-D one. The velocity structures used for the CAP analyses in the Messina Straits and Calabria have been computed by defining 2-D grids of

earthquakes/stations covering the entire target area (Messina Straits and Calabria region, respectively). In both cases we estimated several different models by changing the stations/earthquakes distribution or the starting 3-D velocity model in order to test the stability of the CAP solutions with respect to the velocity structure. Figure 2.1 shows the crustal models used for computing the Green's functions. Green's function have been computed for a distance range from 5 to 500 km with a spacing of 5 km and a focal depth range from 1 to 50 km at 1 km increments.

"Cut and paste" method

The synthetic seismogram for a double-couple mechanism, *s(t)*, is defined as:

$$s(t) = M_0 \sum_{i=1}^{3} A_i(\phi - \theta, \delta, \lambda) \cdot G_i(t)$$
,   (1)

where M_0 is the scalar moment, A_i represent the radiation coefficient and , θ, δ, and λ represent the station azimuth, strike, dip, and rake angles of the source. The $G_i(t)$ are the Green's functions with i=1,2,3 corresponding to the three fundamental faults (i.e., vertical strike-slip, vertical dip-slip, and 45° dip-slip). If $u(t)$ is defined to be the observed data and if the synthetics reproduce perfectly the real data:

$$u(t) = s(t)$$.   (2)

Since the above equation leads to a non-linear problem it is convenient to solve the problem by a grid search method. In order to measure the misfit error between observed and synthetic data we define an object function and search through the parameter space to find the global minimum of the object function. The misfit error is defined as the norm of the difference between observed and synthetic data multiplied by another term

that takes into account the distance range scaling. Mathematically it can be defined as (Zhu and Helmberger, 1996):

$$e = \left\| \left(\frac{r}{r_0} \right)^p \right\| \cdot \| u(t) - s(t) \|$$

(3)

where p is a scaling factor to give the record at distance r the same weight as that at reference distance r_0. To weight Pnl and surface wave we assume a spherical geometrical spreading for body waves ($p=1$) and a cylindrical geometrical spreading for surface waves ($p=0.5$). The scaling factor avoids the problem that if the true-amplitude waveforms are used the closest stations dominate the inversion. The radiation pattern is taken out so the decay with distance is related only to the amplitude decay due to the geometrical spreading. In particular, we use the chi-square, χ^2, defined in Tan et al. (2006), as our object function

$$\chi^2 = \frac{e_{Pnl}}{\sigma^2_{Pnl}} + \frac{e_{surf}}{\sigma^2_{surf}}$$

(4)

where the waveform misfit errors are defined as the following:

$$e_{Pnl} = \left\| u^{Pnl}(t) - s^{Pnl}(t - \Delta T) \right\|$$

(5)

$$e_{surf} = \left\| u^{Rayleigh}(t) - s^{Rayleigh}(t - \Delta T) \right\| + \left\| u^{Love}(t) - s^{Love}(t - \Delta T) \right\|$$

(6)

ΔT represent the time-shift required to align synthetics with data (for conciseness the distance correction term is omitted). In the equation (4) the terms at the denominator are the variance of waveform residuals of Pnl and surface waves. They measure how well the velocity model can explain the observed data. We simply search through the whole parameter space of all the unknowns (depth/strike/dip/rake) and determine the best solution of the source parameters.
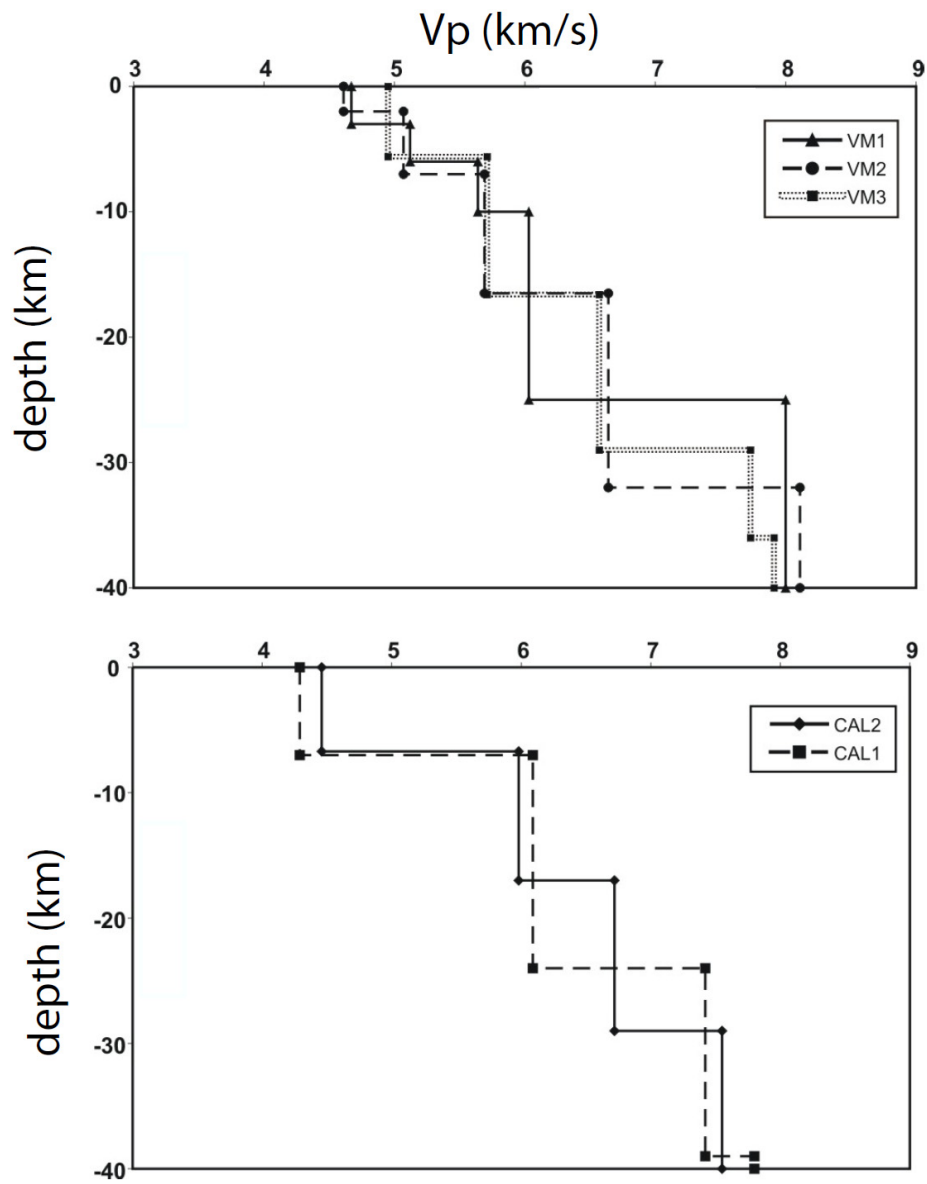
Figure 2.1. Crustal velocity models used in this study to compute the Green's functions.

For additional details we refer to Zhu and Helmberger (1996) and Tan et al. (2006).

Data set

In this study we used seismograms recorded by the Italian National Seismic Network managed by the Istituto Nazionale di Geofisica e Vulcanologia (INGV) and the by CAT-SCAN (Calabria Apennine Tyrrhenian – Subduction Collision Accretion Network) project. During the CAT-SCAN researchers from the Lamont-Doherty Earth Observatory, Istituto Nazionale di Geofisica e Vulcanologia and University of Calabria, deployed 40 portable digital broadband seismographs throughout southern Italy. The stations were equipped with Reftek130 or Reftek72A07 data logger and several three-component sensor types (i.e. CMG40T, CMG3T, L-22, STS2, TRILLIUM40, CMG3ESP). Figure 2.2 shows the location of seismic stations and epicenters used in this study; the earthquakes used in our study are listed in Table 2.1. Each waveform was examined to eliminate recordings with spurious transients or low signal-to-noise ratios and corrected for the instrument response to yield ground velocity. Finally the picking of P-arrivals was reviewed and the horizontal recordings were rotated to radial and transverse components.

Results and discussions

The main advantage of the CAP method is that it has small sensitivity to the velocity model and lateral crustal variation. The technique "cuts" broadband waveforms into the *Pnl* and surface wave segments that could be inverted independently. The surface wave segments are larger in amplitude than the *Pnl* waves and can be affected by the shallow

crustal heterogeneities. The *Pnl* waves have a lower signal-to-noise ratio and are mainly

controlled by the average crustal velocity structure. For this reason we weighted the

body wave segments more by multiplying their amplitudes by a factor of 2. Using the

whole seismogram implies that the inversions are mainly controlled by surface waves.

We preferred to use ground velocity rather than ground displacement mainly because we

used weak-motion data. The earthquakes having magnitude less than 4 have high signal-

to-noise ratio only at the higher frequencies. Furthermore, working with ground velocity

rather than displacement reduces the influence of low frequency site or instrument noise

on the deconvolution. In addition, the moment tensor inversion at regional distances is

possible if the bandpass filtered waveforms are simple in appearance and can be

modeled with a 1-D Earth model. For this reason the choice among the frequency bands

depends on the magnitude of the event. The typical frequency bands we used are from

0.05 Hz to 0.3 Hz for the *Pnl* and from 0.02 Hz to 0.1 Hz for surface waves.

Figures 2.3, 2.4, and 2.5 shows examples of the waveform fits produced by the

CAP inversion for three different events. Black and gray traces indicate the observed

and predicted filtered ground velocity respectively. Figure 2.6 shows the misfit error as a

function of depth for the events in Figure 2.3 and 2.5. It is possible to notice that in both

cases the solution does not change around the minimum indicating the stability of the

final solution.

A good focal mechanism estimate can be obtained using a few stations or even

only two stations with an azimuthal gap of about 180 degrees (Zhu and Helmberger,

1997; Dreger and Helmberger, 1993). Figure 2.7 presents, for the two events in Figure

2.3 and 2.4, the tests we have done for investigating the stability of the final focal

mechanism. We varied, for example, the number of stations used, the azimuthal
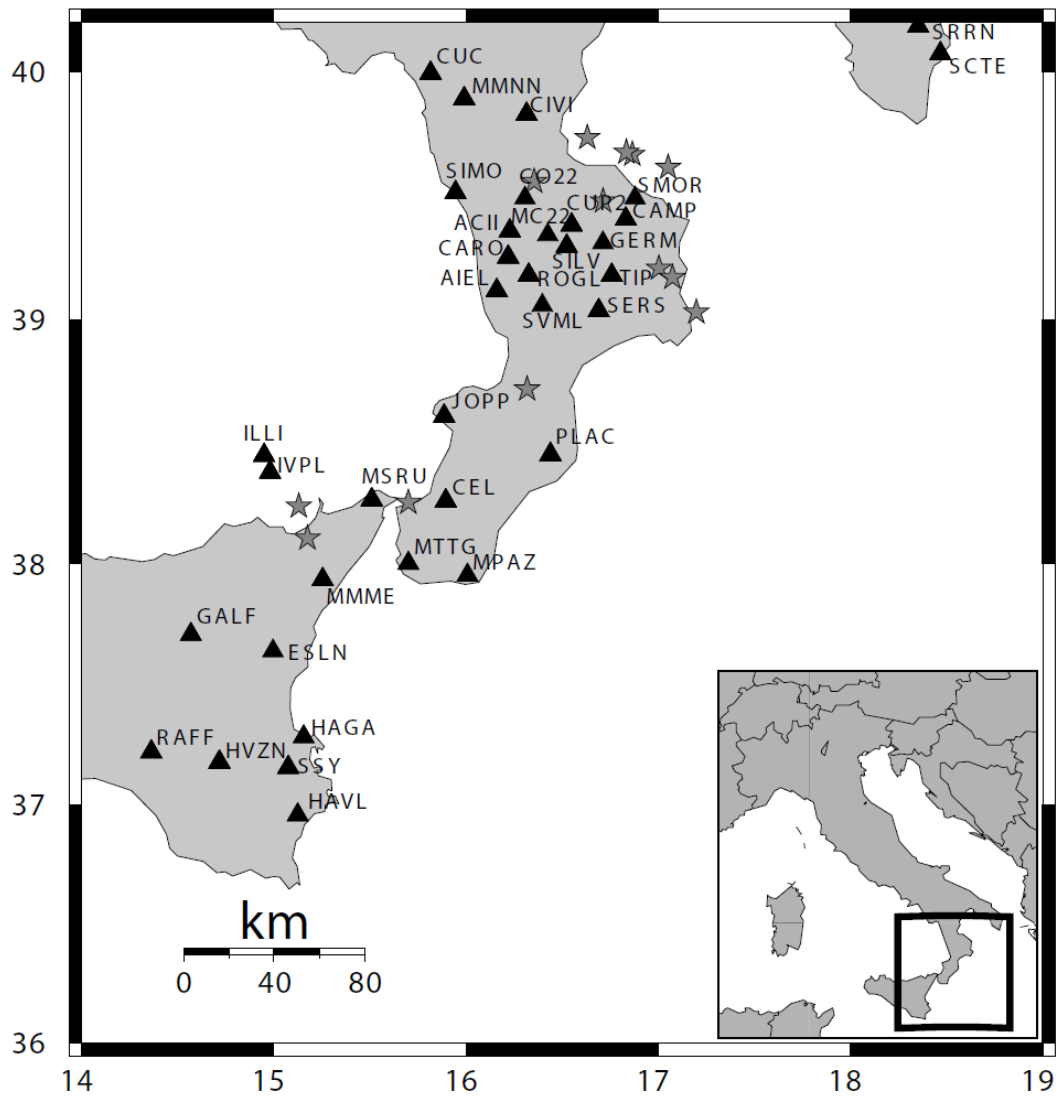
Figure 2.2. Locations of the broadband stations (black triangles) and the earthquakes (gray stars) used in this study.

16

Table 2.1. Source parameters of the earthquakes used in this study

Event ID	Date	O.T.	Lat (°N)	Lon (°E)	H (km)	Strike(°)	Dip(°)	Rake(°)	Mw
20050131	31/01/2005	10.44.50	39.6630	16.8640	30	23	79	-41	4.1
20050423	23/04/2005	19.11.43	39.474	16.711	23	128	58	14	4.1
20051203	03/12/2005	8.33.03	39.2035	17.0021	15	290	64	-18	3.8
20050907	09/07/2005	12.40.33	38.7130	16.3170	16	80	90	-42	3.6
20051118	18/11/2005	18.35.25	39.1665	17.0731	23	120	34	3	3.6
20060227	27/02/2006	4.34.01	38.1017	15.1730	10	62	50	-71	4.1
20060417	17/04/2006	2.44.06	39.6096	17.0504	28	114	74	-3	4.4
20060622	22/06/2007	19.34.58	39.7307	16.631	30	151	42	81	4.6
20070426	26/04/2007	0.49.36	39.5546	16.3542	13	231	22	-23	3.9
20070525	25/05/2007	9.39.45	39.6715	16.8325	25	91	29	-48	4.2
20070801	01/08/2007	0.07.54	39.0247	17.1971	40	80	67	-45	4.1
20070818	18/08/2007	14.04.07	38.2316	15.1291	9	44	50	-23	3.9
20080413	13/04/2008	13.06.57	38.2488	15.6992	14	6	51	-30	2.8

coverage or the use of different velocity models, with the final mechanism being robust. In fact, we found that just a few stations provide enough information to properly constrain the focal mechanism of the earthquake. Furthermore, we note that azimuthal gaps as large as 180° in station distributions do not significantly change the solution.

Panel *C* of Figure 2.7 shows comparison of the focal mechanisms of the earthquakes listed in Table 2.1 obtained applying the CAP method and using different velocity models for the studied earthquakes. The high stability of CAP solutions when the model changes is evident from Figure 2.7c.

For the events we also applied the SLUMT waveform inversion technique (Herrmann, 2008) to get the moment tensor solution as an additional check. The approach models the entire ground velocity waveform and uses a different technique for computing Green's functions (Herrmann, 2002). The method performs a grid search over the focal mechanism parameters of strike, dip and rake angles and source depth (Herrmann, 2008; Herrmann et al., 2008). The focal mechanisms obtained using the two different methodologies are in good agreement.

For a few events in the area there are moment tensor solutions by Li et al. (2007), as well as solutions published by INGV in the RCMT and TDMT catalogues. Figure 2.8 shows a comparison of the source mechanisms obtained using the different approaches. The RCMT are usually published for intermediate sized earthquakes (4.5<M<5.5), and are rarer for smaller earthquakes because the solutions tend to be less constrained in this case (www.bo.ingv.it/RCMT). This is the reason why only three focal mechanisms are available in the area for the time period considered in this study.
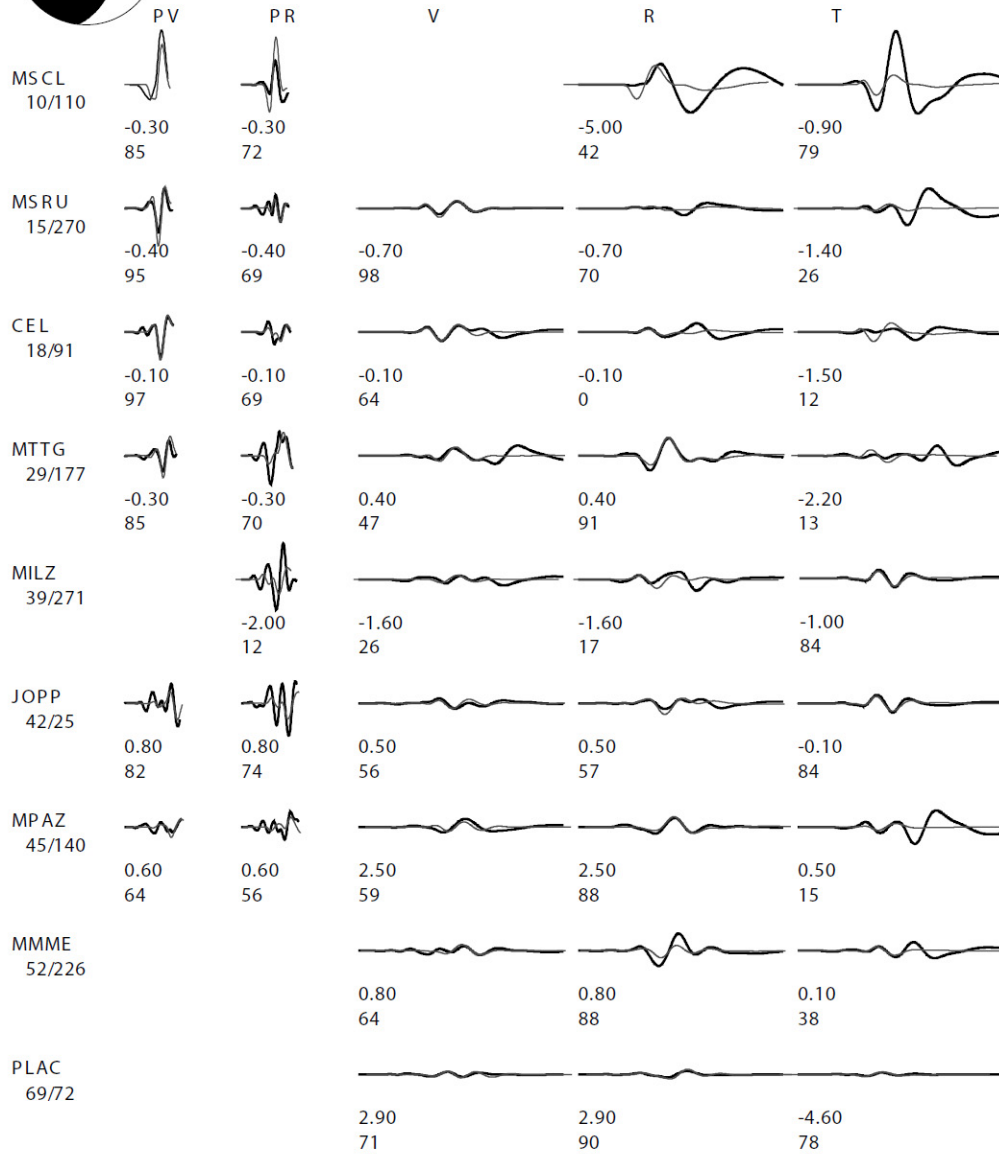
Figure 2.3. Example of waveform fit (Event ID 20080413). Black and gray traces indicate the observed and synthetics data respectively. The left two columns show the waveform fits for the vertical and radial components of the *Pnl* waves, while the next three ones show the waveform fits for the vertical, radial and tangential components of the surface wave segments, respectively. The numbers below each trace segment are the time shifts (in seconds) and the cross-correlation coefficients in percent. The numbers below the name of the seismic station are the distance source-station and azimuth, respectively

19
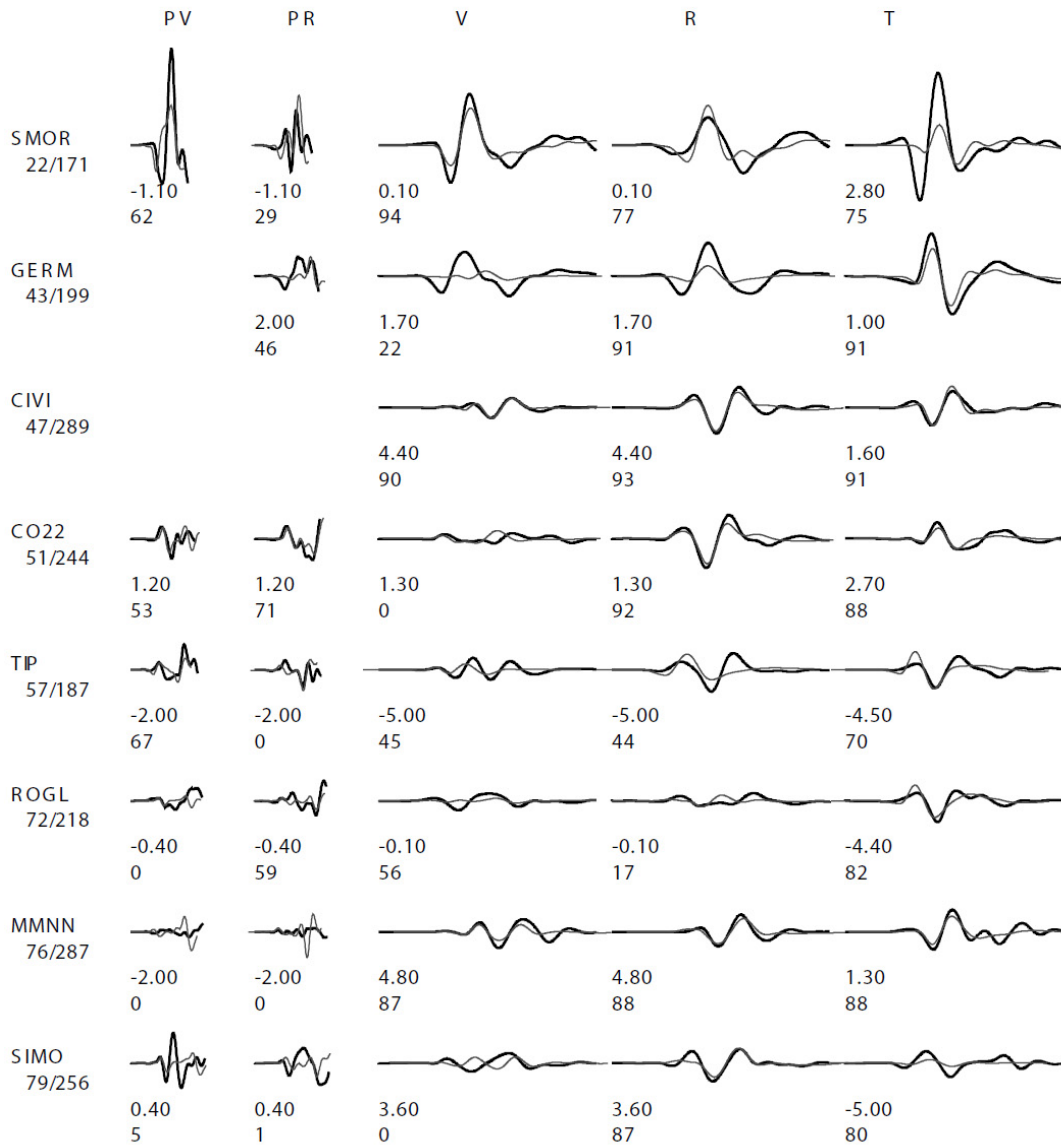
Figure 2.4. Example of waveform fit (Event ID 20050131). See caption of Figure 2.3 for details.
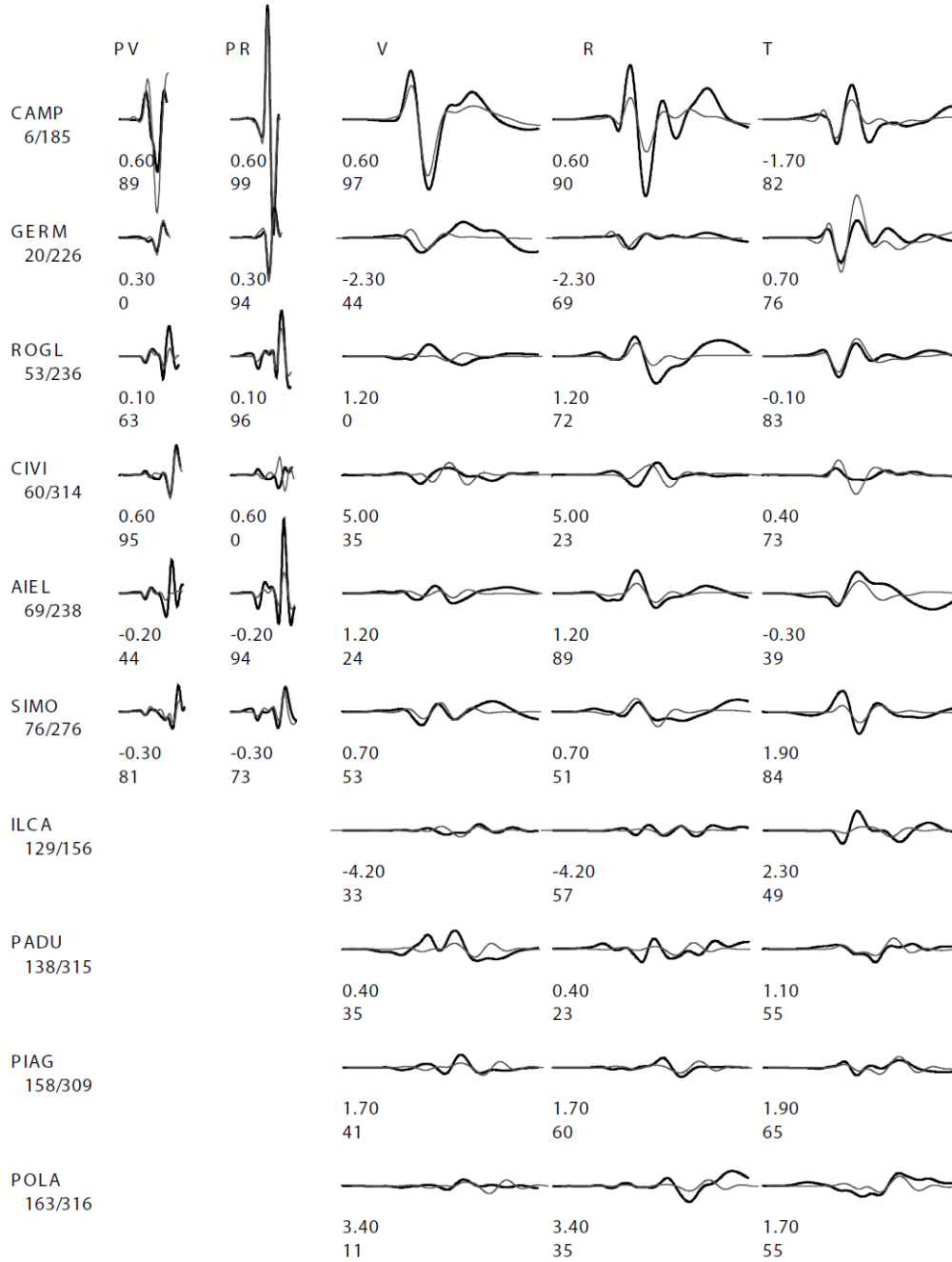
Figure 2.5. Example of waveform fit (Event ID 20050423). See caption of Figure 2.3 for details.
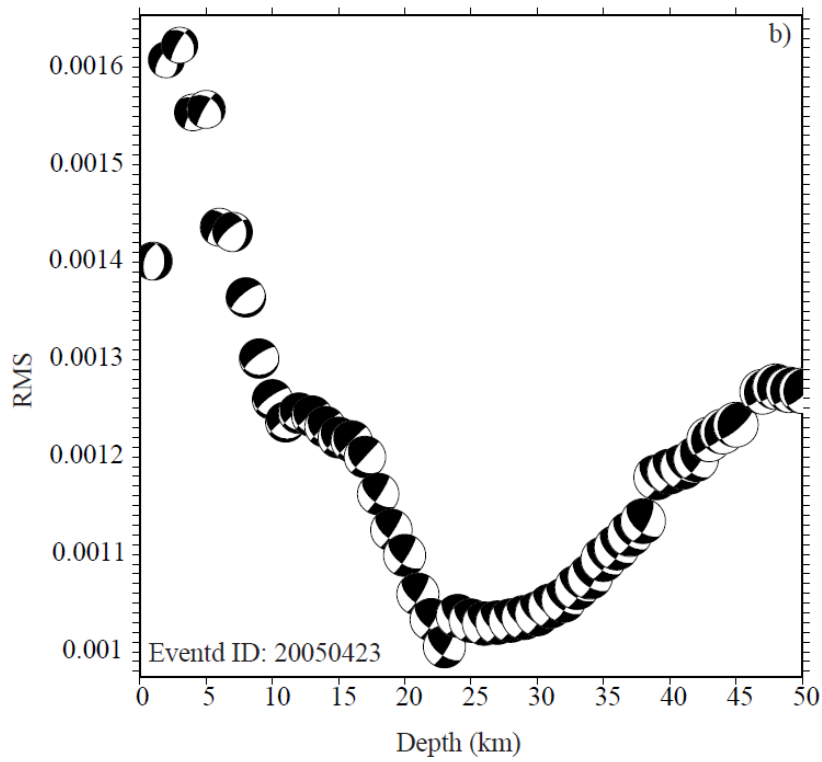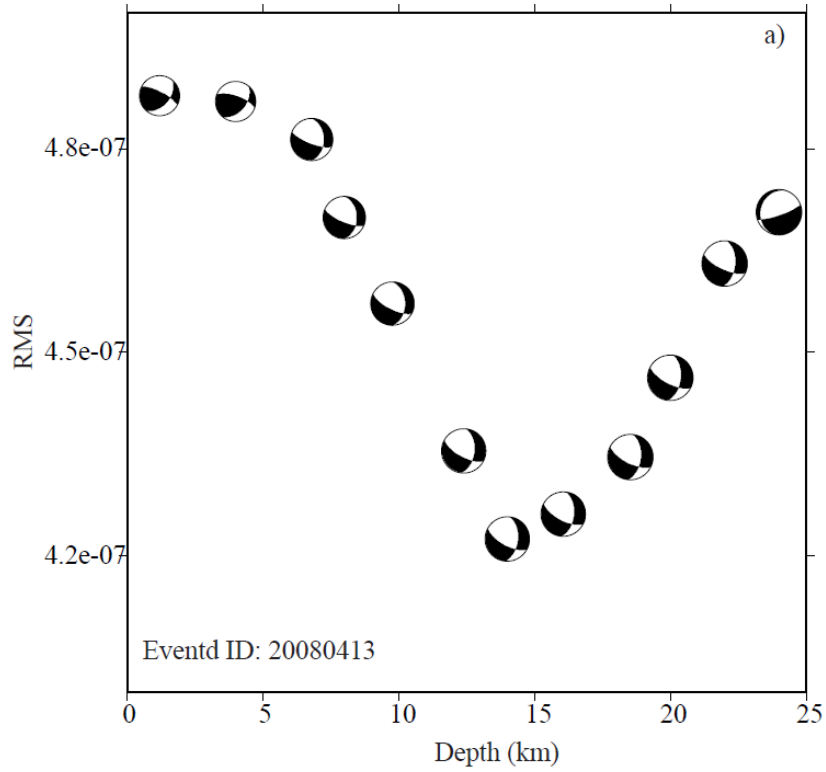
Figure 2.6. Misfit error as a function of depth for the Event ID 20080413 (a) and 20050423 (b). The solution does not change around the minimum, indicating the stability of the final solution.

A)

		STATIONS USED
a)		MSLC, MSRU, CEL, MTTG
b)		MILZ,MMME,MTTG JOPP MPAZ PLAC
c)		PLAC, CEL, MTTG, MPAZ, MSCL
d)		MSLC, MSRU, CEL, MTTG, MILZ,MMME,MTTG JOPP MPAZ PLAC
e)		MSLC, MSRU, CEL, MTTG, MILZ,MMME,MTTG JOPP MPAZ PLAC
f)		MSLC, MSRU, CEL, MTTG, MILZ,MMME,MTTG JOPP MPAZ PLAC

EV ID: 20080413

B)

		STATIONS USED
a)		MMNN, SIMO, ROGL, TIP
b)		SMOR, CIVI, CO22, GERM
c)		SMOR, CO22, GERM, ROGL, TIP
d)		SMOR, CO22, GERM, ROGL, TIP, MMNN, SIMO,CIVI
e)		SMOR, CO22, GERM, ROGL, TIP, MMNN, SIMO,CIVI

EV ID: 20050131

C)

Date			
20050131	CAL1		CAL2
20050423	CAL1		CAL2
20050907	CAL1		CAL2
20051118	CAL1		CAL2
20051203	CAL1		CAL2
20060227	VM1		VM2
20060417	CAL1		CAL2
20060622	CAL1		CAL2
20070426	CAL1		CAL2
20070525	CAL1		CAL2
20070801	CAL1		CAL2
20070818	VM1		VM2
20080403	VM1		VM2

23

Event ID	CAP	TDMT	RCMT	Li et al. (2007)	SLUMT
20050131		N.A.	N.A.	91.8	19.7
20050423		N.A.	N.A.	103.5	45.7
20050907		N.A.	N.A.	30.6	N.A.
20051118		N.A.	N.A.	15.0	N.A.
20060227		N.A.	48.6	N.A.	15.7
20060417		27.9 A	45.1	11.3	21.6
20060622		9.4 A	10.0	58.7	25.3
20070426		55.3 C	N.A.	N.A.	19.8
20070525		17.8 A	N.A.	N.A.	38.9
20070801		103.4 B	N.A.	N.A.	11.3
20070818		44.1 C	N.A.	N.A.	0.0

Figure 2.7. (previous page) Example of tests performed in order to verify the stability of the final focal mechanism. Panel *A* and *B* show several tests for the Event ID 20080413 and 20050131, respectively. In both cases the tests *a*, *b*, and *c* show the focal mechanism obtained by using different stations. Test *d* shows the solution obtained by forcing the epicenter to lie 5 km south in respect of the true location. The tests *e* and *f* shows the mechanisms estimated using different velocity models. In particular, we used the velocity models VM2 and VM3 to obtained the focal mechanisms of the tests *e* and *f* for the Event ID 20080413. The model CAL2 was used to compute the solution (test *e*) reported in panel *B* for the Event ID 20050131. Panel *C* shows the comparison of the focal mechanisms of the earthquakes listed in Table 2.1 obtained applying the CAP method and using the different velocity models for the earthquakes in the Calabrian and Peloritan region respectively. The velocity model used to obtain the focal mechanism is indicated at the right of each focal mechanism plot.

Figure 2.8. (above) Focal mechanisms comparison. Kagan (1991) angles are reported on the right of each solution compared to the respective CAP solution. Quality of TDMT solutions is also reported (see text for details).

The TDMT solutions are obtained by applying the procedure proposed by Dreger (2003). The TDMT solutions are usually obtained using a small number of stations, but with an azimuthal coverage as good as possible. However if the azimuthal coverage is not optimal the final solution can be not well constrained. In this case the solution is labeled as "Quality C" or "Quality D". The given quality of the solution is also dependent on the variance reduction. A solution is labeled as "Quality A" if the moment tensor has variance reduction greater that 60% obtained by using 4-8 stations (Scognamiglio et al. 2009). The focal mechanisms reported by Li et al. (2007) were obtained by applying the CAP method, but using a different velocity model to compute the Green's functions and by adopting different source receiver geometries because of the use of seismograms recorded just from the INGV seismic network. We may note that, in general the results agree well.

The agreement between CAP solutions and the others reported in Figure 2.8 have been numerically checked by applying the method by Kagan (1991). The Kagan angle measures the rotation that should be applied to one earthquake source double-couple to make it coincident with another one. It may vary from 0° (indicating perfect agreement between the two solutions) to 120° (total disagreement), thus values well below 60° indicate a good correspondence while above 60° a mismatch (Pondrelli et al., 2006). The results of comparison are shown in Figure 2.8. The agreement is very good between both CAP vs SLUMT and CAP vs RCMT solutions, 83% between CAP and TDMT solutions (note that the Kagan angles are smaller for "A" quality TDMT solutions) and only 66% between CAP and Li et al. (2007) solutions. In general, the differences among the solutions in Figure 2.8 can be due to a combination of several factors: (i) the adoption of different velocities models to compute the Green's functions, (ii) the use of different

25

stations and different azimuthal coverages; (iii) the use of diverse frequency bands; (iv) the use of ground displacement versus ground velocity. It is important to remark that the CAP method uses higher frequency *P*-waves featuring a greater resolving power than lower frequency methods. Furthermore the use of many stations increases the reliability of the focal mechanism because of large number of waveforms fitted simultaneously. In addition it is possible to notice that some of the TDMT solutions were not well constrained and were labeled as "B" or "C" quality (Figure 2.8). We also notice that the first two events in Figure 2.8 differ in polarity to the solutions proposed by Li et al. (2007). However the good agreement between the CAP and the SLUMT solutions together with the waveform fit reported in Figure 2.5 gives confidence on the final focal mechanisms obtained in this study.

Conclusion

Earthquake source parameters play a key role in several seismological researches. Moment tensor solutions provide the source focal mechanisms (strike/dip/rake of possible fault plane), depth and moment magnitude allowing, for example, to constrain regional seismo-tectonic deformations and the stress field. Focal mechanisms estimated with the traditional method of P-wave first motion are usually affected by inherent uncertainties, and they might be unstable because of insufficient azimuthal coverage and are not easily determined for low magnitude events. In addition the RCMT and TDMD catalogues report only a few moment tensor solutions in the area. Thus the knowledge derived from earthquake focal mechanisms in this area can be considered limited.

In this study we provided moment tensor solutions for several events of small to moderate magnitude in the Calabrian-Peloritan arc. We used waveforms recorded by the Italian National Seismic Network and managed by the INGV and the CAT-SCAN project. We computed the moment tensor solutions using the CAP and SLUMT methods and tested the stability of the final solutions by sensitivity to using different stations or velocity models. Comparisons have been also made with the available published solutions. We concluded that the final focal mechanisms were robustly determined. Furthermore we showed that the application of CAP and SLUMT methods can provide good-quality solutions in the area in a magnitude range not properly represented in the Italian national catalogues and where the solutions estimated from P-onset polarities are often poorly constrained.

In the near future, by applying the CAP and SLUMT methods, we expect to provide several more moment tensor solutions to improve the knowledge of the of the seismo-tectonic regime, the regional stress field features, and the seismic hazard in the Calabrian arc.

CHAPTER 3: Broadband Waveform Inversion of Moderate Earthquakes in the Messina Straits

Introduction

The Messina Straits and the adjoining areas of the Calabro-Peloritan Arc in Southern Italy (Figure 3.1) are characterized by intense active tectonics as evidenced by the occurrence of destructive earthquakes (Boschi et al., 1995; CPTI Working Group, 2004; Guidoboni et al., 2007). The magnitude 7.2 Messina Straits Earthquake of December 28, 1908 was the strongest Italian earthquake of the past century (CPTI, Working Group 2004) and caused more than 60,000 casualties and the destruction of many towns and cities in northeastern Sicily and neighbouring Calabria (Baratta, 1910). The 1908 earthquake may have been caused by the activation of a normal fault located in the Messina Straits, but the exact location and geometry of the fault are still controversial (Boschi et al., 1989; Bottari et al., 1989; Valensise and Pantosti, 1992; Monaco and Tortorici, 2000, Amoruso et al., 2002 and 2006; DISS Working Group, 2007; Pino et al., 2009).

The low level of seismicity in the Messina Straits in the last few decades (Neri et al., 2003, 2004, 2008) has not permitted seismologists to define the locations and mechanisms of the seismogenic faults in this area. Current knowledge about the earthquake mechanisms is represented by the small number of moment tensor solutions published for this area in the Italian CMT catalog (Pondrelli et al., 2006). As discussed later in this chapter, other moment tensor solutions available on the web for this area are ranked as preliminary and await validation
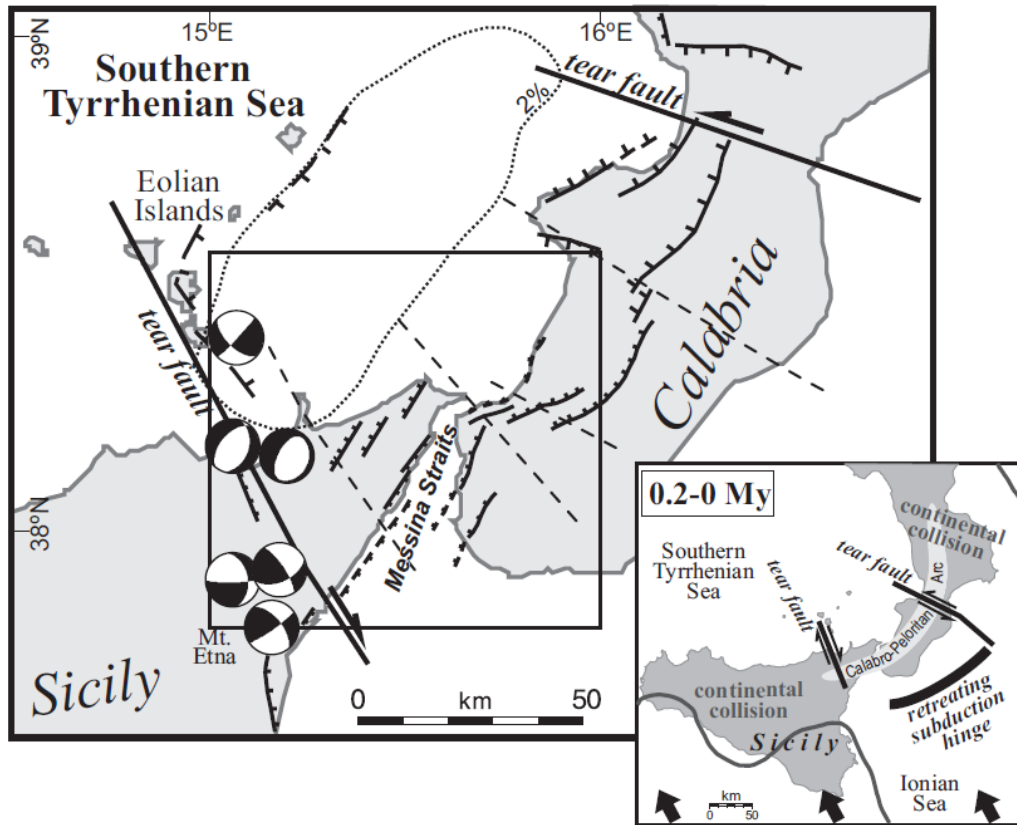
Figure 3.1. The Messina Straits area investigated in the present study is indicated by a square in the main plate of this figure, the smaller frame at the lower right (redrawn from Neri et al., 2009) shows the Calabro-Peloritan Arc region in southern Italy. This smaller frame indicates that while the central portion of the Arc corresponds approximately to the southeast-ward retreating subduction hinge, the northern and southwestern edges of it lie in continental-collision zones which developed after local detachment of the subduction system. The northwest-ward trending arrows in the bottom of the same frame indicate the Nubia-Europe convergence direction (Nocquet and Calais, 2004). The main frame shows the principal fault systems, hatched = normal faulting, half arrow = strike-slip component, dashed = presumed strike-slip but different interpretations in the literature (Fabbri et al., 1980; Finetti and Del Ben, 1986 and 2005; Monaco and Tortorici, 2000). The dotted curve in the southern Tyrrhenian Sea marks the high velocity anomaly found by seismic tomography at 150km depth (Neri et al., 2009) indicating the only part of the subduction system where the slab is still continuous (i.e. detachment has not still occurred). The focal mechanisms reported for the study area in the Italian CMT catalog are also displayed.

(http://mednet.rm.ingv.it/quick_rcmt.php; http://earthquake.rm.ingv.it/tdmt.php). In addition, the solutions estimated with the traditional method of P-wave first motion data (Frepoli and Amato, 2000; Vannucci and Gasperini, 2004; Neri et al., 2004) are affected by inherent uncertainties that do not permit detection of seismogenic structures and local-scale stress changes. Thus the knowledge derived from earthquake focal mechanisms in this area is limited.

We apply the "Cut And Paste" (CAP) method (Zhao and Helmberger, 1994; Zhu and Helmberger, 1996) to determine the focal mechanisms, moment magnitude and depths for earthquakes in the Messina Straits area. This method is based on waveform inversion of *Pnl* and surface-wave segments and has proven to be effective for analyzing earthquakes over a wide range of magnitudes, even those with magnitudes between 2.5 and 4 (Zhu et al., 2006). The application of CAP to small-magnitude events in the Messina Straits area provides an opportunity to significantly increase the number of the local earthquake focal mechanisms, which can then be used to understand current tectonics.

Tectonic framework of the study area

The Messina Straits is located in the Calabro-Peloritan Arc (Figure 3.1), a tectonic structure uplifting at a rate of 0.5-1.2 mm/yr in the last 1-0.7 My (Monaco and Tortorici, 2000). The deformation in the area is mainly accommodated by normal faults (Monaco and Tortorici, 2000, Catalano and De Guidi, 2003, Catalano et al., 2003). The dynamics of this area is controlled by two main tectonic factors: the Nubia-Europe plate convergence locally oriented NNW-SSE (Calais et al., 2003; Nocquet and Calais, 2004; Serpelloni et al., 2007) and the southeast-ward rollback of the Ionian lithospheric slab

which subducts beneath the Tyrrhenian lithosphere (Figure 3.1; Malinverno and Ryan, 1986; Faccenna et al., 1996). The Nubia-Europe convergence velocity in this region has been estimated to be about 0.5 cm/yr (Goes et al., 2004; Nocquet and Calais, 2004; D'Agostino et al., 2008a), and the rollback of the Ionian slab and subduction trench retreat is supposed to be even slower, perhaps a few mm/yr (Devoti et al., 2008; D'Agostino et al., 2008b). Several authors (Spakman and Wortel, 2004 and references therein) argued that this very low outward migration velocity of the Calabro-Peloritan Arc and its fast uplift could suggest a shallow detachment of the subduction slab. A recent seismo-tomographic investigation (Neri et al., 2009) focused on the present state of subduction in this region. They suggested that the deep portion of the subducting lithospheric slab has already detached from the shallow body near the edges of the Arc (e.g. beneath northern Calabria and northeastern Sicily, Figure 3.1) while the slab is still continuous beneath the central part of the Arc, along a 100 km-long NE-trending segment of the subduction system in southern Calabria (Figure 3.1). In addition to filling an information gap indicated by the previous investigators concerning the present state of subduction in this area (see e.g. Spakman and Wortel, 2004) the results by Neri et al (2009) may help the interpretation of the shallow seismicity in the Arc region through proper contextualization of the seismotectonic process occurring at crustal depths above the subducting lithosphere. Seismogenic stress inversion on a regional scale allowed Neri et al. (2005) to detect a clear change from an extensional domain in southern Calabria and Northeastern Sicily to a compressional one in the rest of Sicily. Evidence for this tectonic change was seen in other geological and geophysical investigations (see e.g. Billi et al., 2006 and 2007). The transition was approximately located across a belt running from the Eolian Islands SSE to the Ionian coast of Sicily near Mt. Etna (Figure

31

3.1). The transition from the eastern extensional domain to the western compressional

area may be explained in terms of joint action of two main factors, plate convergence

and rollback of the subducting lithosphere (Neri et al., 2005; Billi et al., 2006 and 2007).

This view matches the findings of the most recent geodetic and seismological

investigations (D'Agostino et al., 2008b; Neri et al., 2009) which support the existence

of a residual rollback of the subduction slab in southern Calabria and continental

collision following slab detachment in western-central Sicily.

Method and data

The study region is approximately bounded by latitudes 37.8N to 38.5N and

longitudes 15.0E to 16.0E and is monitored by the Italian National Seismic Network

managed by the Istituto Nazionale di Geofisica e Vulcanologia (INGV). We started by

compiling a list of all earthquakes in the study area from the INGV seismic catalogue

(http://iside.rm.ingv.it) for the time period from October 2004 to October 2008 (Figure

3.2) with focal depths less than 25 km and magnitudes ML larger than 3. The dataset

was restricted to the earthquakes recorded by a minimum of 4 three-component seismic

stations (Figure 3.2) equipped with broad-band sensors such as Trillium 40's, STS-2-

120's, and Lennartz-3D-20's, located within about 200km from the epicenter. Each

waveform was corrected for the instrument response, examined to eliminate recordings

with spurious transients, double events or low signal-to-noise ratios, and finally

reviewed for the picking of P-arrivals. We also rotated the horizontal recordings to radial

and transverse components of ground velocity with respect to the published location.

The final data set used in this study consisted of about 1000 waveforms from 23

earthquakes. The main parameters of these earthquakes are listed in Table 3.1. The
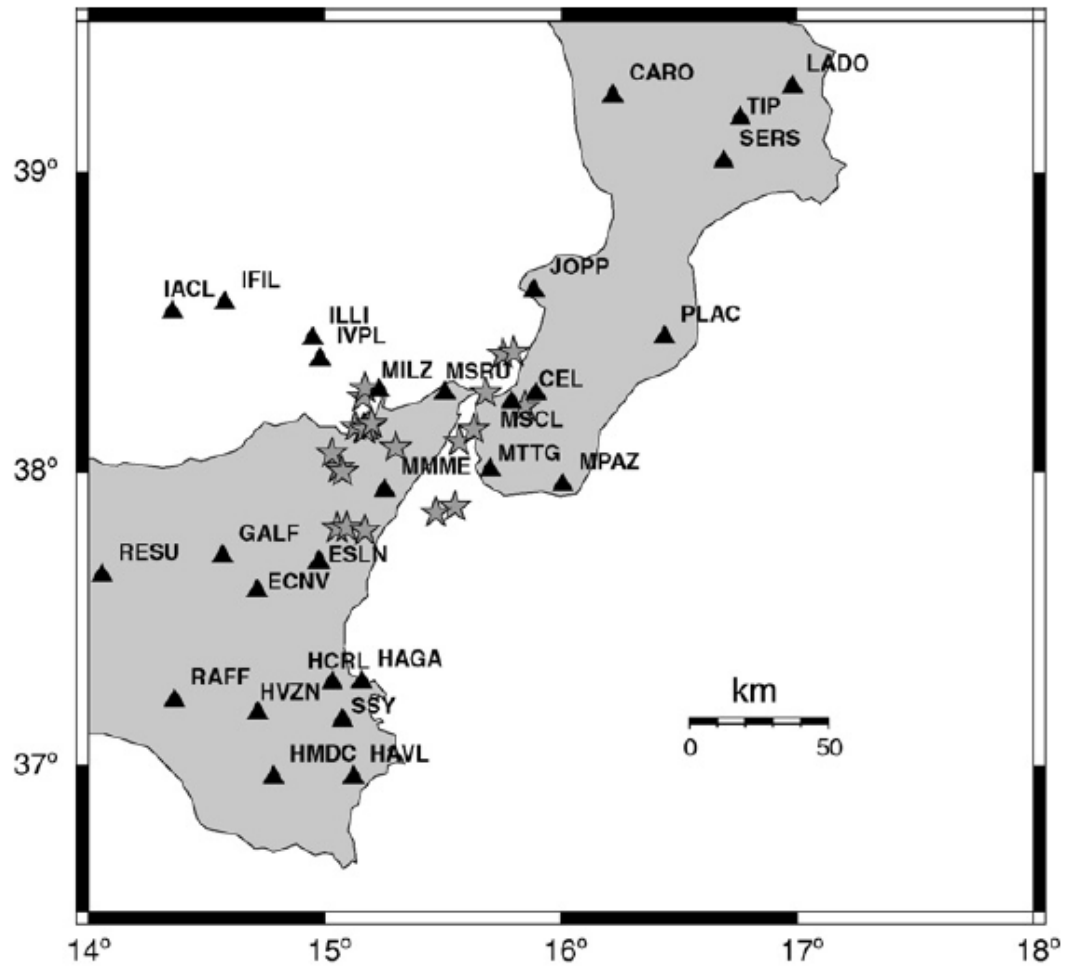
Figure 3.2. Map of the region showing the locations of the earthquakes (stars) and the three-component broad band stations (triangles) used in the present study.

moment tensor solution of each event was obtained by applying the CAP method (Zhu and Helmberger, 1996). In order to get reliable source mechanisms, using waveforms, it is necessary to compute synthetic seismograms, which in turn requires a reasonable velocity/attenuation model for generating Green's functions. We used the frequency-wavenumber (F-K) integration method as described in Zhu and Rivera (2002) to compute Green's functions for a distance range from 5 to 500km with a spacing of 5 km and a focal depth range from 2 to 60 km. We used the 1-D velocity model proposed for the area by Barberi et al. (2004) and added densities based on the Nafe-Drake relation (Ludwig et al., 1970). Qp and Qs values are similar to those used by other researchers. The Qp and Qs values are not critically important because we were dealing with relatively short propagation distances and low frequencies. Table 3.2 presents the crustal model used for computing the Green's functions.

The CAP method minimizes the misfit between the observed and synthetic seismogram using a grid search to obtain the best moment magnitude, source depth and focal mechanism (Zhu and Helmberger, 1996). The misfit is defined as an L2 norm of the difference between the synthetic seismograms and the observed data, after correcting for distance decays of amplitudes. In this study the parameter space of the source orientation (strike, dip, rake) was searched at 10° intervals while the source depth was searched with a 2 km spacing. The moment magnitude was searched at 0.1 intervals in magnitude. An additional grid search with reduced intervals and subsequent interpolation based on the waveform misfits were performed in the vicinity of the grid-search minimum to obtain and further refine the "best solution" (Tan et al., 2006). The uncertainties of focal mechanisms and depths, listed in Table 3.1, were estimated by the

methods and the statistical approaches described by Tan et al. (2006) and Bevington and Robinson (2003).

One of the advantages of the CAP method is that each waveform is broken up into *Pnl* and surface wave segments that are weighted differently in the misfit. This is because they are sensitive to different parts of crustal structure and have different amplitude decay with distance. The surface waves, although large in amplitude, are easily influenced by shallow crustal heterogeneities while the *Pnl* waves are controlled by the averaged crustal velocity structure and therefore are more stable. For this reason we weighted the *Pnl* segments 2-3 times more than the surface wave segments. One particular feature of the CAP technique is that it allows time shifts between synthetics and observed data in order to reduce the dependence of the solution on the assumed velocity model and earthquake location error. The time shifts are also needed in case the Green's functions are not computed at exactly the same distance as the observed data. Figures 3.3 and 3.4 show two examples of the waveform fits produced by the CAP inversion. Observed waveform are indicated by black traces and the synthetics by gray traces. The left two columns show the waveform fits of the vertical and radial components of the *Pnl* waves and, the next three columns show the waveform fits of the vertical, radial, and tangential components of the surface waves. The numbers below each trace segment are the time shifts (in seconds) and the cross-correlation coefficients. A positive time shift indicates that the model prediction is too early and the synthetics are to be delayed to match the observed trace. We used ground velocity instead of ground displacement in the CAP inversion as the magnitudes of the events are smaller than 4 and we needed to avoid the influence of long-period noise embedded in the deconvolved ground displacements. Synthetics and observed ground velocity were

Table 3.1. Source parameters of the earthquakes used in this study. As explained in the text, the CAP method has been used for computation of the focal depth H, the fault parameters Strike, Dip and Rake, and the Magnitude Mw. Focal depth and fault parameter uncertainties have been estimated with the method described in Tan et al. (2006) and papers referred therein.

Event ID	O.T.	Lon (°E)	Lat (°N)	H (km)	ML	Mw	Strike(°)	Dip(°)	Rake(°)	ERR (Strike)	ERR (Dip)	ERR (Rake)
20041011	7.31.41	15.48	37.88	6.6	3.5	3.6	89	90	-45	1	1	1
20041022	21.10.13	15.32	38.08	10.7	3.5	3.4	78	61	-37	0	1	2
20050419	22.36.23	15.66	38.14	7.1	3.2	3.1	220	42	-10	1	2	2
20050423	19.10.48	15.82	38.43	13.6	3.0	2.8	120	50	-64	1	1	2
20050814	22.02.27	15.12	37.80	6.7	3.0	3.1	82	50	-18	1	1	1
20060227a	4.34.01	15.17	38.10	10.1	4.1	4.1	62	50	-71	0	1	2
20060227b	9.11.59	15.18	38.14	10.5	3.5	3.1	39	48	-90	2	1	2
20060227c	14.16.06	15.18	38.14	9.1	3.3	3.1	76	48	-58	1	1	3
20060702	17.52.00	15.10	38.13	10	3.0	2.6	70	59	-49	1	2	3
20060718	7.42.40	15.17	38.12	9.1	3.3	3.1	90	41	-49	1	1	2
20061006	21.16.23	15.57	38.10	9.6	3.2	3.2	18	52	-90	1	1	2
20061104	5.59.22	15.01	38.03	10.6	3.1	3	59	49	-37	1	2	4
20070617	12.11.58	15.79	38.37	10	3.3	2.9	262	38	-43	1	2	1
20070818a	14.04.07	15.13	38.23	9.4	4.0	3.9	44	50	-23	1	1	2
20070818b	14.21.11	15.12	38.19	10	3.2	3.4	26	69	18	2	3	5
20080209	7.46.36	15.56	37.84	6.9	3.1	3	40	90	-10	1	1	2
20080413	13.06.57	15.70	38.25	14.3	3.3	2.8	6	51	-30	2	1	2
20080501	21.05.49	15.07	37.80	2	3.4	3.4	96	76	2	1	1	3
20080513	21.28.30	15.06	37.80	12	3.3	3.5	76	46	-20	1	1	2
20080705	17.04.36	15.87	38.20	2	3.0	2.6	311	59	2	1	1	4
20080901	14.45.40	15.06	37.97	8.1	3.1	3.1	70	31	-80	0	1	3
20080902	9.16.45	15.06	37.99	10.3	3.4	3.3	279	64	-44	1	1	2
20081027	10.55.55	15.13	38.11	2	4.0	3.5	50	28	-71	0	1	2

Table 3.2. Crustal model of the study area used for moment tensor inversion used for the solutions of Figure 3.5 and Table 3.1.

Depth (km)	Vp (km/s)	Vs (km/s)	$P\,(\text{g/cm}^3)$	Qp	Qs
0	4.67	3.08	2.43	600	300
3	5.12	3.17	2.52	600	300
6	5.64	3.29	2.63	600	300
10	6.03	3.59	2.71	600	300
25	8	4.6	3.31	900	450

filtered in the same frequency bands, from 0.02 Hz to 0.1 Hz for the surface waves and from 0.05 Hz to 0.3 Hz for the *Pnl*. These frequency bands were chosen to maximize signal-to-noise ratios of data and to avoid short-wavelength structural heterogeneities. We can see that the synthetic matches well the observed both in shape and amplitude.

Results

Figure 3.5 shows the focal mechanisms of earthquakes in the Messina Straits area estimated by the CAP method. The different shades of gray identify different types of mechanism according to the Zoback classification adopted in the World Stress Map (Zoback, 1992; http://dc-app3-14.gfz-potsdam.de/). The parameters of these events are listed in Table 3.1. ML and Mw indicate, respectively, the local magnitude reported in the INGV catalogue (http://iside.rm.ingv.it) and the moment magnitude derived from this CAP waveform inversion.

Many authors demonstrated that a good focal mechanism can sometimes be obtained using just a few stations or even, in an extreme case, using two stations with an azimuthal gap of about 180 degrees (Zhu and Helmberger, 1997; Dreger and Helmberger, 1993). In order to have an additional check of the CAP focal mechanisms for this area we performed several tests. For some of the earthquakes investigated, we tried different station distributions, such as using only the nearest, the farthest stations or combinations of both. We also changed the azimuthal station distribution and the hypocentral parameters of the event. Figure 3.6 shows the results of this sensitivity testing for one of the earthquakes.
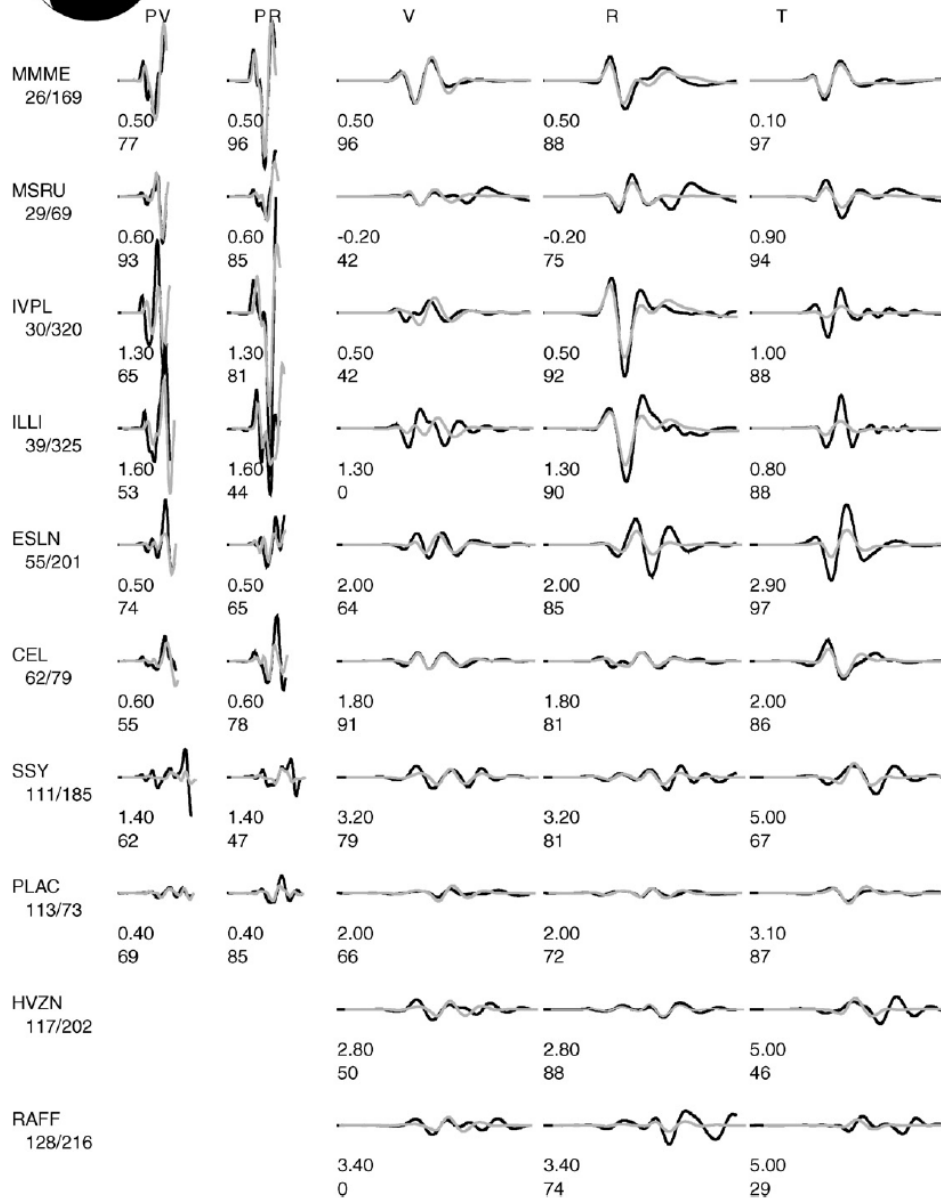
Figure 3.3. Example of waveform fit for the event ID 20060227a (see also Figure 3.5 and Table 3.1). Data are indicated by black lines, synthetics are represented by gray lines. The left two columns show the waveform fits for the *Pnl* waves on the vertical (PV) and the radial components (PR), while the next three ones show the waveform fit for the surface waves: vertical (V), radial (R), and tangential (T) component respectively. The numbers below each trace segment are the time shift (in seconds) and the cross-correlation coefficient, respectively. The name of the station is reported on the left side of each trace fit; the numbers just below it represent the distance from the station and the azimuth.

39

Event: 20070617   Model: VM1   FM: 262 38 -43   Mw: 2.90   rms: 1.900e-07
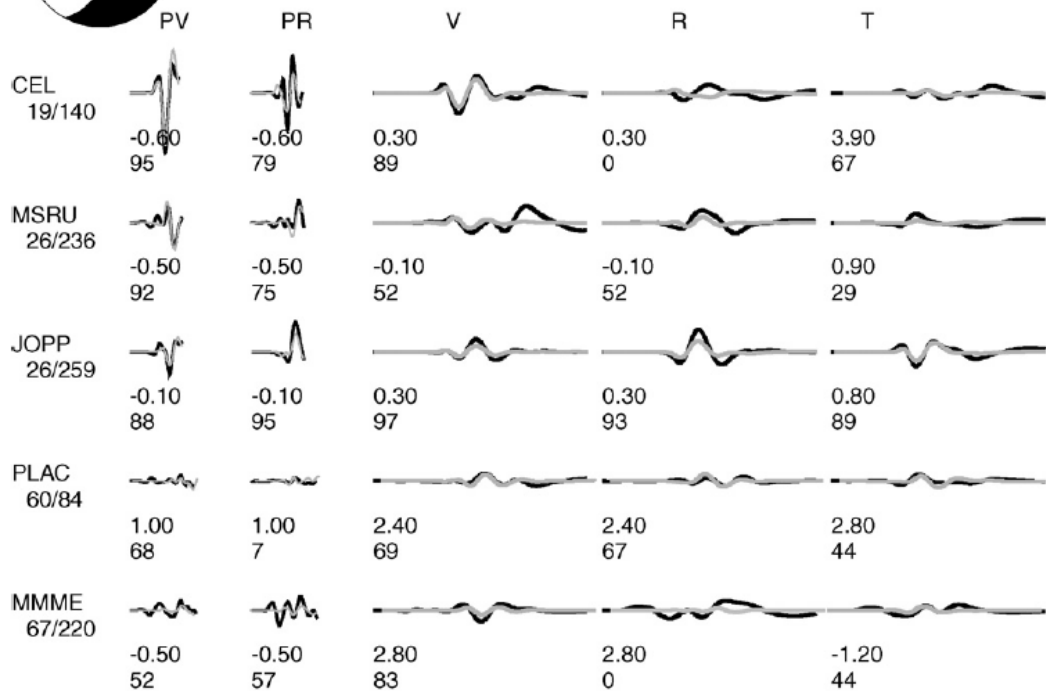
Fig. 4. Example of waveform fit for the event ID 20070617 (Fig. 5 and Table 1). See caption of Fig. 3 for details.

Figure 3.4. Example of waveform fit for the event ID 20070617 (Fig. 3.5 and Table 3.1). See caption of Figure 3.3 for details.
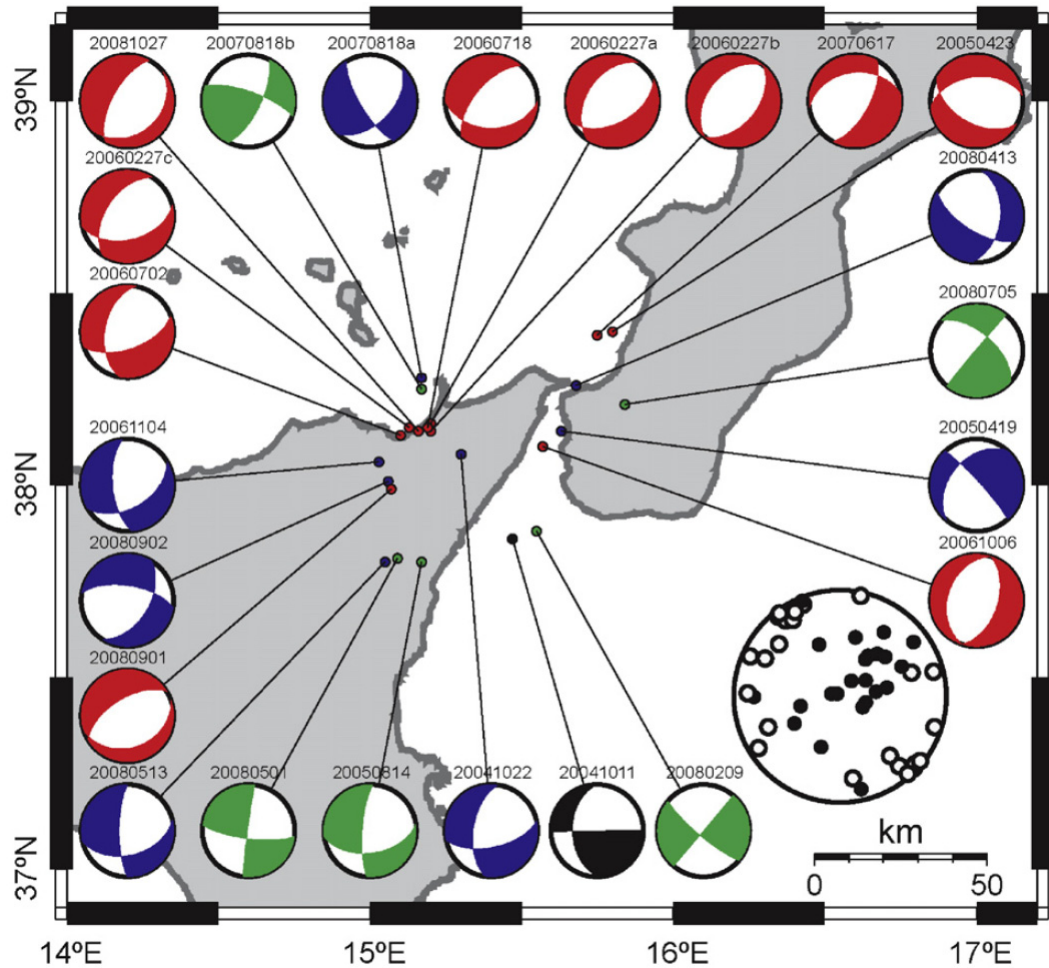
Figure 3.5. Focal mechanisms estimated in the present study by the CAP waveform inversion method. The different colours identify different types of mechanism according to the Zoback classification adopted in the World Stress Map (Zoback, 1992; http://dc-app3-14.gfz-potsdam.de/): red = normal faulting, NF, blue = predominantly normal faulting with strike-slip component, NS; green = strike-slip faulting, SS; black = unknown stress regime, U. The polar plot of P- and T-axes of these events is also shown (black and white dots correspond to P and T axes, respectively). The main parameters of the earthquakes are reported in Table 3.1.

41
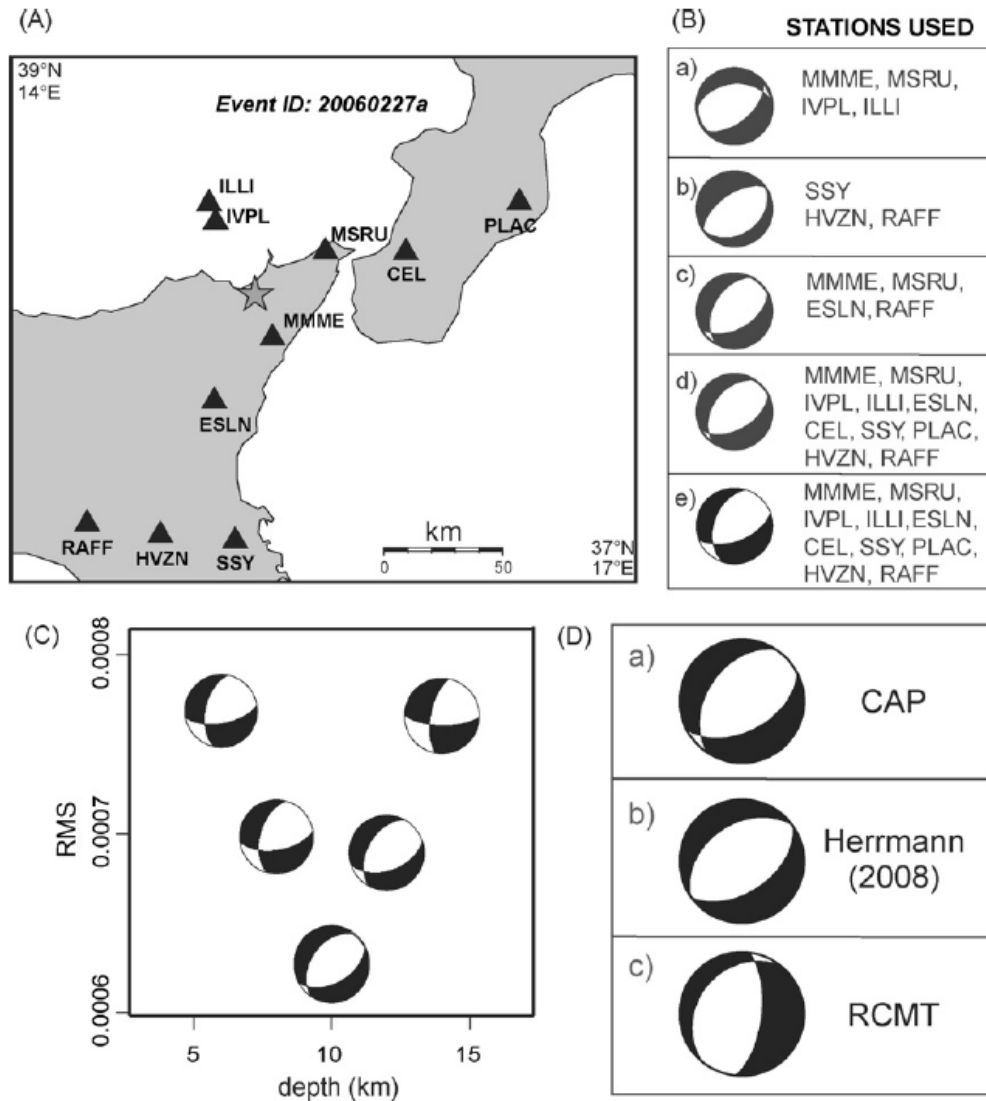
Figure 3.6. Examples of tests and comparisons made to check the quality of the CAP solutions obtained in the present work. The panel A shows the location of the event ID 20060227a and of the stations used in the tests displayed here. The beach balls in the panel B represent the solution obtained using some nearby stations (a), some farther stations (b), a combination of them with an azimuthal gap of almost 180 degrees (c), forcing the epicenter to lie 5 km south of the true location (d) and using only the surface wave segments (e). The solutions obtained at different depth levels around the CAP focal depth of the event are displayed in the panel C with the corresponding values of the predicted-observed waveform misfit. Finally the panel D shows, for comparison, our CAP solution, the focal mechanism we estimated by the method of Herrmann (2008) and the regional CMT solution released by INGV (http://www.bo.ingv.it/RCMT/searchRCMT.html).

42

The focal mechanism is robustly determined. In fact, we found that just a few stations provide enough information to properly constrain the focal mechanism of the earthquake. Furthermore, we note that azimuthal gaps as large as 180° in station distributions do not significantly change the solution. Finally, we may observe that the solution is stable in the error range of the focal depth estimated by CAP. For some events we also applied the waveform inversion technique of Herrmann (2008) to get the moment tensor solution as a check on our computations. His approach models the entire ground velocity waveform and uses a different technique for computing Green's functions. Using the crustal model given in Table 3.2 to obtain the Green's functions, a grid search over the focal mechanism parameters of strike, dip and rake angles and source depth (Herrmann, 2008; Herrmann et al., 2008) was performed. The focal mechanisms obtained using the two different methodologies are in good agreement. Figure 3.6D shows a comparison of the source mechanisms obtained for the event ID 20060227a using CAP and Herrmann's (2008) methods, and displays also the published INGV-RCMT solution of the same event (Ekstrom et al.,1998; Pondrelli et al., 2006). The RCMT are usually released for intermediate sized earthquakes (4.5<M<5.5), more rarely for smaller earthquakes because the solutions tend in this case to be less constrained (www.bo.ingv.it/RCMT). We may note in the figure the good agreement between the CAP and Herrmann's solutions, while the RCMT solution appears a little different from the others. Finally, we have checked the stability of the mechanisms of Figure 3.5 by varying the earth structure parameters within ranges defined according to the most recent tomographic inversions and velocity models available for the study area (see e.g. Barberi et al., 2004). For this test we started from the tomographic models of Barberi et al. (2004) and computed in both structures the P-wave theoretical travel-times

corresponding to the source-station pairs used for the CAP inversion leading to Figure 3.5. Then, from the time-distance plots obtained for the respective structures we derived the 1D velocity models indicated as VM2 and VM3 in Figure 3.7. The same figure shows also the VM1 model used for computation of the focal mechanisms of Figure 3.5 and reported in Table 3.2. The differences among these models represent wave propagation across the laterally heterogeneous crust of the study area (Neri et al., 2002; Finetti, 2005; Pontevivo and Panza, 2006). The high stability of CAP solutions when the model changes is evident from Figure 3.7.

Discussion and conclusion

Figure 3.5 shows that normal faulting is the main style of seismic deformation in the Messina Straits area. Using the Zoback's WSM terminology (Zoback, 1992; http://dc-app3-14.gfz-potsdam.de/) we count 10 normal faulting mechanisms (NF), 7 normal-strike (NS), 5 strike-slip (SS) and 1 undefined (U). In the same figure, the polar plot of P- and T-axes shows a roughly NW-SE preferential orientation of the extension axes. In addition, we may note from the map that the regime of faulting significantly changes from north to south: normal faulting prevails clearly in the north while it appears mixed to strike-slip in the south. According to WSM terminology we count 9 NF earthquakes, 3 NS and 2 SS in the northern sector A of the study area (Figure 3.8) and 4 NS, 3 SS, 1 NF and 1 undefined in the southern sector B. Testing different space partitions of the study area by changing the location and orientation of the dashed separation line of Figure 3.8 we have also checked that the sub-volumes A and B

44
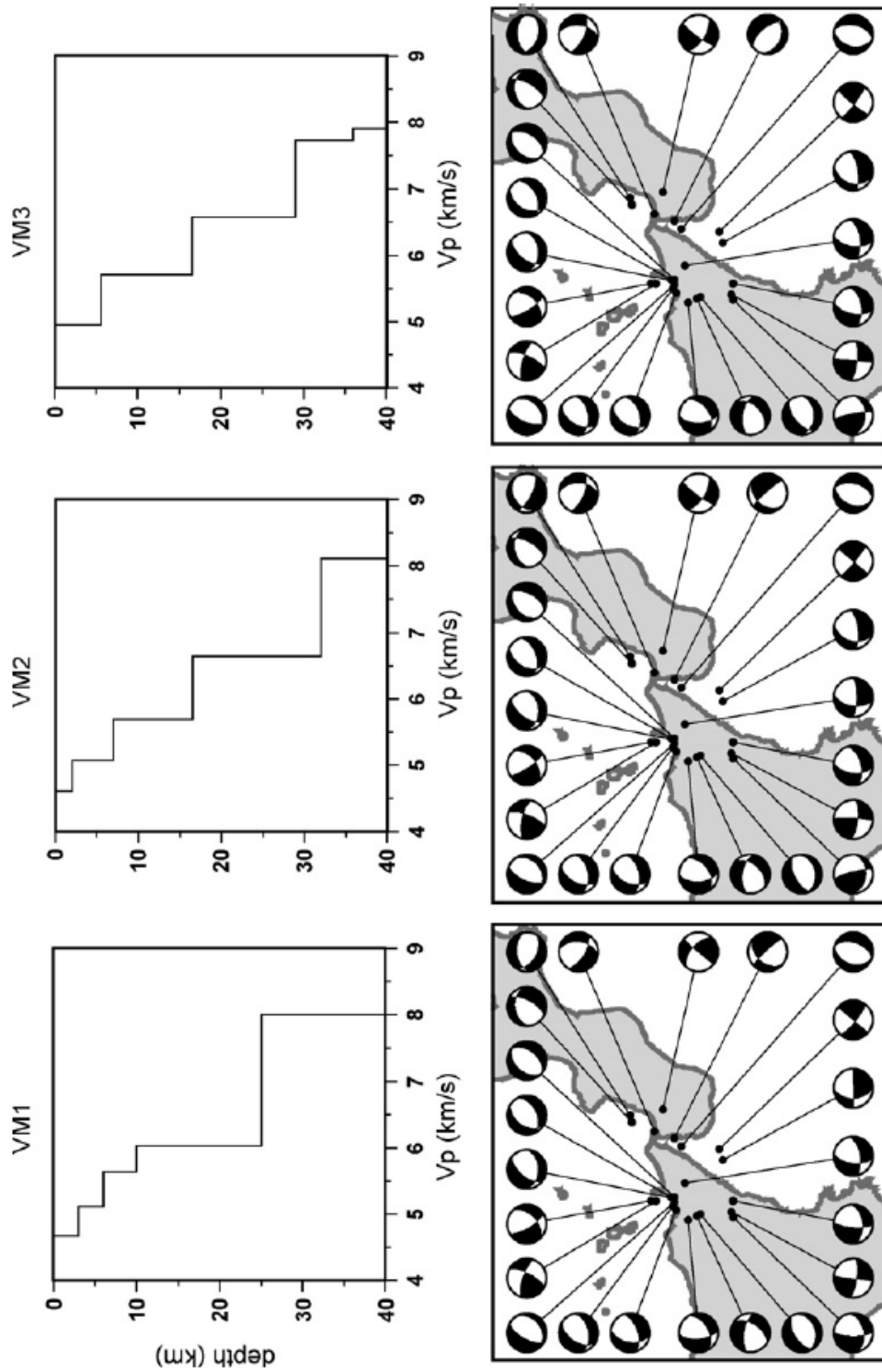
Figure 3.7. Comparison of the CAP mechanisms of the earthquakes listed in Table 3.1 estimated with different velocity models (VM1, VM2, VM3). See text for details.

effectively allow for the best separation between the normal faulting earthquakes and the others (maps and percentage histograms relative to the large number of trials performed are not reported for conciseness).

The CAP focal mechanisms of Figure 3.5 bring new knowledge on the earthquake process in the Messina Straits area. Here, the focal mechanism information available before the present study included (a) the waveform inversion solutions of the Italian CMT catalog (http://www.bo.ingv.it/RCMT) validated by quality evaluation processes which guarantee high reliability of data, (b) other waveform inversion solutions such as Quick-RCMT (http://mednet.rm.ingv.it) and TDMT (http://earthquake.rm.ingv.it/tdmt.php) ranked as preliminary because they routinely enter into the databases with nearly automathic procedures at the earthquake occurrence, and (c) traditional focal mechanisms from inversion of P-onset polarities (see e.g. Caccamo et al., 1996; Frepoli and Amato, 2000; Neri et al. 2004 and 2005; Vannucci and Gasperini, 2004). The traditional focal mechanism solutions have focal parameter errors small enough to allow detection of strong stress variations between the Calabrian Arc and Western-Central Sicily major domains, but the errors are too large for detection of more subtle stress changes in the transitional area between the main domains. The network geometry used for focal mechanism studies is limited by the lack of OBSs in the wide offshore sectors of the study region and this is a major factor reducing the quality of these solutions. The preliminary Quick-RCMT and TDMT solutions (item 'b') will undergo validation or modification in the near future through accurate review by specialists (see, e.g. Pondrelli et al., 2006; Scognamiglio et al., 2009). High-reliability solutions available for the Messina Straits area are displayed in the top-left of Figure 3.8

46

in gray shading together with the CAP solutions estimated in the present study in black. The data outline a clear north-to-south variation of the seismic deformation style marked by the dashed line separating the sub-volumes A and B. The polar plots of P- and T-axes in A and B show the different styles of deformation, with the P-axes more clustered near the center in the case of plot A.

These findings fit in the framework of the most recent interpretation of the regional geodynamics and furnish additional constraints to the model (Figure 3.8). As mentioned above, the Ionian lithosphere subducting beneath the Tyrrhenian crust has detached from the shallow body along the subduction front except in the central part, corresponding to the approximately 100 km-long, northeast-trending segment of southern Calabria (Figure 3.1; see also Neri et al., 2009). In this area, the residual, very slow SE-ward rollback of lithosphere and retreat of the subduction trench generates normal faulting on the shallow structures, in particular on the faults parallel to the Arc (see geostructural data from Monaco and Tortorici, 2000; Figures 3.1 and 8). In Western and Central Sicily (Figures 3.1 and 3.8) the detachment of the subducting slab (already occurred) combined with the persistence of northwest-ward plate convergence has produced a regime of continental collision as evidenced by geophysical and geological evidence (Neri et al., 2005; Billi et al., 2006, 2007). Our study area (indicated by the rectangle in Figure 3.8) is transitional between the extensional domain of south-western Calabria and the compressive domain of Western-Central Sicily. The co-existence of normal faulting and strike-slip mechanisms that we have found in the present study provides new data in support of the above interpretation of the local geodynamics. Normal faulting (with NW-SE preferential direction of extension) is the response to the residual rollback of the subducting slab and south-eastward trench retreat still occurring at very low speed in

47

southern Calabria. In fact, seismogenic normal faulting characterized by this study is more pronounced in the northern portion of the area, e.g. in the sub-area A more favorably oriented with respect to trench retreat representing the source of extension (Figure 3.8). The subducting trench retreat combined with the continuing plate convergence due to northwestward Nubia motion generates a dextral transfer zone across northeastern Sicily and the Messina Straits and, therefore, explains the strike-slip mechanisms found to prevail in the southern part B of our study area (Figure 3.8).

In conclusion, the present application of the CAP method fills a remarkable lack of knowledge existing on the seismogenic mechanisms in the study area and provides a tool for further studies in the whole region. Combined with the findings of previous investigations (Billi et al., 2006, 2007; D'Agostino et al., 2008b: Neri et al., 2009a) the new focal mechanisms furnished by this study, and the corresponding north-to-south change of seismic deformation from normal faulting to strike-slip detected in the Messina Straits area, mark with an increased level of detail the transition between the extensional domain related to subduction trench retreat in southern Calabria and the compressional one due to continental collision in western-central Sicily. These findings furnish additional constraints to the regional geodynamic model and contribute to current investigations of seismotectonics and seismic hazard in the area struck by the strongest Italian earthquake of the past century.
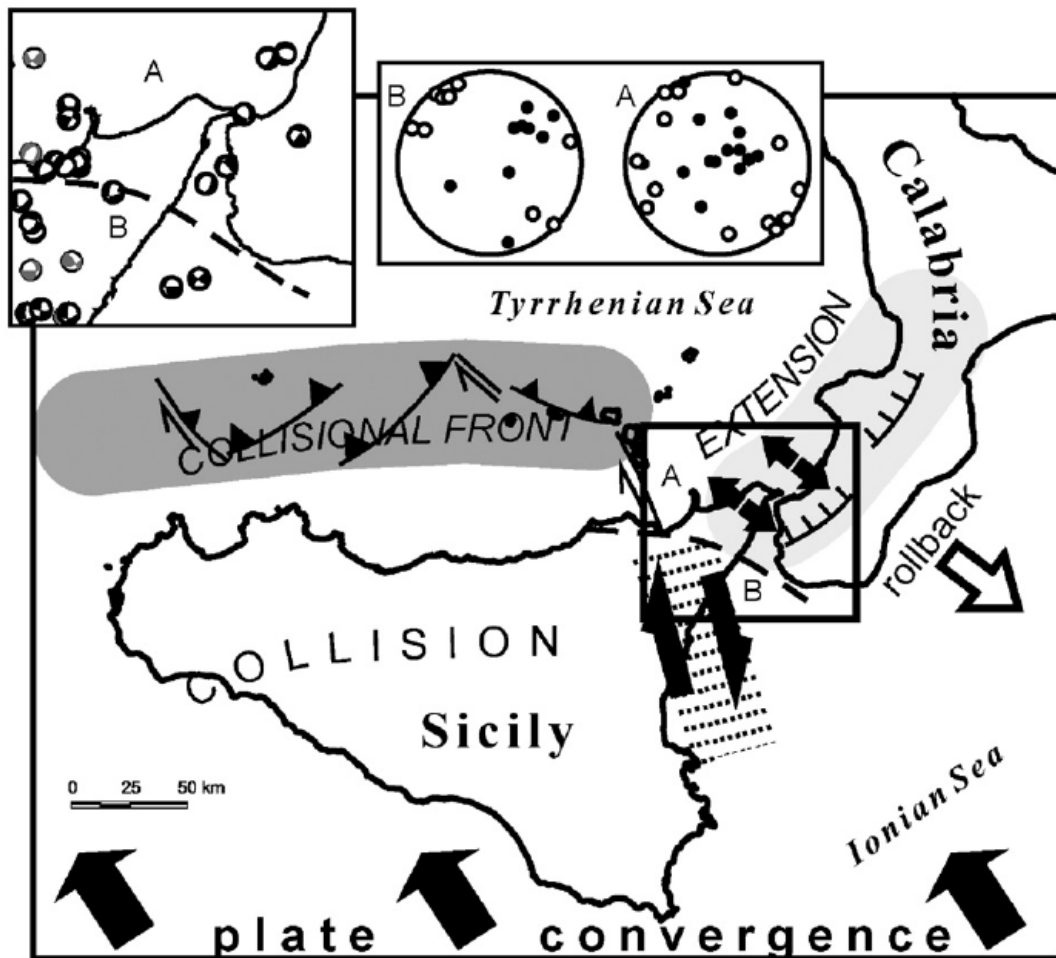
Figure 3.8. Main findings of this work. The focal mechanisms estimated by the CAP method (black) and those taken from the Italian CMT catalog (grey) are shown in the top, together with the polar plots of P and T axes relative to sub-areas A and B, respectively. Black and white dots in the polar plots correspond to P and T axes, respectively. The basic geodynamic information (direction of plate convergence, continental-collision domain, sense of rollback of the subduction slab) has been taken from the literature (Faccenna et al., 1996; Nocquet and Calais, 2004; Billi et al., 2007; Serprelloni et al., 2007). The normal faulting is found to be dominant in sector A (more favorably positioned with respect to the southeast-ward retreat of subduction hinge) and strike-slip components evident in sector B (located across the transfer zone between the extensional and compressional domains) offer a new, more detailed picture of the geodynamic pattern in the transitional area between the extensional domain of southern Calabria and the compressional domain of western-central Sicily.

CHAPTER 4: High-Frequency Earthquake Ground Motion Scaling in Calabria, Southern Italy

Introduction

The Italian peninsula across the Mediterranean Sea is part of the tectonic plate boundary between the Eurasian and the African plates (Fig. 4.1), which continue to move closer to each other. The Calabrian Subduction System results from the fragmentation of formerly continuous Western Mediterranean subduction zone. It developed in a geodynamic setting characterized by N-S convergence between Africa and Eurasia, and by a strong rollback of the slab that induced the opening of back arc extensional basins (Gueguen et al., 1998; Faccenna et al., 2001). From a geodynamic point of view southern Italy is divided into two regions. The Southern part, the so-called Calabrian Arc, is the area where the Ionian lithosphere subducts beneath the Tyrrhenian Sea; the subduction is characterized by an eastward rollback (e.g.,Malinverno and Ryan, 1986; Doglioni et al., 1996). North of the Calabrian Arc there are the so-called Southern Apennines that constitute the accretionary prism of the Adriatic plate subduction (e.g., Doglioni et al., 1996, and references therein). On the basis of geological evidence the hinge of this subduction has been migrating northeastward up to the Pliocene; at present it is thought to be quiescent. The tectonic process of the Southern Apennines is dominated by a NE-SW oriented tensile stress field (Amato and Montone, 1997). The latter generates a series of normal fault systems with longitudinal trend. The Calabrian Arc in its northern portion has an almost North-South trend. It is also apparently characterized by

extensional activity oriented along its axis. An additional seismic feature of the southern Tyrrhenian region is deep earthquake activity along a northwestward dipping Benioff plane (Peterschmitt, 1956: Caputo et al.. 1970: Gasparini et al., 1982: Anderson and Jackson, 1987). Deep seismicity is one of the features which led Barberi et al. (1973) to hypothesize the existence of an active subduction process in the region and to interpret the southern Tyrrhenian area as a back-arc basin.

In fact, the study area is also characterized by an intermediate and deep seismicity clustered and aligned along a narrow (less than 200 km) and steep (about 70°) Wadati-Benioff zone striking NE-SW and dipping toward the northwest down to 500 km of depth (Neri et al., 2009). In the last thirty years about a dozen sub-crustal earthquakes with magnitude greater than 5 occurred in the study area.

Calabria is one of the most active seismic areas in Italy and has a high earthquake hazard. Based on the historical records, the area has suffered intensity X or higher several time in the past (e.g. 1905; 1908 etc; Boschi et al. 1995). The high seismic potential of the area, its population density, the large number of potential building with poor construction criteria, and the inadequacy of the application of the building codes make South Italy an area of high seismic risk where modern hazard studies are needed. The attenuation properties of the crust can be evaluated using the background seismicity as suggested by Chouet et al. (1978) and later demonstrated by Raoof et al. (1999) and Malagnini et al (2000). In other words, it is possible to develop regionally-calibrated attenuation relationships even where strong-motion data are not available. The prediction of the ground shaking for engineering application is often obtained using empirical predictive relationships (Kramer, 1996; Douglas, 2003) which usually are developed by regressing a large number of strong-motion data.
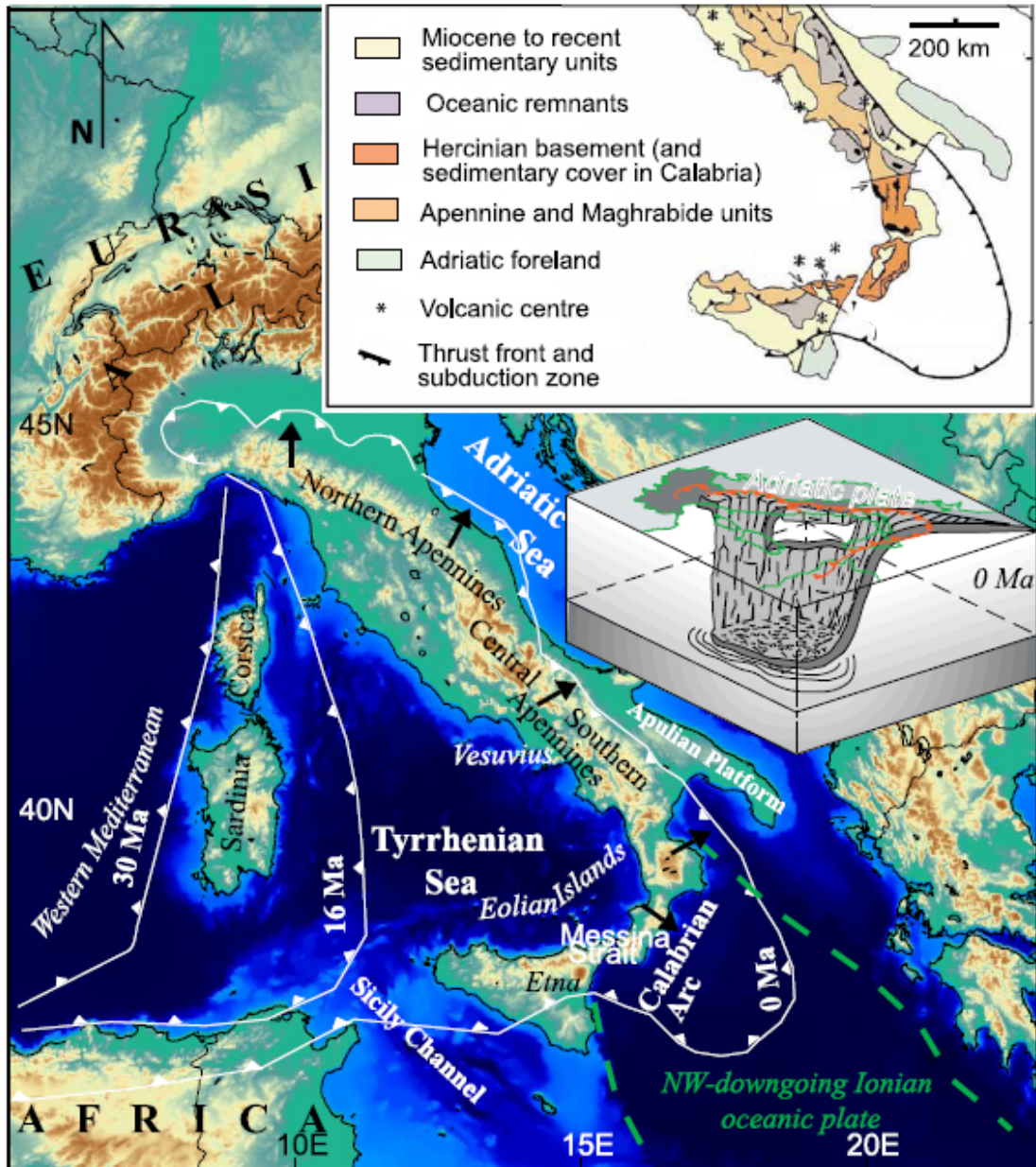
Figure 4.1: Topographic map of Italy and surrounding regions (from Baccheschi et al. 2007). White lines and triangles indicate the position of the thrust front of the western Mediterranean subduction zone at 30, 16 and 0 Ma (Gueguen et al., 1998). The upper inset is a geological map (from Rosenbaum et al., 2002) of the study The lower inset is a schematic block view of the present day subducting lithosphere beneath the Italian region (from Lucente and Speranza 2001)

Modeling is carried out through the use of Random Vibration theory (RVT) (Cartwright and Louguent-Higgins, 1956) to obtain a functional form describing the empirical excitation and the distance-scaling relationships.

In this chapter we use the same methodology for data processing and analysis applied in different parts of the world: California (Raoof et al. 1999; Malagnini et al. 2007), northwestern United States (Herrmann and Dutt, 1999; Jeon and Herrmann 2004; Fatehi, 2008), central United States (Herrmann and Malagnini, 1996), Mexico (Ortega et al., 2003), Greece and Crete (Pino et al., 2001), Italy (Malagnini et al., 2000a,c: 2002; Morasca et al. 2006), Central Europe (Malagnini et al., 2000b, Bay et al, 2003), Turkey (Akinci et al., 2001, 2006), India (Bodin et al., 2004), and China (Xu et al, 2010).

The purpose of this work is to describe quantitatively the regional attenuation and source characteristics for constraining the amplitude of strong motion expected from future earthquakes in the area. The results obtained can be used for engineering design and also suitable for upgrading the most recent hazard map of Italy. The results can also be used to improve tools like ShakeMap® used for emergency response efforts. ShakeMap is a tool used to portray the extent of potentially damaging shaking following an earthquake. It can be used for emergency response, loss estimation, and public information. Istituto Nazionale di Geofisica e Vulcanologia (INGV) runs this tools for Mediterranean earthquakes and in particular for the Italian ones. *ShakeMap* shows the distribution of ground shaking in the region, information critical for emergency management decision making. Having this information in real time will result in lives saved and reduction in property damage. After a damaging earthquake, emergency managers must quickly find answers to important questions such as the localization of the most serious damage, and the areas with the less damage and the identification of the

resources that must be mobilized. In this context a rapid and automatic response for the affected area is really important, which is why the development of an attenuation relationship is a priority.

Data set

The data set analyzed in this work consists of more than 10600 three/component seismograms from about 350 regional earthquakes, recorded between December 2003 and October 2005. The magnitude of the events ranged between M=2.5 and M=4.7, whereas the path lengths ranged between a few kilometers and about 280 km. In this study we used seismic recordings obtained from two different projects: the SAPTEX (Southern APennines Tomography Experiment) (Cimini et al. 2006) and CAT-SCAN (Calabria Apennine Tyrrhenian – Subduction Collision Accretion Network) array; both are temporary experiments. Figure 4.2a shows the distribution of the seismic instruments for the SAPTEX deployment in Southern Italy. The deployment of the portable digital seismographs began at the end of June 2001 and finished at the end of 2005. However 2003 and 2004 were the years with the maximum number of operating seismic stations. The geometry of the array included Calabria, the Aeolian islands and the southern part of the Apulia (Fig. 4.2b). Each station was equipped with a 24 bit RefTek 72A07 digitizer, a three-component Lennartz 3D-5 s sensor (LE-3D/5s) with natural frequency and damping of 0.2 Hz and 0.70, respectively, a hard disk with capacity of 1, 2 or 4 Gb, two 70 Ah-12 V batteries, and two 45-Watt solar panels at sites where electrical power was unavailable. A GPS antenna provided the absolute timing for the system. Digitizers were set to operate in continuous mode recording, with unitary preamplifier gain and sampling rate of 50 sample per second (sps) to record both teleseisms and local/regional

seismicity. For the output a fixed record length of 3600 s (hourly files) and a compressed data format was adopted, which required changing the 1-Gb hard disks about once a month at the noisiest stations (*e.g.*, volcanic sites). At 50 sps, the amount of uncompressed raw data produced by each station is about 52 Mb/day. The frequency response of the LE-3D/5 s extended band sensors (velocity response flat from 0.2 to 40 Hz, decaying with 40 db/decade below the natural frequency) and the chosen sampling rate of 50 sps allowed the recording of weak ground motions in the frequency band between about 0.1 and 20 Hz (Cimini et al., 2006). In this band, the main sources of seismic noise are the sea (marine microseismic band 0.05-1 Hz), the wind and cultural noise. The second set of data comes from the CAT-SCAN (Calabria Apennine Tyrrhenian – Subduction Collision Accretion Network) array (Figure 4.2) deployed in southern Italy from 2004 and 2005. Researchers from the Lamont-Doherty Earth Observatory, the Istituto Nazionale di Geofisica e Vulcanologia and the University of Calabria, deployed almost 40 portable digital broadband seismographs throughout southern Italy. Each station was equipped with Reftek130 or Reftek72A07 data logger and different three-component sensors (CMG40T, CMG3T, L-22, STS2, TRILIUM40, CMG3ESP).

Figures 4.3 and 4.4 show the characteristics of the data set used during this study. They show the source-distance distribution (Fig. 4.3), the number of recordings as a function of magnitude (Fig. 4.4a) and as a function of depth (Fig. 4.4b). In the present study we consider only the shallow events excluding from the original data set those ones having a depth greater than 40 km. Figure 4.5 shows the epicentral distribution of the events used in the present study.

Data processing

The approach we used focuses on the use of seismograms of background seismicity, so strong-motion recordings are not required for our analysis. Details of the data processing technique are provided in Malagnini et al. (2000a, 2002). Each waveform is examined to eliminate those having low signal-to-noise ratio and/or anomalous glitches; every seismogram is corrected for instrument response to ground velocity in m/sec. The P- and S- wave first arrival picks are also reviewed. Each corrected time series is then filtered at 11 different center frequencies (f_c=0.25, 0.40, 0.6, 0.85, 1.25, 1.75, 2.5, 3.5, 5.0, 7.0, 9.0 Hz). A bandpass filter at every f_c is built as the contribution of two 8-poles butterworth filters: a low-pass filter and a high-pass filter with corner frequency, respectively, at $\sqrt{2}\,f_c$ and $1/\sqrt{2}\,f_c$.

A general form of a regression model to characterize the observation is as follows:

$$A_{ij}(f_c)=EXC_i(f_c)+SITE(f_c)+D(r,r_{ref},f_c) \tag{1}$$

where $A_{ij}(f_c)$ represents the logarithm of peak amplitude of ground-motion velocity read on each filtered seismogram recorded at the hypocentral distance r; $EXC_i(f_c)$ is the excitation term representing the motion at a reference distance r_{ref}; $SITE(f_c)$ represents the site term and describes a site modification that is caused by wave propagation effects near the site; and $D(r,r_{ref},f)$ is the crustal propagation term and represents an estimate of the average crustal response for the region. A piece-wise linear function defined by fixed-distance nodes was used to define the $D(r,r_{ref},f)$ functional (Yazd, 1993, Anderson and Lei 1994; Harmsen, 1997).

The number and the spacing between the nodes are selected according to the expected amplitude with distance. In relation (1) we can arrange all our observation in a
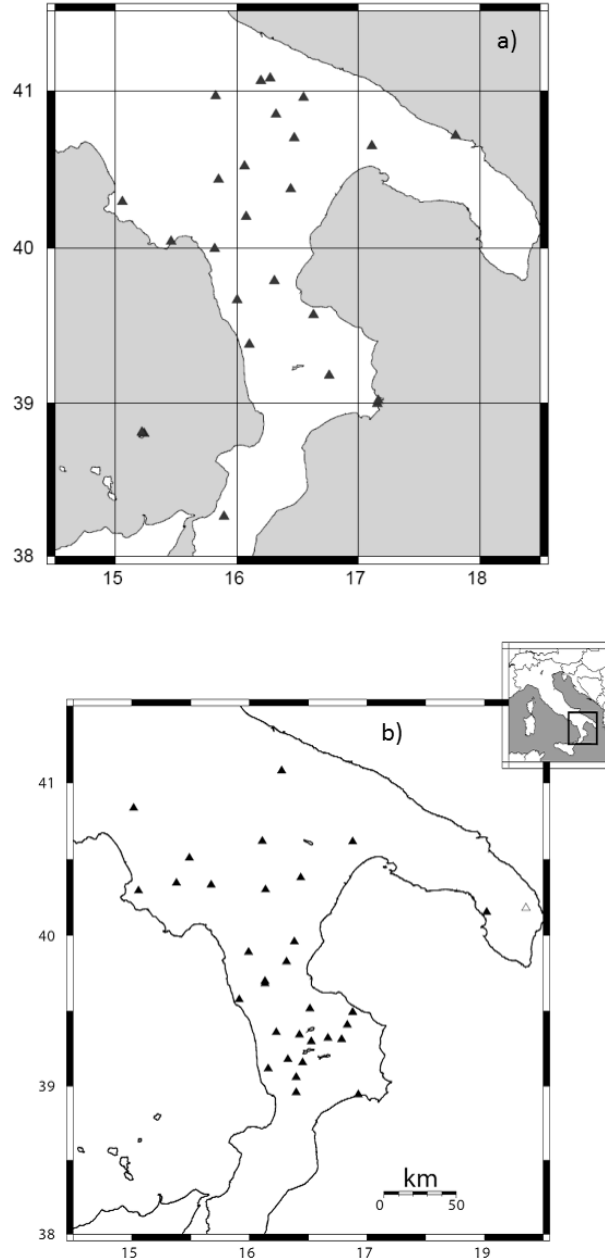
Figure 4.2:a) The figure shows the station distribution for the SAPTEX (Southern APennines Tomography Experiment; Cimini et al. 2006). The SAPTEX array was planned with the main goal of resolving the crustal and upper mantle structure beneath southern Italy. b)The map show the station distribution for the CAT-SCAN (Calabria Apennine Tyrrhenian – Subduction Collision Accretion Network) array deployed from 2004 and 2005 by a joint project among different Institutions: Istituto Nazionale di Geofisica e Vulcanologia, Lamont-Doherty Earth Observatory and the University of Calabria. The black triangles represent the active stations that recorded during the duration of the experiment. Note that two stations, SX11 and SX17 have the same name of two SAPTEX project stations.
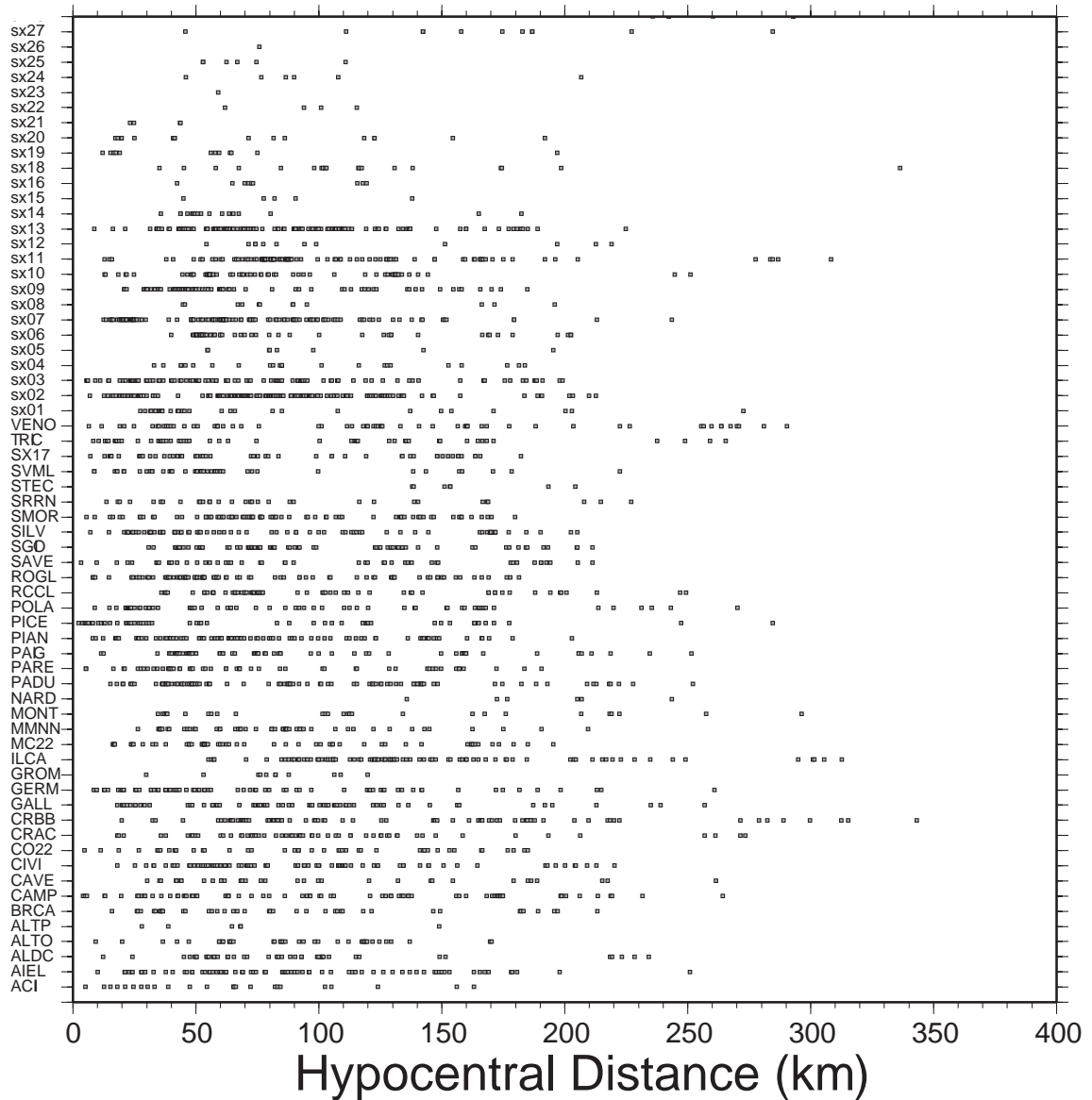
Figure 4.3: Plot of observations at each station as a function of hypocentral distance. Good regression results require overlapping observations between individual stations as well as an overall uniform distribution. The data are sufficient to describe the $D(r=r_{ref},r_{ref},f)$ between 10 and 250 km.

58
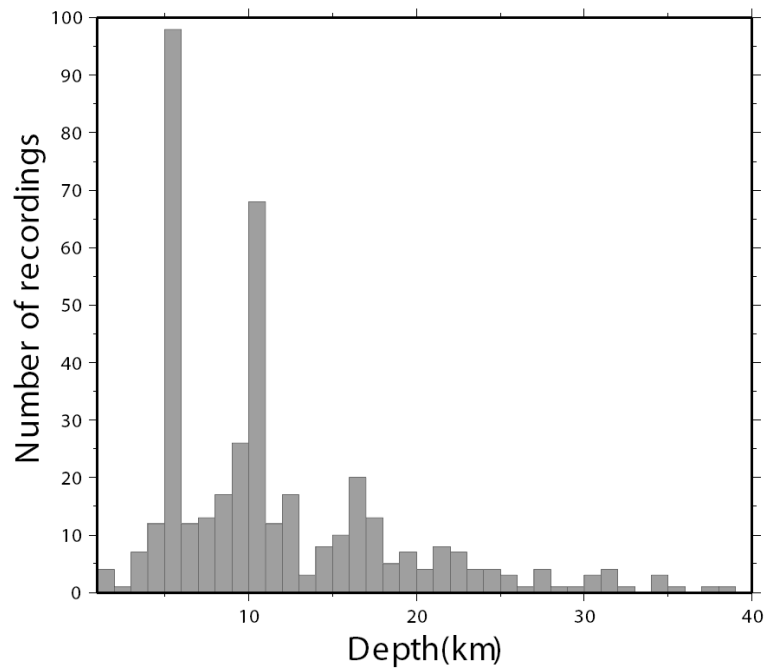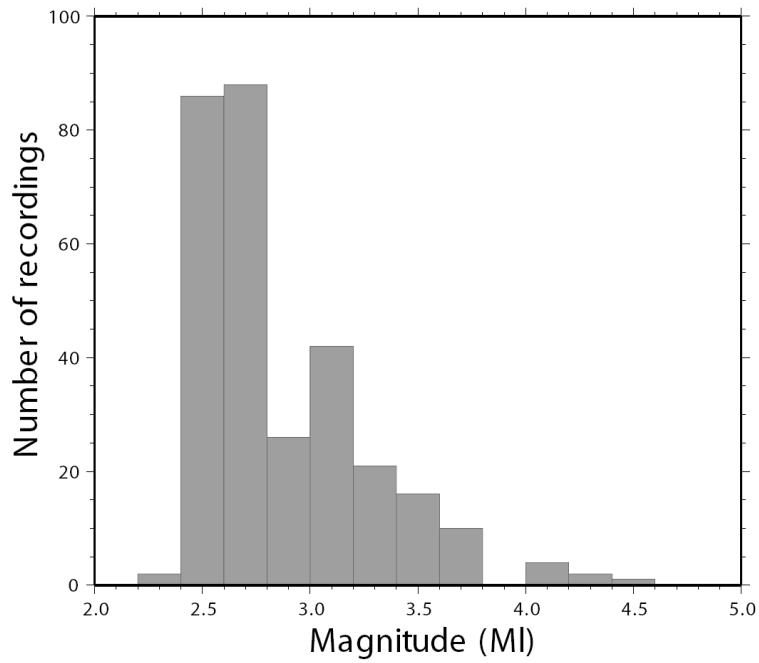
Figure 4.4: a) Number of earthquakes as a function of local magnitude; b) Number of earthquakes as a function of depth. In this study we did not consider the events with depth greater than 40 km. The top figure shows the significant contribution of earthquakes with Ml < 3.5 to the compiled data set.
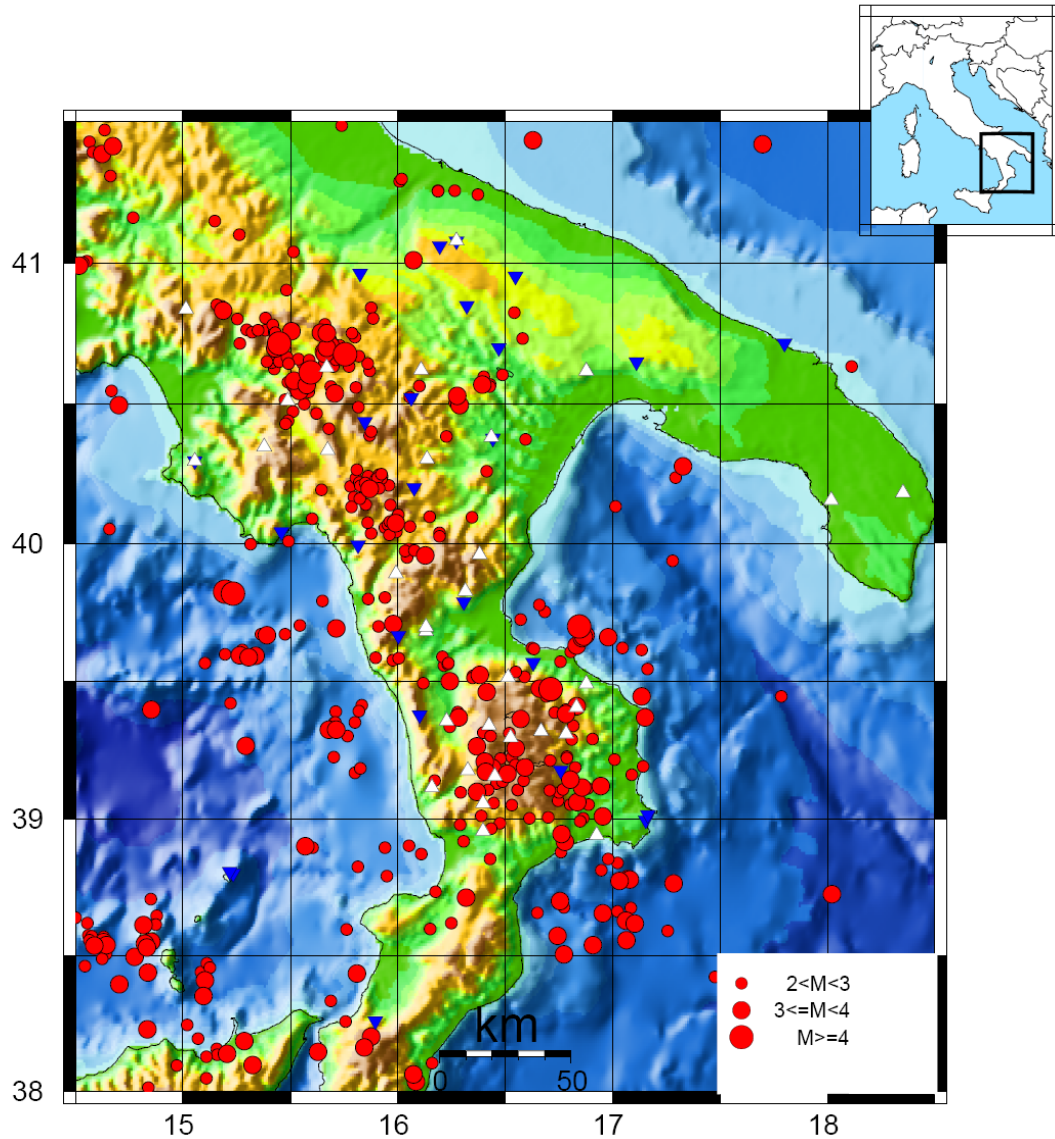
Figure 4.5: The map shows the epicentral distribution of the events (red dots) used in the present study. The size of the dots is proportional to the magnitude of the events. The withe triangles are the stations of the CATSCAN experiment while the blue ones are those belonging to the SAPTEX array.

large matrix and then invert to obtain source, path and site terms. According to

Malagnini et al. (2000a) the regression needs two constraints:

$$D(r=r_{ref}, r_{ref}, f_c)=0 \qquad\qquad (2a)$$

$$\sum SITE(f_c)=0 \qquad\qquad (2b)$$

They are introduced to reduce the degrees of freedom of the system. In this study

we chose r_{ref}=40 km. The first constraint defines the distance where the excitation term

is projected; the effect of the second one is that common site effects are mapped on the

excitation term.

Results

By using (1), we are able to arrange all our observations at frequency f in a large

matrix, and simultaneously invert for source, path (attenuation), and site terms.   The

Fourier velocity spectra of the ground at the site is assumed to be modeled by the

relation that combines source, propagation and site effects:

$$A(f) = C(2\pi f)M_0 s(f)g(r)\exp\left[\frac{-\pi f}{\beta Q(f)}\right]v(f)\exp(-\pi f k_0)$$

where β is the shear-wave velocity, $Q(f)$ is the crustal attenuation , g(r) is the

geometrical spreading (it can be defined on the basis of consideration about the crustal

structure of the region of interest), the parameter k_o is *a* spectral decay factor that

depends on the shallow geology, M_0 is the seismic moment, $v(f)$ is the generic rock site

amplification, like the one used by Atkinson and Silva (1997). s(f) represents the shape

of source displacement spectrum:

$$s(f) = \frac{1}{1 + \left(\dfrac{f}{f_a}\right)^2}$$

where $f_a = 4.9 \; 10^6 \; \beta \; (\Delta\sigma/M_0)^{1/3}$, $\Delta\sigma$ is defined as the stress drop and being C the constant that controls the low-frequency spectral amplitude. The C constant has the following form:

$$C = \frac{RVF}{4\pi\rho\beta^3}$$

where R represents the radiation pattern, V is the portion of total shear-waves energy into horizontal components, F is the effect of the free surface, and ρ represent the density .

Duration of ground-motion is, in general, a function of fault size and of the dispersion of elastic waves along the path between the source and the seismic station (Herrmann, 1985). Our definition of effective duration of ground-motion is the same of that given by (Raoof et al. 1999). For each seismogram the duration is determined and its definition is given as the width of the time window that limits the 5%-75% portion of the seismic energy following the S-wave first arrival. Duration is an input parameter to RVT, and it must be empirically quantified as a function of hypocentral distance at each sampling frequency. Regressions were carried out separately on peak values of filtered ground velocity and on Fourier spectral amplitudes at the same set of selected central frequencies, f. To obtain the filtered time histories around a target frequency f_{0i}, we apply a high-pass butterworth (8-pole, $f_{ci} = f_{0i}/(2)^{1/2}$) followed by a low-pass butterworth (8-pole, $f_{ci} = (2)^{1/2} f_{0i}$). In Figure 4.6 the duration for all the recordings available are reported.

The empirical attenuation term is modeled by using the following functional form:

$$D(r, r_{ref}, f) = \log[g(r)] - \log[g(r_{ref})] - \frac{\pi f (r - r_{ref})}{\beta Q(f)}$$

(3)

where $g(r)$ is the geometrical spreading function, β is the shear-wave velocity (3.5 km/sec) and

$$Q(f) = Q_0 \left(\frac{f}{f_{ref}} \right)^\eta$$

(4)

For the study area, after a trial-and-error modeling of the regression results, we found a model having $Q_0=190$, $\eta=0.65$ and $f_{ref}=1.0Hz$, so that equation (4) becomes

$$Q(f) = 190(f)^{0.65}$$

(5)

for a geometrical spreading of:

$$g(r) = \begin{cases} r^{-1.0} & 1 < r < 100km \\ r^{-0.5} & r > 100km \end{cases}$$

The color curves in Figure 4.7 represent the empirical propagation term at different central frequencies, while the black lines represent the theoretical predictions. As shown in Figure 4.7 the (D_r, r_{ref}) term was forced to zero at the reference distance of 40 km. The distance of 40 km satisfies these conditions, and it is the same in similar studies in other regions, so we can eventually compare the results.

In the equation (1) the term $EXC(f_c, r_{ref})$ represents the ground motion excitation at the Earth's surface at the reference distance. It depends on source excitation as a function of magnitude to the reference distance and the network average site condition.
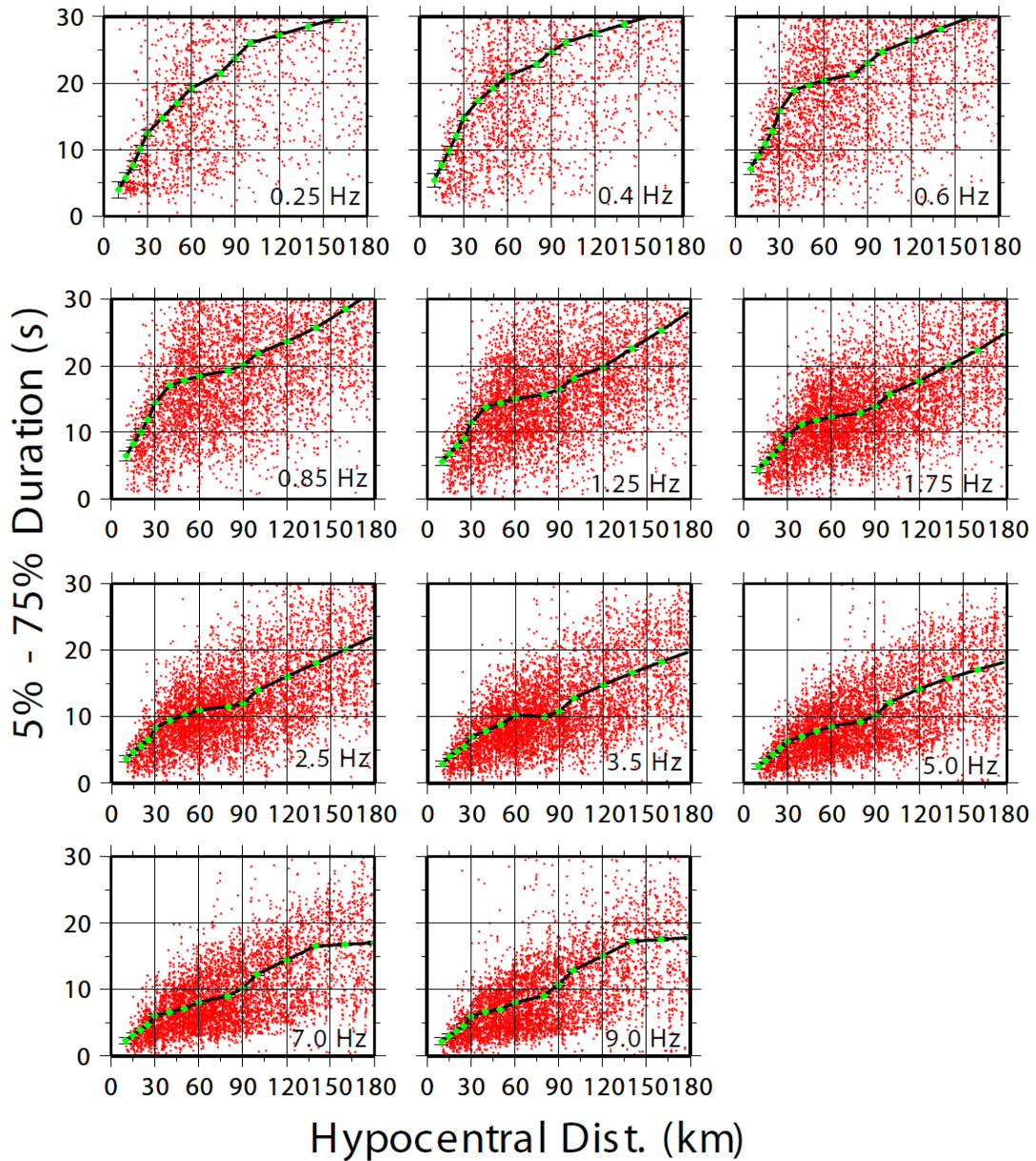
Figure 4.6: Duration of the seismic signals and associated standard errors as a function of hypocentral distances for each frequency studied. Duration is computed on each individual seismogram in the data set as the time windows bracketing the 5%-75% of the integrated seismic energy that follows the S-waves onset. Estimates of the duration computed on each individual recording are indicated by red small dots. Large green diamonds indicate the L1-norm estimates of the duration function that were used for RVT prediction of peak amplitudes. The solid black line is a piecewise linear curved used to link used to link the green diamonds.

The excitation terms, in the Fourier domain, are modeled by using the following functional form:

$$exc(f, r_{ref}) = C(2\pi f)M_0 s(f)g(r_{ref})\exp\left[-\frac{\pi r_{ref}}{\beta Q(f)}\right]v(f)\exp(-\pi f k_0)$$

(6)

including the crustal attenuation , $Q(f)$, the geometrical spreading $g(r=r_{ref})$ we modeled; the parameter k_o and the generic rock site amplification $v(f)$, like the one used by Atkinson and Silva (1997).

The shape of source displacement spectrum is:

$$s(f) = \frac{1}{1+\left(\dfrac{f}{f_a}\right)^2}$$

(7)

where $f_a = 4.9\ 10^6\ \beta\ (\varDelta\sigma/M_0)^{1/3}$ with

$$C = \frac{RVF}{4\pi\rho\beta^3}$$

(8)

where R=0.80; V=0.707; F=2.0; ρ=2.8g/cm3; β=3.5km/s.

For our study area we found $\Delta\sigma$ =25MPa and k_0=0.040s;

The term $\exp(-\pi k_0 f)$ is used to fit the spectral shape of the excitation function at high frequencies. The source parameters, $\Delta\sigma$ and k_0, are determined in a trial-and-error procedure. In order to properly calibrate the $\Delta\sigma$, and k_0 we constrained the scaling relations by using moment magnitudes derived from regional moment tensor inversion described in Chapter 2 and Chapter 3. Our model does well in fitting the scaling relationship for the largest earthquakes in the dataset. Figure 4.8 compares the predicted excitation terms to the observed.
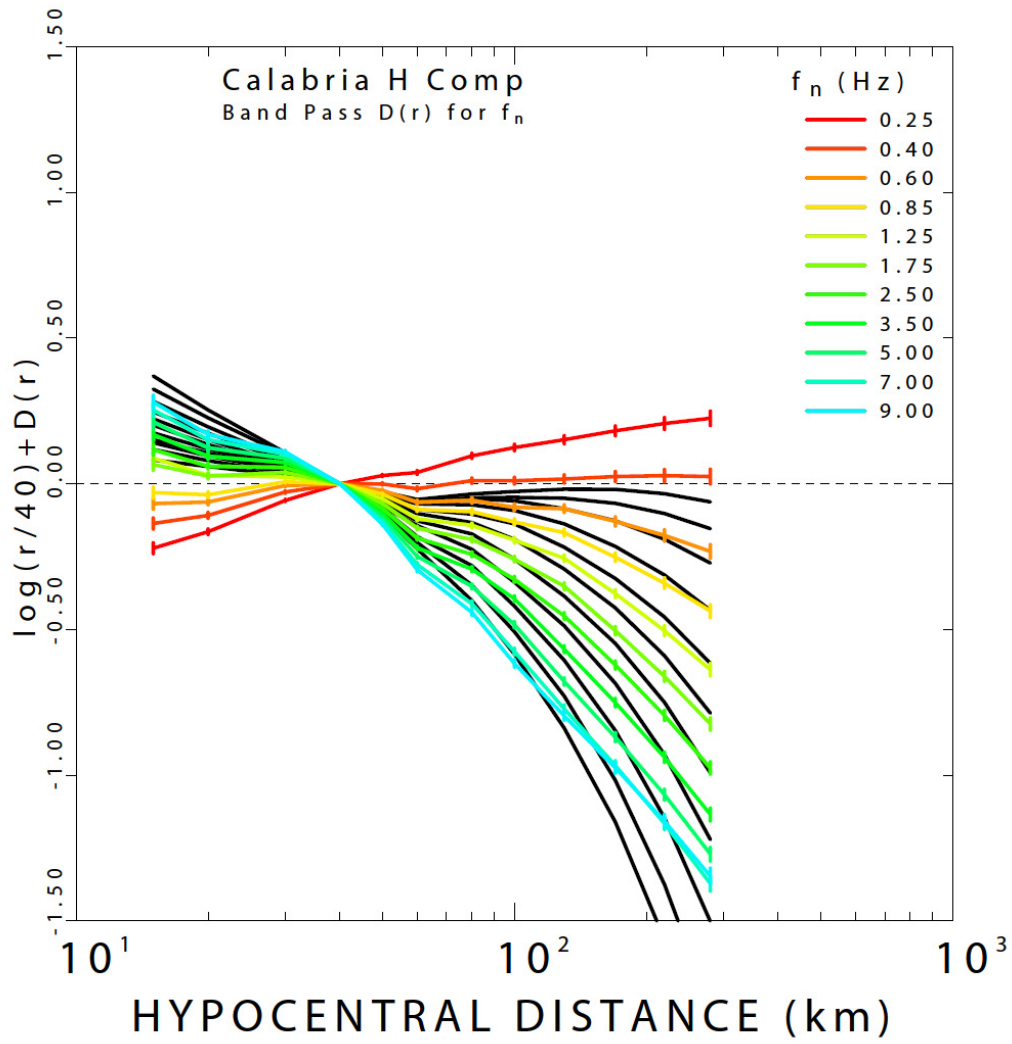
Figure 4.7: Colored curves are the empirical propagation term at the central frequencies of 0.25, 0.40, 0.60, 0.85, 1.25, 1.75, 2.50, 3.50, 5.00, 7.00, 9.00 Hz, resulting from the regression of the peak value of the data set waveforms. The attenuation term was forced to be zero at the reference distance of 40 km. Black lines are our theoretical predictions, which were obtained for each central frequency through the use of RVT. These predictions are in good agreement with observation for f_c greater or equal to 0.6 Hz

Figure 4.9 shows the influence of κ_0 on the high-frequency amplitudes of small events, and the tradeoff between κ_0 and the stress parameter for large earthquakes. A tradeoff exists between the stress parameter and κ_0. κ_0 governs the high-frequency decay of the theoretical excitation terms, as well as the $\Delta\sigma$, which affects the radiated spectra beyond their corner frequencies. In the frequency band of our interest, however, the effect of the stress parameter is strongest for the largest earthquakes, while κ_0 completely controls the behavior of the small earthquakes at high frequency. For this reason, it is necessary first to find estimates of the high frequency parameter, k_0, by examining the spectra of small events, and than, knowing k_0, of the stress parameter of the larger events.

During the inversion the sum of all site terms is forced to zero for each frequency. This constraint represents what would be recorded at the reference hypocentral distance by the average network site. The site term measures the deviation from the mean seismic spectra for each station, which is due to the physical properties of the shallow geology at the recording site. Comparisons can be done among different Italian regions in which this kind of studies have been conducted. It has been found that the western Alps (Morasca *et al.*, 2006), eastern Alps (Malagnini *et al.*, 2002), Southern Appenines, central Italy (Malagnini et al 2000a) and eastern Sicily (Scognaniglio et al 2005) have different characteristics for the attenuation parameters. For instance the crustal wave propagation in eastern Sicily is more efficient than in other Italian regions. The combination of the geometrical spreading function and the parameter $Q(f)$ is strictly related to the crustal characteristics. Figure 4.10 reports the attenuation values for each region for a visual comparison.
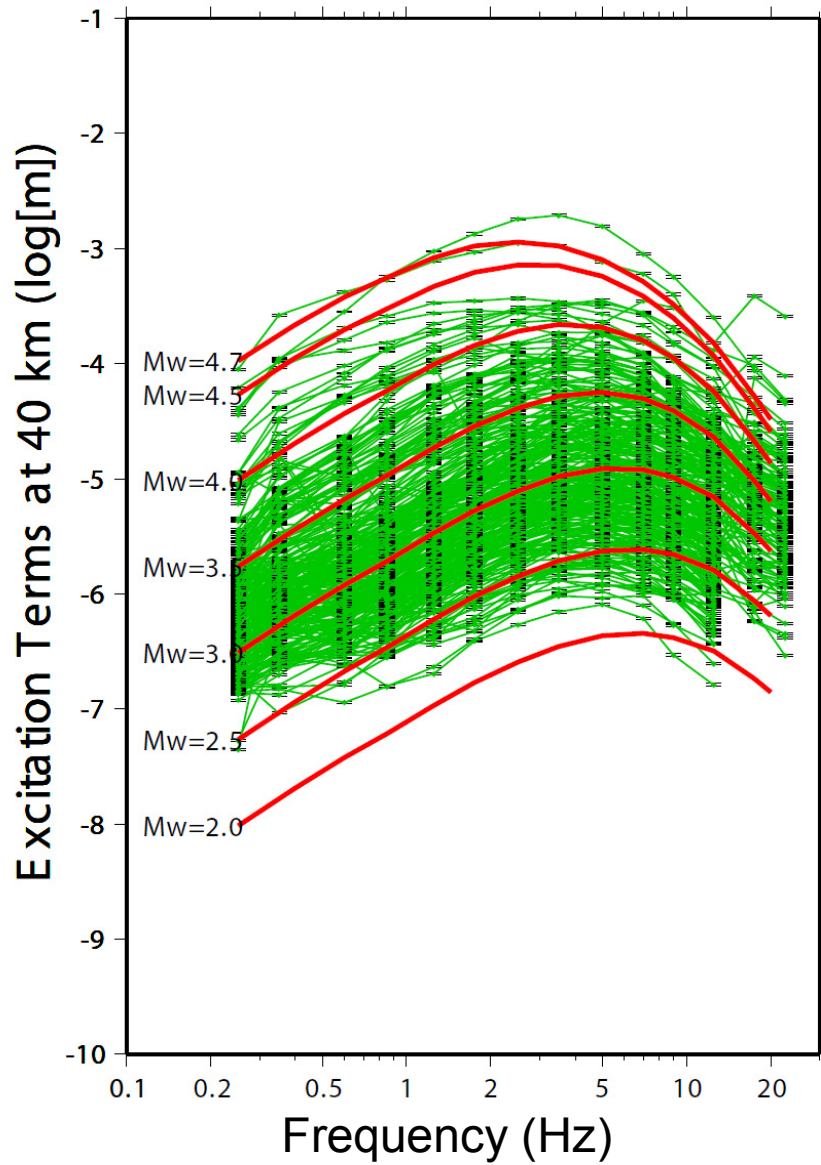
Figure 4.8: Estimated excitation terms (in the time domain) of the peak-filtered velocity at the reference distance of 40 km. Red lines are the theoretical prediction performed using the RVT and the source parameters in Table 3.1. Green lines are the observed data.
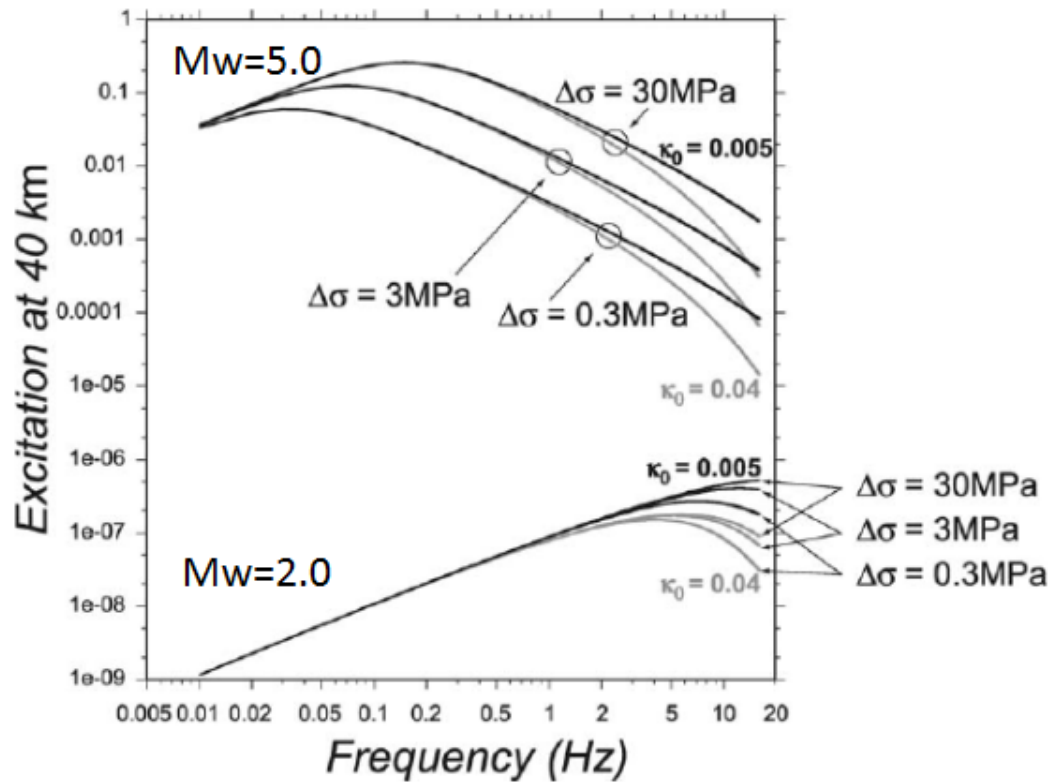
Figure 4.9: Demonstration of tradeoff existing between the stress parameter and k_0. We show velocity spectra at two reference magnitudes (*M*w 2.0 and *M*w 5.0), derived by using the Brune spectral model with three different values for the stress parameter, and for two different values of the high-frequency attenuation parameter k_0. Spectra are propagated to the reference distance of 40 km using the propagation characteristics of the crust. The two values of k_0 generically refer to rock sites (0.005 sec), and to moderately attenuating sites (0.04 sec). The three values of stress parameter are within a normal range of variability.

As an example, Figure 4.11 shows the comparison of simulated PGA and PGV as a function of distance for moment magnitude of 5 and 6 obtained using the SMSIM programs (Boore, 2003; http://www.daveboore.com/software_online.htm). It is clear how the predictions of the ground motion are different in the different areas, therefore the regional calibration of attenuation properties and source scaling is a really important task.

Conclusion

We obtained quantitative evaluation of the southern Italy ground-motion parameters in order to decrease the uncertainties for seismic hazard. Our results are obtained through regressions of more than 10,000 bandpassed waveforms. We modeled the crustal propagation features and the geometrical spreading as the following:

$$Q(f) = 190(f)^{0.65}$$

and

$$g(r) = \begin{cases} r^{-1.0} & 1 < r < 100km \\ r^{-0.5} & r > 100km \end{cases}$$

While a trade-off exists between Q_0 and $g(r)$, on the contrary the parameter η is controlled by the frequency dependent variation of the D(r) at a fixed distance.

By using the same approach used in this study, other authors have found different Q(f) relations for other Italian regions. In the western Alps Q(f)=310 (f)$^{0.2}$ (Morasca et al., 2006), while in the eastern Alps Q(f)=260(f)$^{0.55}$ (Malagnini et al., 2002). Lower Q-values were found in the Apennine area (Q(f)=140 (f)$^{0.25}$; Malagnini et al. 2010). In
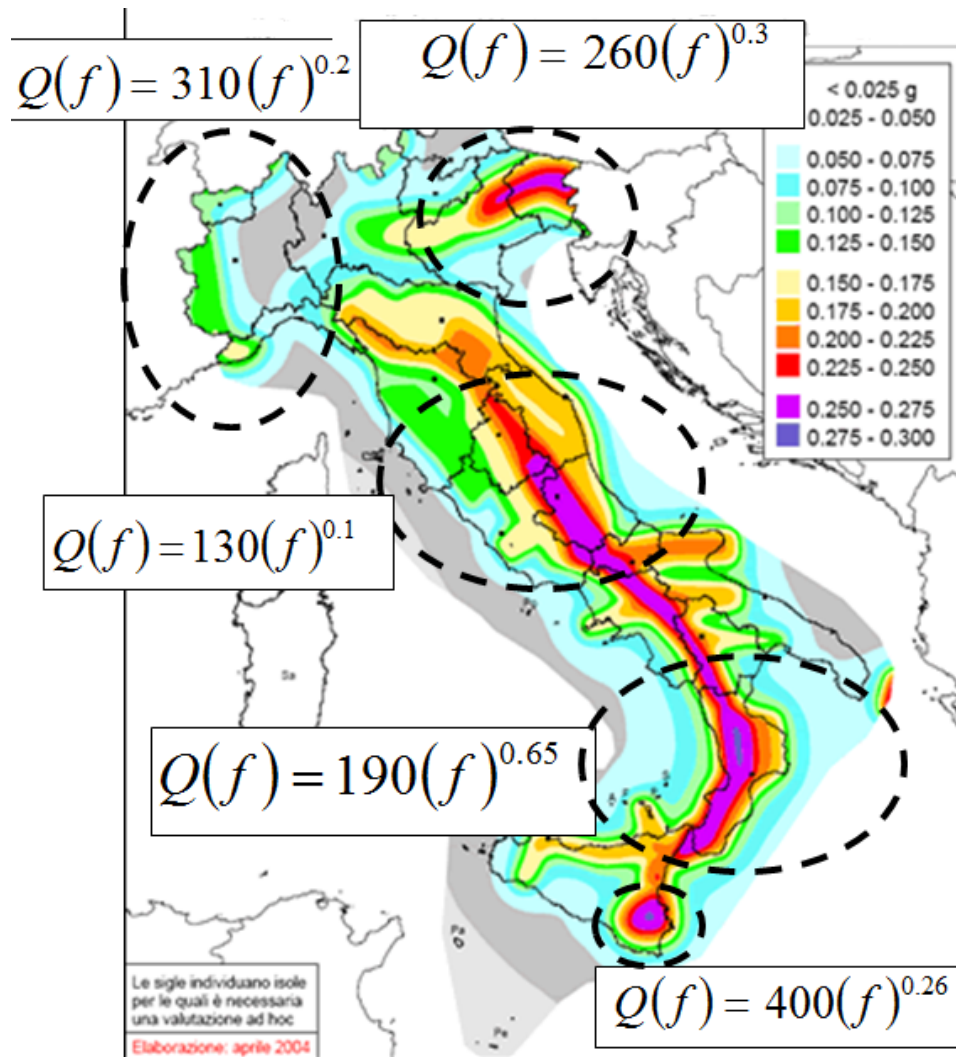
Figure 4.10: Attenuation values for different Italian regions: western Alps (Morasca *et al.*, 2006), eastern Alps (Malagnini *et al.*, 2002), Southern Appenines (this study), central Italy (Malagnini et al 2000a) and eastern Sicily (Scognaniglio et al 2005). The values are plotted on the Italian seismic hazrd map (http://zonesismiche.mi.ingv.it; "Mappa di pericolosità sismica del territorio nazionale").

71
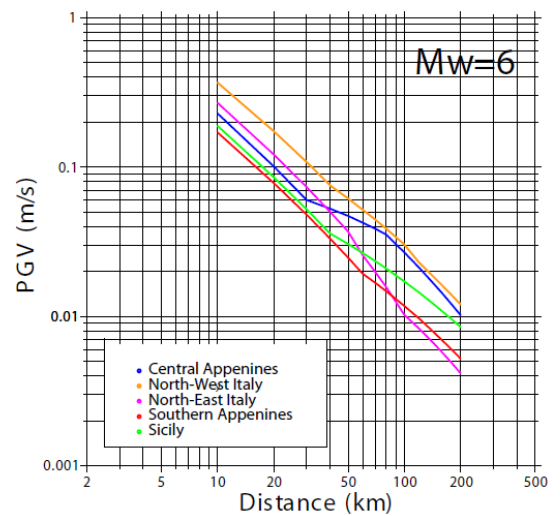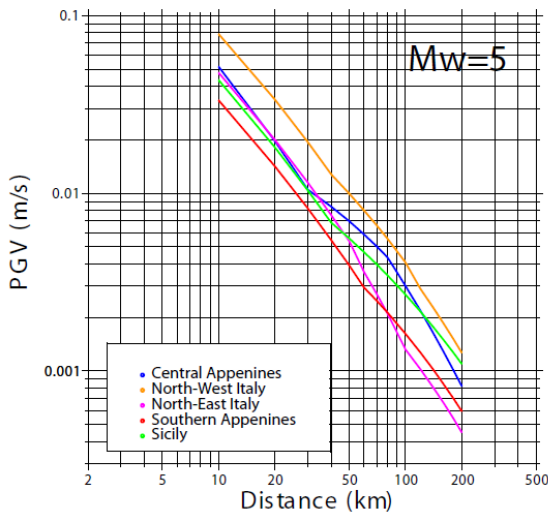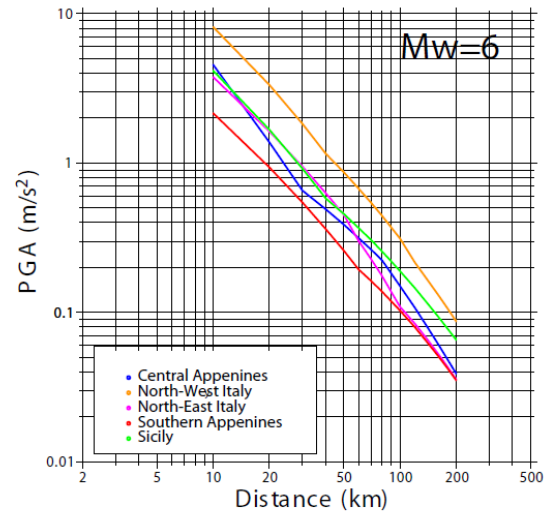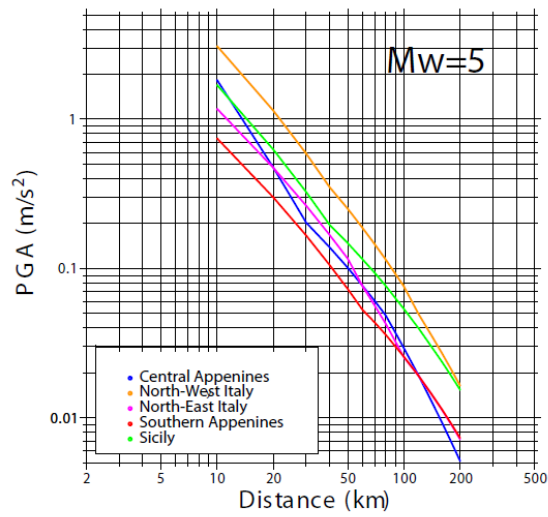
Figure 4.11: Comparison of different estimates of PGA and PGV for different Italian regions as a function of moment magnitude Mw

eastern Sicily Scognamiglio et al. (2005) found $Q(f)=400(f)^{0.26}$. These differences are linked with the different geologic and tectonic settings of the areas and they play a key role in hazard studies.

We reproduced the seismic spectra at the reference distance using a Brune spectral model with a stress drop 250 bar, a generic rock site amplification factor $v(f)=1.0$, and the high-frequency cutoff parameter $k_0=0.04$sec.

CHAPTER 5: An Attenuation Relationship for Southern Italy

Introduction

Since Italy is a seismically active region it is really important to define an attenuation relation for the area because of increasing exposure and vulnerability to the effects of earthquakes. The estimation of ground motion for a particular region and also site-specific investigation is essential for the design of engineered structures. Seismic hazard assessment requires a strong motion attenuation relationship (Kramer, 1996) to estimate ground motions from specific parameters characterizing the nature of earthquake source, the distortion effect of the shallow geology and the effects of the transmitting medium on the seismic waves. A number of such relationships have been developed for many regions of the world (Ambraseys et al., 1996; Boore and Joyner, 1991; Toro and McGuire, 1987; Atkinson and Boore, 1995; Campbell, 1997; Sadigh, 1997), mainly by regressing strong-motion data. These studies have shown that the ground motion levels can differ significantly in different tectonic regimes, for example depending on whether stresses are extensional or compressional.

In the previous chapter we defined a regional calibrated attenuation model for the crust and the source parameters that can be used as input for stochastic finite fault simulations. In particular in this chapter we describe predictive relationships for the ground motion in the studied area by regressing the peak ground acceleration (PGA) from our dataset augmented with some simulations of large magnitude earthquakes that are missed in our data set since the study is characterized by low magnitude events area in the last 30 years.

D'Amico et al . (2010d) showed that regional propagation parameters, obtained from independent weak-motion database, may be used for evaluation of ground motion parameters for earthquakes of magnitude up to 7.6. Consequently, we found it reasonable to simulate the PGA values of large earthquakes in order to have a complete data-set for regression. In fact, in our original data-base there are no observations of PGA values for large earthquakes (e.g. M > 5).

Estimates of expected ground motion at a given distance from an earthquake of a given magnitude are fundamental inputs to earthquake hazard assessments. The determination of seismic design criteria for engineered structures depends upon reproducible estimates of the expected lifetime of the structures. Different researchers use different "source to site" distance measures. For instance, r_{jb} (the Boore and Joyner distance) is the closest horizontal distance to the vertical projection of the rupture; r_{rup} is the closest distance to the rupture surface; r_{seis} represents the closest distance to the seismogenic rupture surface (Marone and Scholz, 1998); r_{epi} and r_{hypo} are the epicentral an the hypocentral distances respectively. There are also several site classification schemes used in different papers ranging from qualitative description of the near surface material to very quantitative definitions based on shear wave velocities.

Different tectonic environments give rise to different ground motion attenuation relationship. Regardless of the tectonic regime, rupture directivity also may affect ground motion attenuation relationship (Somerville et al., 1997). For larger events, a special problem arises, at short distances, with the source-to-site distance measure, because the distance metrics based on a point-source model are no longer appropriate. As a consequence, different attenuation relations differ in the distance metric that they use. In addition to being a source of confusion, this causes problems when trying to

quantitatively compare or combine different ground-motion models. For these reasons, Scherbaum et al. (2004) used well established scaling laws to determine explicit distance conversion relations using regression analysis on simulated data. They demonstrate that, for all practical purposes, most popular distance metrics can be related to the Joyner-Boore distance using models based on gamma distributions to express the shape of some "residual function".

Predicting ground motion

In order to predict the expected ground motion parameters in terms of peak ground acceleration (PGA) and peak ground velocity (PGV) as a function of distance and magnitude we used the latest version of EXSIM program (Boore, 2010) originally developed by Motazedian and Atkinson (2005). It is a modified version of the FINSIM (finite fault simulation) code developed by Beresnev and Atkinson (1998).

The simulations, for moment magnitude from 4 to 7 (with an incremental steps of 0.5), were carried out by using the regional propagation parameters obtained in Chapter 4 and rectangular faults having length and width proportional to the moment magnitude according the relationship proposed by Wells and Coppersmith (1994). We selected about 20 faults in the southern Apennines from the Database of Individual Seismogenic Sources (DISS – Basili et al. 2008) managed by the Istituto Nazionale di Geofisica e Vulcanologia (Fig 5.1, Table 5.1). The Database contains the results of the investigations of the active tectonics in Italy during the past 20 years and highlights the results of several decades of research work (www.ingv.it/DISS). Each "Individual Seismogenic Source" (Fig. 5.2) is defined by geological and geophysical data (see Table 5.1) and is characterized by a full set of geometric (strike, dip, length, width and depth),

kinematic (rake), and seismological parameters (single event displacement, magnitude, slip rate, recurrence interval).

Each fault was assigned a random slip distribution. Beresnev and Atkinson (2002) showed that only the gross features of slip distribution on a fault plane that do not diverge significantly from the average value of slip may be reliable; all other complexities could be extremely uncertain. We thus find it reasonable to assume a random slip distribution in order to simulate a wide range of ground motion parameters due to the activation of several faults. During each simulation the fault plane is discretized into several subfaults. Site effects at a specific station are very important and may be used for engineering purpose to define the regional predictive low and the seismic hazard. When the site contribution to the ground shaking is known it could be removed from records in order to determine a spectral model available to predict the regional ground shaking, especially if the site response shows important signal distortion due to the local geology. A generalized site response concept is useful to create detailed shaking map for a region where the different outcropping lithologies are known. The generic site response represents the average response expected for a site with specific superficial geologic characteristics, and without important distortion effects due to the superficial geology. The knowledge of generic site response of different soil kinds allows to produce detailed shaking maps for large regions, where it is possible to detail the superficial geology for the different kind of lithologies. Boore and Joyner (1997) determined the site response average amplification for two different kind of rock largely common in United States, characterizing the sites on the basis of Vs30, the average shear-wave velocity in the upper 30 meters.
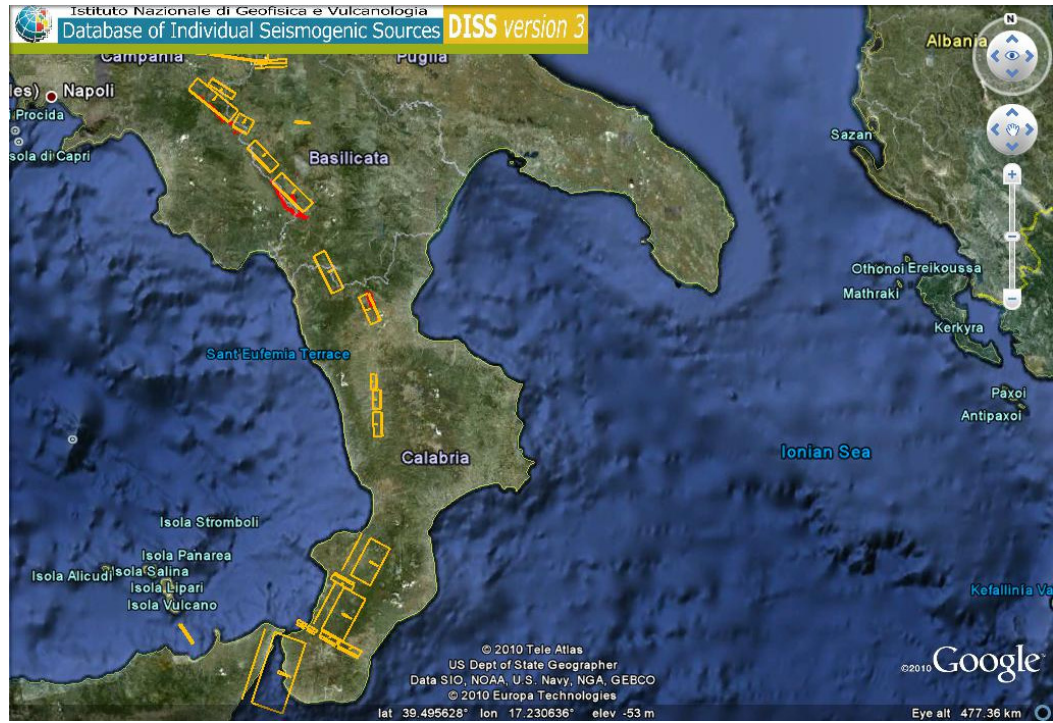
Figure 5.1: Location of the active faults reported in Table 5.1 and used for the simulations.

Table 5.1: Principal types of data used to characterize the parameters of seismogenic sources

Fault Name	LAT	LONG	LENGTH (km)	WIDTH (km)	MIN DEPTH (km)	MAX DEPTH (km)	STRIKE	DIP	RAKE	MAX Mw
Agri_Valley	40.35	15.78	23	13.5	1.00	12.70	316	60	270	6.5
Castrovillari	39.78	16.24	15.6	10.3	1.00	9.90	158	60	270	6.2
Melandro_Pergola	40.53	15.60	17.9	11.3	1.00	10.80	317	60	270	6.3
Upper_Mesima_Basin	38.59	16.19	22	13.5	3.00	9.80	30	30	270	6.6
Gioia_Tauro_Plain	38.64	16.02	25	15	3.00	10.50	30	30	270	6.6
Messina_Strait	38.06	15.61	40	20	3.00	12.70	20	29	270	7
Mercure_Basin	39.97	15.99	22	12.7	1.00	12.00	335	60	270	6.4
Aspromonte_NW	38.27	15.82	5	4.5	3.00	7.20	300	70	270	5.3
Sicilia_Offshore	38.30	15.76	5	4.5	3.00	7.20	300	70	225	5.3
Aspromonte_NE	38.23	15.39	10	7.5	3.00	10.00	300	70	225	5.8
Aspromonte_E	38.18	16.05	12.5	8.8	3.00	11.30	300	70	225	6
Nicotera_Rosarno	38.49	16.02	12.5	8.8	2.00	11.30	120	70	315	6
Patti_Gulf	38.26	15.05	12.1	8.6	1.50	10.00	147	83	180	6.2
Colliano	40.80	15.29	28	15	1.00	14.00	310	60	270	6.8
San_Gregorio_Magno	40.68	15.48	9	15	1.00	14.00	300	60	270	6.2
Pescopagano	40.85	15.35	15	10	1.00	10.40	124	70	270	6.2
Melfi	40.98	15.66	17.2	11	12.00	22.80	269	80	180	6.4
Potenza	40.68	15.85	7.9	6.2	14.80	21.00	95	88	175	5.8
Luzzi	39.44	16.25	7.6	6.3	1.00	6.70	180	65	270	5.8
Castiglione_Cosentino	39.35	16.26	10	7.5	1.00	7.50	180	60	270	6
Dipignano	39.24	16.26	12.7	8.9	1.00	8.90	180	62	270	6.2
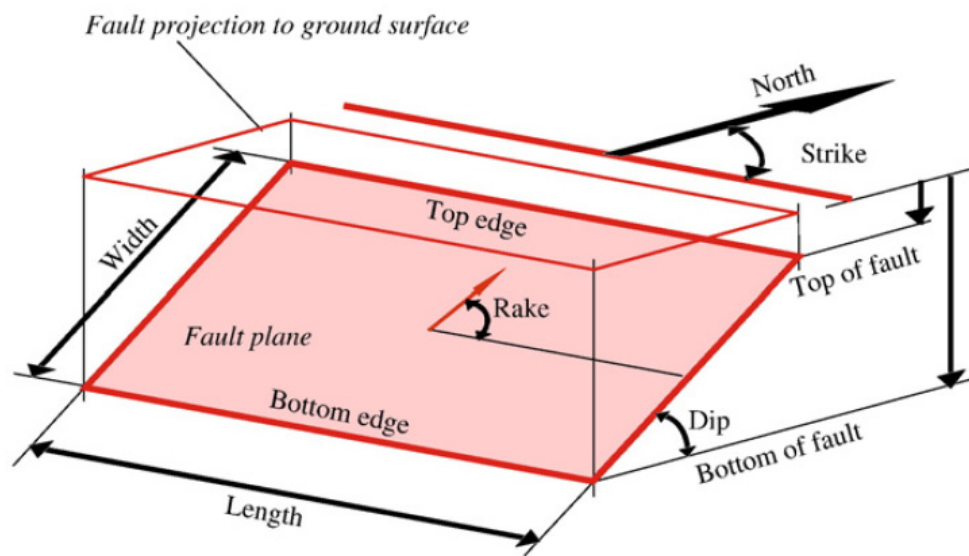
Figure 5.2: Schematic representation of an Individual Seismogenic Source and its characteristics (from Basili et al. 2008).

The first one is represented by very hard rock Vs30 =2900 m/s, typically present in eastern North America. The second one is represented by rocks present in coast California, for which Vs30=620 m/s. In this study in order to consider different site condition we will refer to the NEHRP classification (BSSC, 1994). The data set used for the regression is reported in Figure 5.3.

Methodology

We employ two-stage regression procedure (Joyner and Boore, 1981, 1993; Ambraseys et al., 1996; Boore et al., 1997). We fit the simulated strong-motion data by multiple linear regressions using the equation (modified after Joyner and Boore, 1981 and Ambraseys et al., 1996):

$$\log y = \sum_{i=1}^{N} a_i E_i + br + c \log r + dS + \varepsilon \qquad (5.1)$$

where:

$E_i = 1$ for earthquake i

$E_i = 0$ otherwise

$S = 1$ for soft rock sites

$S = 0$ for generic rock sites

$r = (d^2 + h^2)^{1/2}$

$\varepsilon = $ residuals

and y is peak horizontal acceleration (in cm/s^2), N is the number of earthquakes in the data sample, and d is the closest horizontal distance site to the vertical projection of the fault rupture (in km). Values a_i, b and c are coefficients determined by the first linear regression for a chosen

81
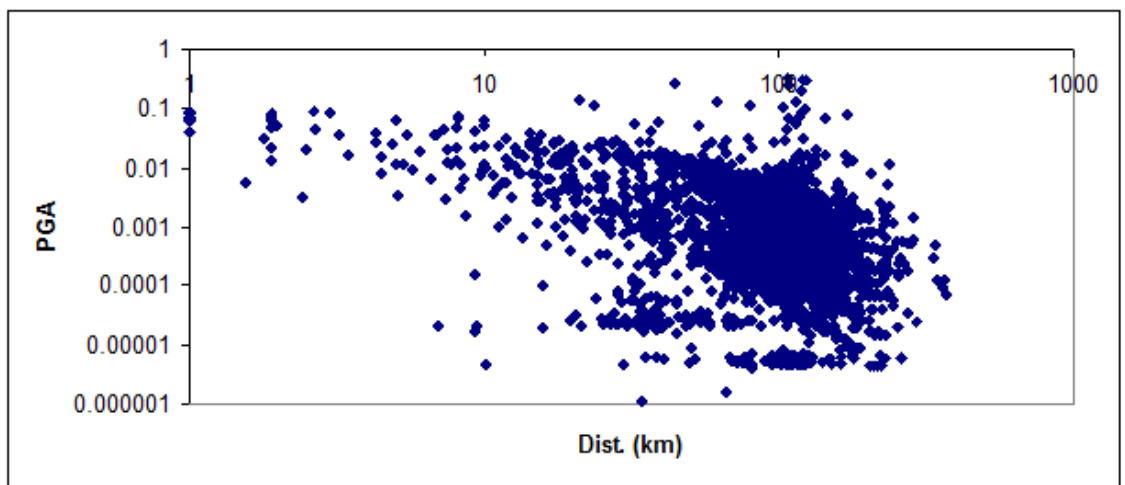
Figure 5.3: Data set used for the regression

value of h, and h is determined by a simple grid-search procedure to minimize the sum of squares of the residuals. Since, our data set does not have stations located on hard rock site, we obtained the coefficients only for stiff and soft soil sites. In this equation, $\varepsilon=\sigma P$; σ is the standard deviation of the residuals. The value of P is based on the assumption that the prediction errors are normally distributed and P=0.84 confidence level for $\pm 1\sigma$ values. By using E_i and S, we divided the data into classes; this is a well-known technique in regression analysis (Draper and Smith, 1966; Weisberg, 1980; Joyner and Boore, 1981; Boore et al., 1997). The procedure decouples the determination of magnitude dependence from the determination of distance dependence. If the regression analysis were done in terms of magnitude and distance simultaneously, errors in measuring magnitude would affect the distance coefficients obtained from the regression. In this approach, each earthquake has the same weight in determining magnitude dependence and each recording has the same weight in determining distance dependence (Joyner and Boore, 1981). The coefficient, h, is sometimes referred to as a "fictitious" depth measure (Boore et al., 1997) implying that interpretation of h is not clear and its value is estimated as part of the regression. Abrahamson and Silva (1997) have reported that h yields a marginally better fit to the data at short distances. In this study, the distance measure, d, is the closest horizontal distance to the vertical projection of the rupture. In cases that we could not describe the rupture surface, especially for small earthquakes, we used epicentral distance instead of this measure. The parameter h is introduced to allow for the fact that the source point may not be the closest point on the rupture. In fact, the value obtained for h incorporates all the factors that tend to limit or reduce motion near the source, including any tendency for the peak horizontal

acceleration to be limited by the finite strength of near-surface materials. The value of h also incorporates any factors that tend to enhance the motion near the source, especially, directivity effect (Joyner and Boore, 1981). After the a_i values are obtained by the first linear regression, they were used to find, by least squares, a first or second order polynomial representing the magnitude dependence:

$$a_i = \alpha + \beta M_i + \gamma M_i^2 \qquad (5.2)$$

Here, M is moment magnitude α, β, and γ are the coefficients determined by the second linear regression. To estimate σ, the total standard error after two regressions, we assumed that magnitude and distance parameters do not have any correlation between each other. By using convergence theorem, we can write following equation:

$$\sigma = \sqrt{\sigma_1^2 + \sigma_2^2} \qquad (5.3)$$

where, σ_1 is the standard deviation of the residuals from the regression described by equation (5.1) and σ_2 is the standard deviation of the residuals from the regression described by equation (5.2).

After the regression of our PGA dataset we obtained for the following form the coefficients.

α=-3.87;

β=1.22;

b=0.03;

c=-1.73;

d=0.02
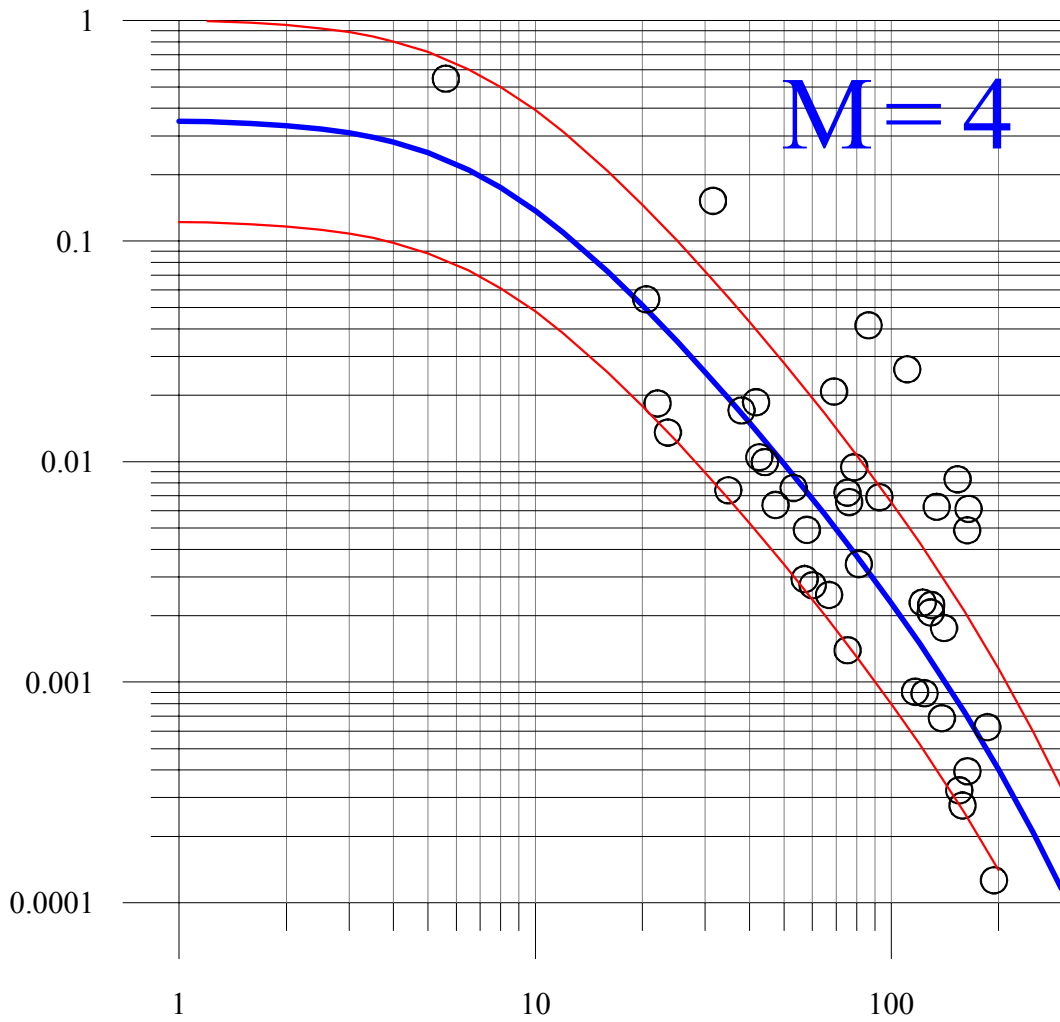
Figure 5.4: Predicted PGA (cm/s^2) values as a function of distance (in km) for M=4.0 event (blue line) and ±1σ values (red lines). Observed PGA values for M=4.0 events (circles). The observed PGA data were obtained through the differentiation of the ground velocity waveform and taking the peak values of them.

Figure 5.4 shows an example for M=4 using the coefficient obtained from the regression. The figure shows the predicted peak ground acceleration as a function of distance for an earthquake having magnitude equal to four (blue line); the two thin red lines represent the "one standard deviation" bounds. The circles are the observed PGA values coming from the events having M=4 present in our data set. It is possible to notice that some of the observed data are out of the "standard deviation limits", this is due to the possible site effect that tend to amplify the peak ground acceleration at certain sites. Figure 5.shows predicted PGA as a function of magnitude and distance by using the models developed in this study. The predictions are given for moment magnitude 4, 5, 6, and 7.

As an example we apply stochastic strong ground motion simulations for finite faults (Boore, 2010; Motazedian and Atkinson 2005; Beresnev and Atkinson 1998) to estimate the spatial distribution of peak ground acceleration from the destructive 1908 Messina earthquake. It caused more than 100,000 casualties on 28 December 1908. As the earthquake source we have chosen the normal fault proposed by the DISS catalogue (Basili et al. 2008). It is an east-dipping source with shallowest depth beneath the Sicilian side of the Straits area (Figure 5.6). We computed peak ground acceleration values based on the attenuation models derived in study and chosen sources, and converted to macroseismic intensities using the empirical formulas given by the USGS ShakeMap® package. This type of study could play a key role in the area because the Messina Straits and the southern segment of the Calabrian Arc are characterized by the highest seismicity in Italy, with earthquake magnitudes that exceed M 7.0 (e.g. the 1905 and 1908 events, and a complex sequence of five large earthquakes that occurred from February to March 1783).
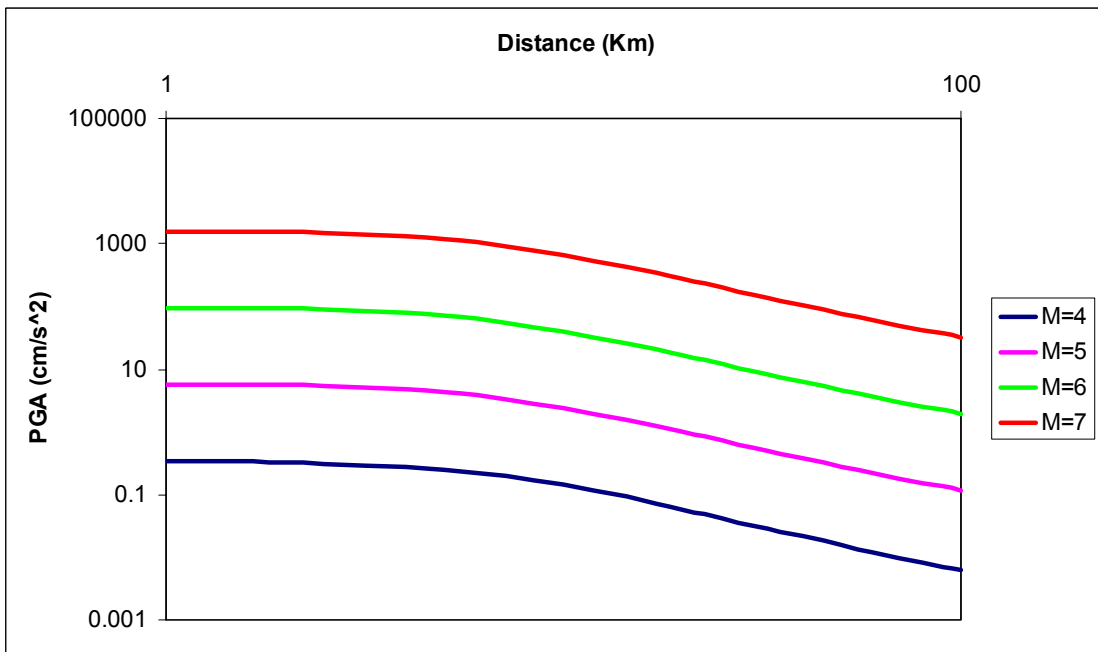
Figure 5.5: Magnitude and distance scaling predicted values by using the models developed in this study. The predictions are given for magnitude 4, 5, 6, and 7.

To take into account the amplification effect of the soil overlying the bedrock, at first, we assigned a soil category (B, C or D) to the geological formations, based on the Vs30 values (*Rasà R. and Pino P. personal communication*). Then, we used the NEHRP boundary site conditions to get the appropriate amplification factors.

Figure 5.7a shows synthetic PGA distribution maps for the 1908 earthquake area obtained for the est-dipping source and the observed microseismic data (Fig. 5.7b). The predicted intensities from the DISS source show good agreement with observed intensity in the central and northern parts of the study area, whereas they are relatively high in the southern part. The differences could be due to several factors such as local site effects not mapped in this study or the uncertainties on the magnitude and the actual earthquake source. In fact, although the 1908 Messina earthquake marked a turning point in the seismic history of southern Italy and NE Sicily, scientists still do not have enough data or methods to determine the exact location and especially the geometry (specifically the dip direction) of the seismogenic fault. The final scope of this exercise was to compare distribution of the synthetic intensities with the available macroseismic data. In fact, as shown using the GoogleMap® tools, the city of Messina is located in a narrow land between high mountains and the sea. A repeat of an earthquake like the 1908 one could interrupt the railroads, highways and state roads. As it is clear form Figure 5.8 they run parallel to each other making the risk of interruption even higher especially in the point where there will be large values of peak round accelerations and velocities. For example from Figure 5.7 it is possible to notice that the railroad the highway, A18, and the state road, SS114, run parallel to each other and in a very narrow piece of land confined between mountains and the sea.
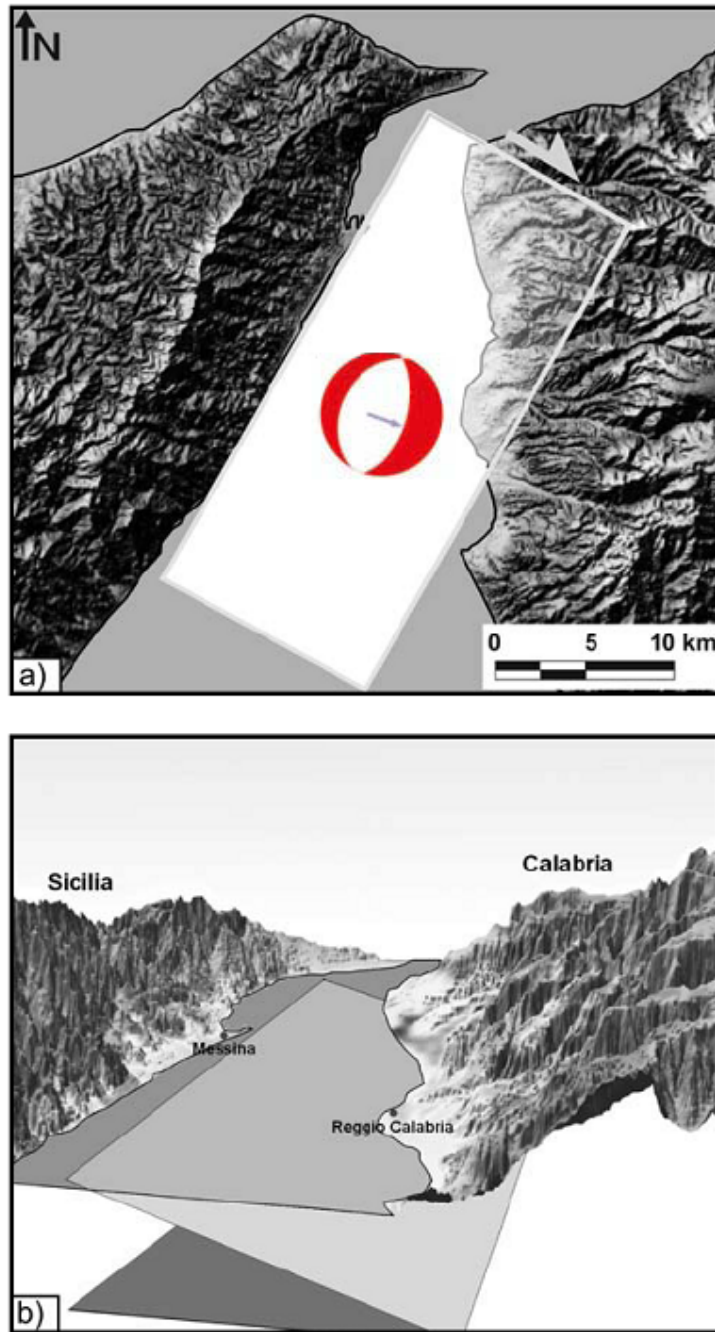
Figure 5.6: 1908 Messina earthquake source proposed by the DISS catalogue (Basili et al. 2008).
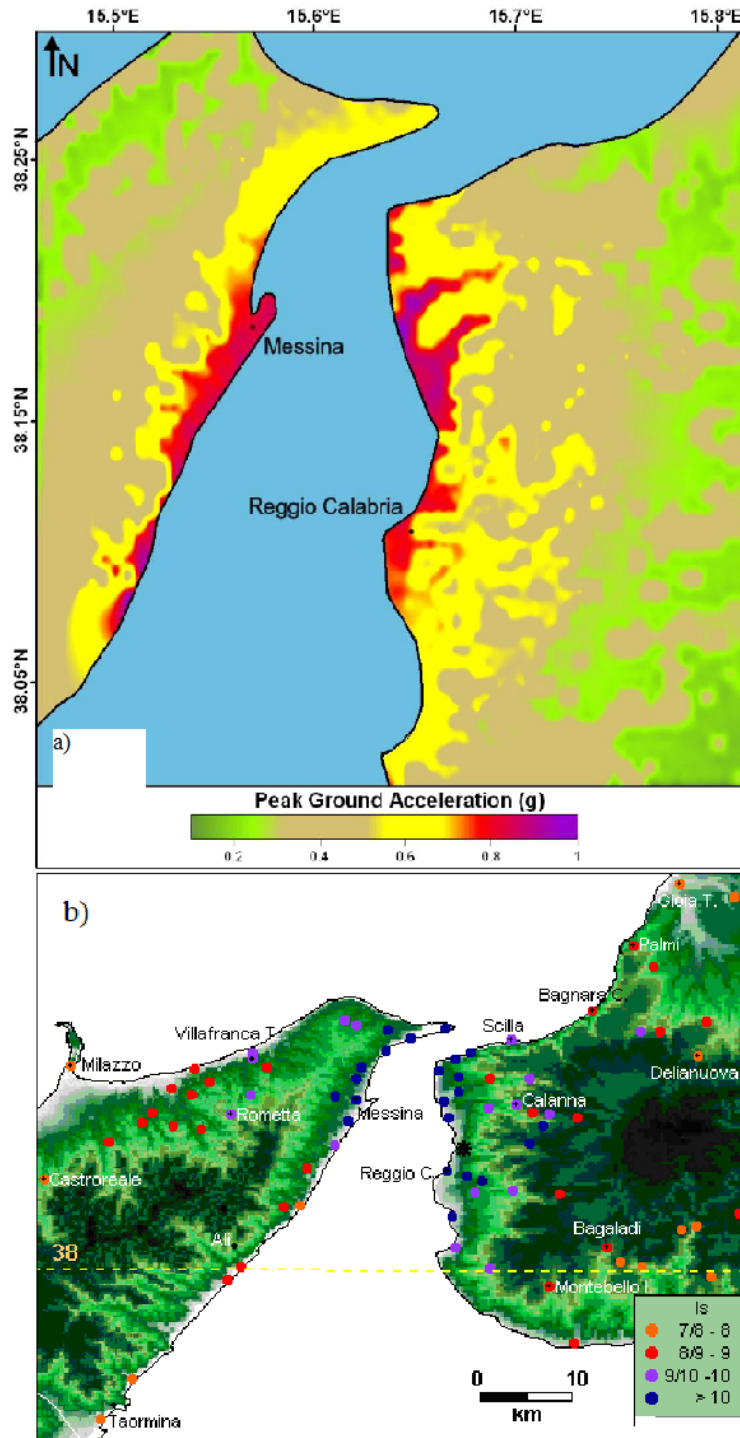
Figure 5.7: a) synthetic PGA distribution maps for the 1908 earthquake area obtained for the west-dipping source and the observed microseismic data (b).
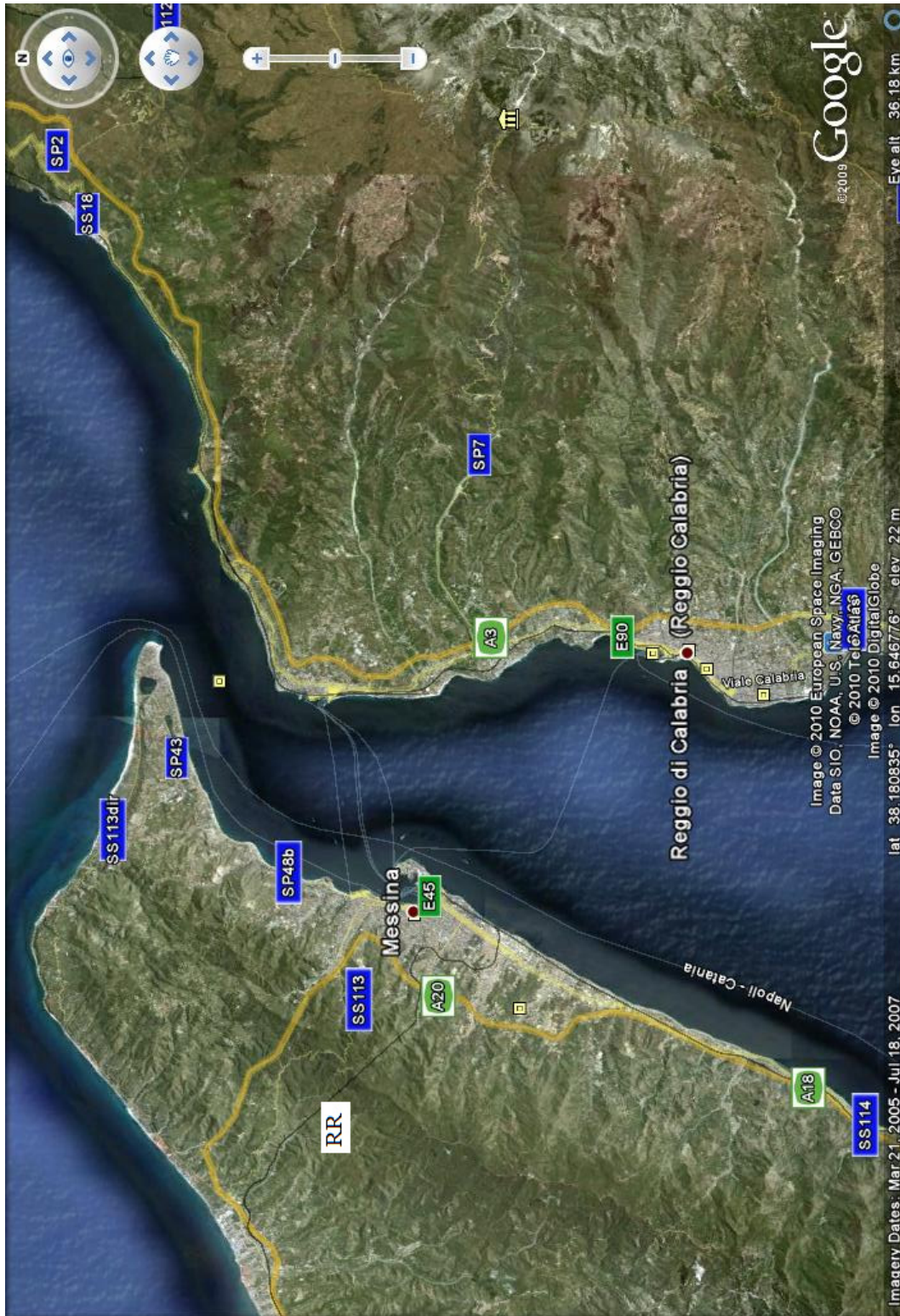
Figure 5.8: GoogleMap® showing the area where the simulation where made. The main railroad (RR), highways (A3-E90; A18; A20) and state road (SS114, SS113, SP48; SP7) are shown.

Both from the simulations and the microseismic data it is evident that the area could be largely affected by strong ground shaking that could create severe damage. A similar situation is present in the northern part of Messina. This represents a critical point for the Civil Protection decision makers because in the worst scenario the communication routes for emergency responders and rescue teams could be completely blocked. In fact, the points described above are the only connections with the two other main cities in Sicily, Palermo and Catania which are respectively located to the west and the south of Messina. If both land routes are interrupted, the rescue team could reach the city only by sea and/or using helicopters since there is no place for small aircraft to land. A similar situation could happen in the Calabria side where the main city, Reggio di Calabria, suffers the same geographical problem as Messina.

Conclusion

It is well known that the estimation of strong ground motions in regions of high seismicity is an extremely important first step in seismic design, hazard analysis, and hazard mitigation. In this chapter, we used stochastic finite-fault simulation technique based on a dynamic corner frequency developed by Motazedian and Atkinson (2005) to simulate the strong ground motions of several earthquakes in Southern Italy and in particular, we simulated the strong ground motion of the 1908 Messina earthquake.

For the simulations we adopted the duration, regional path effects and geometrical spreading model derived in the previous chapter. For each simulation the fault size has been taken form the DISS data base while the local site effects including the kappa operator (estimated in the previous chapter) and soil amplifications are taken according the NEHERP classification.

In conclusion, despite certain discrepancies mostly due to source complexity, stochastic finite-fault modeling based on a dynamic frequency approach confirms to be a reliable and practical method to simulate ground motion records of moderate and large earthquakes especially in regions of widespread structural damage but sparse ground motion recordings. Using the synthetic data set augmented with the few available data in the region we calibrated a ground motion attenuation relationship for the peak ground acceleration in Southern Italy.

CHAPTER 6: Conclusions

The main goal of this thesis is to develop an attenuation relationship for Southern Italy. The results of this work can be used for upgrading the Italian hazard map as well as for engineering designs. They also can be useful to implement *Shake Map®* in order to generate a rapid earthquake response.

The regional ground motion scaling in Southern Italy has been studied and this represents the first attempt in the area. The results of this study are carried out by using weak-motion modeling the average features of regional wave propagation in Southern Italy. These parameters describe the averaged attenuation characteristic of the study area. This has been possible for the first time thanks to the deployment of a large number of temporary seismic stations in the area which allowed to have a good data set. In order to model the regional propagation parameters it was necessary compute the moment tensor solutions for several earthquakes to have estimations of the moment magnitudes and source focal mechanisms. For the earthquakes investigated we tried different station distributions (for example using only the nearest, the farthest stations or combinations of both). We also changed the azimuthal station distribution and the epicentral parameters of the event. We showed that the final solution is robustly determined. The methods provide a good-quality solutions in the area in a magnitude range (2.5-4.5) not properly represented in the Italian national catalogues. We also used this results to constraint regional seismo-tectonic deformations in the Messina Strait area. Combined with the findings of previous investigations (Billi et al., 2006, 2007; D'Agostino et al., 2008b: Neri et al., 2009) the new focal mechanisms furnished by this study mark with an increased level of detail the transition between the extensional domain related to

subduction trench retreat in southern Calabria and the compressional one due to continental collision in western-central Sicily.

Our results on the attenuation properties of the crust confirm the regional dependence of ground motion, in terms of attenuation and stress parameter. In fact, we have shown that the attenuation properties of the crust are different from the other part of Italy and these differences have to be taken into account for seismic hazard studies.

Finally, we calibrated also an attenuation relationship for Peak Ground Acceleration (PGA). We regressed PGA values from our data set augmented with some simulated PGA values of large earthquakes that were missed in our dataset since the study area is characterized only by low magnitude event in the instrumental history. We predicted the expected ground motions for the region using a stochastic approach. In the implementation of the stochastic method, the attenuation effects of the propagation path are modeled through the empirical $Q(f)$, geometrical spreading $g(r)$ and stress obtained in the present study.

We demonstrated that the weak-motion based region-specific high-frequency spectral parameters can be successfully used to predict average expected ground motion amplitudes through the stochastic approaches and these values can be regressed to calibrated a regional attenuation relationship to be used in the area both for engineering and seismic hazard goals.

In conclusion, once the regional parameters are calibrated for the area, the described approach allows even the predictions of ground motion parameters (such as PGA, etc.) even for large earthquakes. This is really important because it will be possible to make ground motion predictions for regions where strong-motion data are lacking or for high risk seismic areas in which just data from moderate earthquakes are

available. Moreover, simulations offer a great advantage in real time estimation of peak ground motion for emergency response operations (e.g. ShakeMap®).

We finally stress the fact that that the development of global empirical ground motion predictions equations obtained combining data from regions with different attenuation characteristics may not be always correct.

References

Abrahamson, N. A., and Silva, W. J., 1997. Empirical Response Spectral Attenuation Relations for Shallow Crustal Earthquakes, Seism. Res. Lett., 68, 94-127.

Amato A., and Montone, P., 1997. Present day stress-field and active tectonics in Southern Peninsular Italy, Geophys. J. Int., 130, 519-534.

Ambraseys, N. N., and Simpson K. A., 1996. Prediction of vertical response spectra in Europe, Earthquake Eng. Struct. Dyn., 25, 401–412.

Ambraseys, N. N., Simpson, K. A., Bommer J. J., 1996. Prediction of horizontal response spectra in Europe, Earthquake Eng. Struct. Dyn., 25, 371–400.

Amoruso, A., Crescentini, L., Neri, G., Orecchio, B., Scarpa, R., 2006. Spatial relation between the 1908 Messina Straits earthquake slip and recent earthquake distribution. Geophys. Res. Lett. 33, doi:10.1029/2006GL027227.

Amoruso, A., Crescentini, L., Scarpa, R., 2002. Source parameters of the 1908 Messina Straits, Italy, earthquake from geodetic and seismic data. J. Geophys. Res., 107, B4, 10.1029/2001JB000434.

Akinci, A., Akyol, N., D'Amico, S., Malagnini, L., Mercuri, A. 2006. Ground-Motion scaling in Western Anatolia (Turkey). Seismological Research Letters, 77, 264-265.

Akinci, A., Malagnini, L., 2009. The 2009 Abruzzo earthquake, Italy. IRIS Newsletter, 1, 3.

Akinci A., Malagnini, L., Sabetta, F., 2009. Strong ground motion characteristic from the 6 April 2009 L'Aquila earthquake, Italy. AGU Fall Meeting.

Akinci, A., L. Malagnini, N. A. Pino, L. Scognamiglio, R. B. Herrmann, and H. Eyidogan, 2001. High-frequency ground motion in the Erzincan region. Turkey: inferences from small earthquakes, Bull. Seism. Soc. Am., 91, 1446–1455.

Anderson, H. and Jackson, J., 1987. The deep seismicity of the Tyrrhenian Sea. Geophys. J. R. Astron. Soc., 91, 613-637.

Anderson, J. G., and Lei Y., 1994. Non-parametric description of peak acceleration as a function of magnitude, distance, and site in Guerrero, Mexico, Bull. Seism. Soc. Am. 84, 1003–1017

Assatourians, K., and Atkinson G., 2007. Modeling Variable-Stress Distribution with the Stochastic Finite-Fault Technique. Bull. Seism. Soc. Am., 97, 1935-1949.

Atkinson, G. M. and Boore, D. M., 1995. Ground-Motion Relations for Eastern North America, Bull. Seism. Soc. Am., 85, 17-30.

Atzori, S., I. Hunstad, M. Chini, S. Salvi,C. Tolomei, C. Bignami, S. Stramondo, E. Trasatti, A. Antonioli, and E. Boschi 2009, Finite fault inversion of DInSAR cosismic displacement of the 2009 L'Aquila earthquake (Central Italy), Geophys. Res. Lett., 36, L15305, doi:10.1029/2009GL039293.

Baccheschi, P., Margheriti, L., Steckler, M. S., 2007, Seismic anisotropy reveals focused mantle flow around the Calabrian slab (Southern Italy), Geophys. Res. Lett., 34, L05302, doi:10.1029/2006GL028899.

Baratta, M., 1910. La catastrofe sismica Calabro Messinese (28 dicembre 1908). Rel. Soc. Geogr. Ital., Tip. Riva-Zolla-Bellinzona, Voghera.

Basili, R., Valensise, G., Vannoli, P., Burrato, P., Fracassi, U., Mariano, S., Tiberti, M. M., Boschi, E., 2008. The Database of Individual Seismogenic Sources (DISS), version 3: Summarizing 20 years of research on Italy's earthquake geology, Tectonophysics, 453, 20–43.

Barberi, F., Gasparini. P., Innocenti. F. and Vfllari, L., 1973. Volcanism of the southern Tyrrhenian Sea and its geodynamic implications. J. Geophys. Res., 78, 5221-5232.

Barberi G., Cosentino, M.T., Gervasi A., Guerra I., Neri G., and Orecchio B.; 2004: Crustal seismic tomography in the Calabrian Arc region, south Italy. Phys. Earth Planet. Int., 147, 297-314.

Bay, F., Fah, D., Malagnini, L., Giardini, D., 2003. Spectral shear-wave ground motion scaling for Switzerland, Bull. Seism. Soc. Am., 93, 414–429.

Beresnev, I. A., Atkinson G., 1998. FINSIM—a FORTRAN program for simulating stochastic acceleration time histories from finite faults, Seism. Res. Lett. 69, 27–32.

Beresnev, I. A., Atkinson, G.M., 2002. Source parameters of earthquakes in eastern and western North America based on finite-fault modeling, Bull. Seismol. Soc. Am. 92, 695-710.

Bevington, P. R., and Robinson, D. K., 2003. Data reduction and error analysis, McGraw-Hill, New York.

Billi, A., Barberi, G., Faccenna, C., Neri, G., Pepe F., Sulli A., 2006. Tectonics and seismicity of the Tindari Fault System, southern Italy: Crustal deformations at the transition between ongoing contractional and extensional domains located above the edge of a subducting slab, Tectonics, 25, doi:10.1029/2004TC001763.

Billi, A., Presti, D., Faccenna, C., Neri, G., Orecchio B., 2007, Seismotectonics of the Nubia plate compressive margin in the south-Tyrrhenian region, Italy: clues for subduction inception, J. Geophys. Res., 112, B08302, doi:10.1029/2006JB004837.

Bodin, P., Malagnini L., Akinci A., 2004. Ground motion scaling in the Kachchh basin, India, deduced from aftershocks of the 2001 Mw7.6 Bhuj earthquake, Bull. Seism. Soc. Am. 94, 1658–1669.

Boore D. M., 2010. Comparing stochastic point- and finite-source ground-motion simulations: SMSIM and EXSIM, Bull. Seism. Soc. Am, 99,3202-3216.

Boore, D. M., and Joyner, W. B., 1991. Estimation of Ground Motion at Deep-Soil Sites in Eastern North America, Bull. Seism. Soc. Am., 81, 2167-2185.

Boore, D. M., 2003. Prediction of ground motion using the stochastic method, Aki Symposium, Pageoph 160, 635–676.

Boore, D. M., Joyner, W. B., Fumal, T. E., 1993. Estimation of response spectra and peak acceleration from western North America earthquakes: an interim report, U.S. Geol. Surv. Open-File Rept. 93-509, 72 pp.

Boore, D. M., Joyner, W. B., Fumal, T. E., 1997. Equations for Estimating Horizontal Response Spectra and Peak Acceleration from Western North American Earthquakes: A Summary of Recent Work, Seism. Res. Lett., 68 (1), 128-153.

Boschi, E., Pantosti, D., Valensise, G., 1989. Modello di sorgente per il terremoto di Messina del 1908 ed evoluzione recente dell'area dello Stretto. Proceedings VIII Meeting Gruppo Nazionale di Geofisica della Terra Solida, Rome, 245–258.

Boschi, E., Ferrari, G., Gasperini, P., Giudoboni, E., Smiriglio, G. ,Valensise, G., 1995. Catalogo dei forti terremoti in Italia dal 461 A.C. al 1980, ING, Roma_SGA Bologna.

Boschi, E., Guidoboni, E., Ferrari, G., Mariotti, D., Valensise, G., Gasperini, P.,(eds.); 2000: Catalogue of Strong Italian Earthquakes from 461 B.C. to 1997. Ann. Geofis., 43, 609-868.

Bottari, A., Capuano, P., De Natale, G., Gasparini, P., Neri, G., Pingue, F., Scarpa, R.,1989, Source parameters of earthquakes in the Strait of Messina, Italy, during this century. Tectonophysics, 166, 221–234.

BSSC, 1994. NEHRP recommended previsions for seismic regulations for new buildings, Part 1, FEMA 222A, Federal Emergency Management Agengy, 290 pp.

Caccamo, D., Neri, G., Saraò, A., Wyss, M., 1996. Estimates of stress directions by inversion of earthquake fault-plane solutions in Sicily. Geophys. J. Int. 125, 857–868.

Calais, E., DeMets, C., Nocquet, J.-M., 2003. Evidence for a post-3.16-Ma change in Nubia-Eurasia-North America plate motions?. Earth Planet. Sci. Lett., 216, 81-92.

Campbell, K. W., and Y. Bozorgnia (1994). Near-source attenuation of peak horizontal acceleration from worldwide accelerograms recorded from 1957 to 1993, in Proc.

Fifth U.S. National Conference on Earthquake Engineering, EERI, Berkeley, California, Vol. 1, 283–292.

Campbell, K. W., 1997. Empirical Near-Source Attenuation Relationships for Horizontal and Vertical Components of Peak Ground Acceleration, Peak Ground Velocity and Pseudo-Absolute Acceleration Response Spectra, Seism. Res. Lett., 68 (1), 154-179.

Caputo, M.. Panza, G.F., Postpischl, D.. 1970. Deep structure of the Mediterranean Basin. J. Geophys. Res.. 75(26): 4919- 4923.

Cartwright, D.E.,. Longuet-Higgins, M.S, 1956. The statistical distribution of the maxima of a random function, Proc. R. Soc. London, 237, 212-232.

Catalano, S., De Guidi, G., 2003. Late Quaternary uplift of northeastern Sicily: relation with the active normal faulting deformation. J. Geodyn., 36, 445-467.

Catalano, S., De Guidi, G., Monaco, C., Tortorici, G., Tortorici, L., 2003. Long-term behaviour of the late Quaternary normal faults in the Straits of Messina area (Calabrian arc): structural and morphological constraints. Quat. Int., 101-102, 81-91.

Chouet, B., K. Aki, M. Tsujiura, 1978. Regional variation of the scaling law of earthquake source spectra, Bull. Seism. Soc. Am. 68, 49–79.

Cimini G.B, P. De Gori, A. Frepoli, 2006. Passive seismology in Souther Italy: The SAPTEX array. Ann. Geophys., 49, 2, 825-840.

Cirella A., Piatanesi A., Cocco M., Tinti E., Scognamiglio L., Michelini A., Lomax A., Boschi E., 2009. Rupture history of the 2009 L'Aquila (Italy) earthquake from non-linear joint inversion of strong motion and GPS data, Geophys. Res. Lett., 36, L19304. doi:10.1029/2009GL039795.

CPTI Working Group; 2004: Catalogo Parametrico dei Terremoti Italiani, versione 2004 (CPTI04), INGV, Bologna, http://emidius.mi.ingv.it/CPTI/home.html (last access 2010-March-01).

CSI, Working Group, 2001: Catalogo della Sismicità Italiana, Istituto Nazionale di Geofisica e Vulcanologia, http://csi.rm.ingv.it (last access 2010-March-01).

D'Agostino, N., A. Avallone, D. Cheloni, E. D'Anastasio, S. Mantenuto, and G. Selvaggi, 2008a, Active tectonics of the Adriatic region from GPS and earthquake slip vectors, J. Geophys. Res., 113, B12413, doi:10.1029/2008JB005860.

D'Agostino, N., Cheloni, D., Bernardi, F., Hunstad, I., Palombo, B., Selvaggi, G. 2008b. Il contributo della geodesia alla definizione del modello sismotettonico dello Stretto di Messina: analisi della deformazione intersismica e cosismica. Riassunti estesi del

convegno 1908 – 2008 Scienza e Società a cento anni dal Grande Terremoto. Miscellanea INGV, 03.

D'Amico, S., Orecchio, B., Presti, D., Zhu, L., Herrmann, R. B., Neri, G., 2008: Moment tensor solutions in the area of the 1908 Messina earthquake: preliminary results. Miscellanea INGV, 8, 43-44.

D'Amico, S., Koper, D., Herrmann, B., Akinci, A., Malagnini, L., 2010a. Imaging The Rupture Of The Mw 6.3 April 6, 2009 L'aquila, Italy Earthquake Using Back-Projection of Teleseismic P-Waves, Geophys. Res. Lett., 37, L03301, doi:10.1029/2009GL042156.

D'Amico, S., Orecchio, B., Presti, D., Zhu, L., Herrmann, R. B., Neri, G., 2010b. Moment tensor solutions for moderate earthquakes in the Messina straits, southern Italy, Phys. Earth Plan. Int., 179, 97–106, doi:10.1016/j.pepi.2010.01.012.

D'Amico, S., Orecchio, B., Presti, D., Gervasi, A., Zhu, L., Guerra, I., Neri, G., Herrmann, R. B., 2010c. Testing the stability of focal mechanism solutions for small and moderate earthquakes in the Calabrian-Peloritan arc region (southern Italy). Boll. Geof. Teo. Appl., in press.

D'Amico, S., Akinci, A., Malagnini, L., 2010d. Predictions of high-freqeuncy ground-motion in Taiwan based on weak motion data. Geophys. J. Int., submitted

Devoti, C., Riguzzi, F., Cuffaro, M., Doglioni C., 2008. New GPS constraints on the kinematics of the Apennines subduction. Earth Planet. Sci. Lett., doi:10.1016/j.epsl.2008.06.03.

DISS Working Group, 2007. Database of Individual Seismogenic Sources (DISS), Version 3.0.4: A compilation of potential sources for earthquakes larger than M 5.5 in Italy and surrounding areas. © INGV 2007 - Istituto Nazionale di Geofisica e Vulcanologia, Roma, http://www.ingv.it/DISS/.

Doglioni, C., Harabaglia, P., Martinelli, G., Mongelli, F., Zito, G., 1996. A geodynamic model of the Southern Apennines, Terra Nova, 8, 540-547.

Douglas, J., 2003. Earthquake ground motion estimation using strong-motion records: a review of equations for the estimation of peak ground acceleration and response spectral ordinates, Earth-Science Reviews, 61, 43–104.

Draper, N. R. and Smith, H., 1966. Applied Regression Analysis, Wiley, New York, 407 pp.

Dreger, D. S., 2003. TDMT_INV: Time domain seismic moment tensor inversion, in International Handbook of Earthquake and Engineering Seismology, W. H. K. Lee, H. Kanamori, P. C. Jennings, and C. Kisslinger (Editors), Vol B, Academic Press, An Imprint of Elsevier Science, London, 1627 pp.

Dreger, D. S., and Helmberger, D. V.; 1993: Determination of source parameters at regional distances with single station or sparse network data. J. Geophys Res., 98, 1162-1179.

Ekstrom, G. A., Morelli, A., Boschi, E., Dziewonsky, A. M., 1998. Moment tensor analysis of the central Italy earthquake sequence of September – October 1997, Geophys. Res. Lett., 25, 1971-1974.

Fabbri, A., Ghisetti, F., Vezzani, L., 1980. The Peloritani-Calabria range and the Gioia basin in the Calabrian Arc (south Italy): Relationships between land and marine data. Geol. Rom., 19, 131– 150.

Faccenna, C., Becker, T. W. , Lucente, F.P., Jolivet, L., Rossetti, F.. 2001. History of subduction and back-arc extension in the central Mediterranean, Geophys. J. Int., 145, 809– 820.

Faccenna, C., Davy, P., Brun, J.P., Funiciello, R., Giardini, D., Mattei, M., Nalpas, T., 1996. The dynamics of back-arc extension: an experimental approach to the opening of the Tyrrhenian Sea. Geophys. J. Int., 126, 781–795.

Fan, G., and Wallace, T., 1991. The determination of source parameters for small earthquakes from a single, very broadband seismic station, Geophys. Res. Lett., 18, 1385– 1388.

Fatehi, A., and Herrmann, R. B., 2008. High-Frequency Ground-Motion Scaling in the Pacific Northwest and in Northern and Central California, Bulletin of the Seismological Society of America, 98, 709–721, doi: 10.1785/0120070051.

Finetti, I. R., 2005. Depth contour map of the moho discontinuity in the central Mediterranean region from new CROP seismic data. In I.R. Finetti (Editor). CROP PROJECT: Deep Seismic Exploration of the Central Mediterranean and Italy, Elsevier, Amsterdam, 597-606.

Finetti, I. R., and Del Ben, A., 1986, Geophysical study of the Tyrrhenian opening, Boll. Geofis. Teor. Appl. 110 75-156.

Finetti, I. R., and Del Ben, A., 2005, Ionian Thetys Lithosphere Roll-Back Sinking and Back-Arc Tyrrhenian Opening. In I.R. Finetti (Editor). CROP PROJECT: Deep Seismic Exploration of the Central Mediterranean and Italy, Elsevier, Amsterdam,, 483-503.

Frepoli, A., and Amato, A., 2000. Fault plane solutions of crustal earthquakes in southern Italy (1988–1995) seismotectonic implications. Ann. Geophys. 43, 437–467.

Gasparini, C., Iannaccone. G.. Scandone, P. and Scarpa. R.. 1982. Seismolectonics of tile Calabrian Arc. Tectonophysics 84: 267 286.

Goes, S., Giardini, D., Jenny, S., Hollenstein, C.,, Kahle, H.G,, Geiger, A., 2004, A recent tectonic reorganization in the south-central Mediterranean, Earth Planet. Sc. Lett., 226, 335-345.

Gueguen, E., C. Doglioni, M Fernandez, 1998. On the post-25 Ma geodynamic evolution of the western Mediterranean, Tectonophysics, 298, 259–269.

Guidoboni, E., Ferrari, G., Mariotti, D., Comastri, A.,, Tarabusi, G., Valensise, G., 2007. CFTI4Med, Catalogue of Strong Earthquakes in Italy (461 B.C.-1997) and Mediterranean Area (760 B.C.-1500). INGV-SGA. Available at http://storing.ingv.it/cfti4med/.

Harmsen, S. (1997). Estimating the diminution of shear-wave amplitude with distance: application to the Los Angeles, California, urban area, Bull. Seism. Soc. Am. 87, 888–903.

Herrmann, R. B., 2002. An overview of synthetic seismogram computation, Computer Programs in Seismology, Saint Louis University, pp. 183.

Herrmann, R. B.; 2008. Toward automated focal mechanism and moment determination for the continental U.S. – an ANSS product. Final Technical Report USGS Grant 05HQGR0047, 16 pp.

Herrmann, R. B., and Dutt, J., 1999. High frequency vertical ground motion in the Pacific Northwest using PNSN data, Seism. Res. Lett. 70, 216

Herrmann, R. B., and Malagnini, L., 1996. Absolute ground motion scaling in the New Madrid Seismic Zone, Seism. Res. Lett. 67, 40.

Herrmann R. B., Withers M., and Benz H.; 2008: The April 18, 2008 Illinois earthquake: an ANSS monitoring success, Seism. Res. Lett., 79, 830-843.

Jeon Y.S., and Herrmann, R. B., 2004. High-frequency ground-motion scaling in Utah and Yellowstone. Bull. Seism. Soc. Am. 94, 1644-1657.

Joyner, W. B. and Boore, D. M., 1981. Peak Horizontal Acceleration and Velocity from Strong-Motion Records Including Records from the 1979 Imperial Valley, California, Earthquake, Bull. Seism. Soc. Am., 71 (6), 2011-2038.

Joyner, W. B. and Boore, D. M., 1993. Methods for the Regression Analysis of Strong-Motion Data, Bull. Seism. Soc. Am., 83 (2), 469-487.

Kagan, Y.Y.; 1991: 3-D rotation of double-couple earthquake sources. Geophys. J. Int., 106, 709–716.

King, J.L., and Tucker, B.E., 1984. Observed variations of earthquake motion across a sediment filled valley, Bull. Seism. Soc. Am., 74, 137-151.

Kramer, S.L.,1996. Geotechnical Earthquake Engineering. Prentice Hall, Upper Saddle River, NJ.

Langston, C. A.; 1981; Source inversion of seismic waveforms: The Koyna, India, earthquakes of 13 September 1967, Bull. Seismol. Soc. Am., 71, 1 –24.

Li, H., Michelini A., Zhu L., Bernardi F., and Spada M., 2007. Crustal Velocity Structure in Italy from Analysis of Regional Seismic Waveforms. Bull. Seism. Soc. Am., 97, 2024–2039, doi: 10.1785/0120070071.

Lucente, F. P., and F. Speranza 2001, Belt bending driven by deep processes: Geophysical evidences from the northern Apennines (Italy), Tectonophysics, 337, 51– 62.

Ludwig, W.J., Nafe, J. E., Drake, C. L., 1970. Seismic refraction, in The Sea, A. E.Maxwell, (Editor) Vol. 4, Wiley-Interscience, New York, 53–84.

Malagnini, L., Akinci, A., Hermann, R. B., Pino, N. A. , Scognamiglio L., 2002. Characteristics of the ground motion in northeastern Italy, Bull. Seism. Soc. Am. 92, 2186–2204.

Malagnini, L., Hermann, R. B., Di Bona, M., 2000a. Ground-motion scaling in the Apennines (Italy), Bull. Seism. Soc. Am. 90, 1062–1081.

Malagnini, L., Herrmann, R. B., Koch, K., 2000b. Regional ground motion in scaling in Central Europe, Bull. Seism. Soc. Am. 90, 1052– 1061.

Malagnini, L., Herrmann R. B., 2000c. Ground motion scaling in the region of the 1997 Umbria-Marche earthquake (Italy), Bull. Seism. Soc. Am. 90, 1041–1051.

Malagnini, L., Mayeda, K., Akinci, A., Bragato, P. L., 2004. Estimating absolute site effects, Bull. Seism. Soc. Am., 94, 1343-1352.

Malagnini, L., Mayeda, K., Uhrhammer, R., Akinci, A., Herrmann, R. B., 2007. A regional ground motion excitation/attenuation model for the San Francisco region, Bull. Seism. Soc. Am., 97; 3; p. 843-862; DOI: 10.1785/0120060101.

Malagnini, L., Akinci, A., Mayeda, K., Munafo, I., Herrmann, R. B., Mercuri, A., 2010. Characterization of Earthquake-induced ground motion from the L'Aquila seismic sequence of 1009, Italy. Geophys. J. Int., in press

Malinverno, A., Ryan, W.B.F., 1986. Extension in the Tyrrhenian sea and shortening in the Apennines as result of Arc migration driven by sinking of the lithosphere. Tectonics, 5, 227–245.

Mancilla, F., Ammon, C. J., Herrmann, R. B., Morales, J., 2002. Faulting parameters of the 1999 Mula earthquake, southern Spain, Tectonophysics, 354, 139-155.

Marone, C., and Scholz, C., 1998. The depth of seismic faulting and the upper transition from stable to unstable slip regimes, Geophys. Res. Lett., 15, 621–624.

Monaco, C., Tortorici, L., 2000. Active faulting in the Calabrian arc and eastern Sicily. J. Geodyn., 29, 407–424.

Morasca, P., Malagnini, L., Akinci, A., Spallarossa, D., Herrmann, R.B., 2006. Ground motion scaling in the western Alps. J. Seismol., 10, 315-333.

Motezedian, D., and Atkinson, G. M., 2005. Stochastic finite-fault modeling based on a dynamic corner frequency, Bull. Seism. Soc. Am. 95, 995-1010.

Moya, A., Aguirre, J., Irikura, K., 2000. Inversion of source parameters and site effects from strong motion records using genetic algorithms, Bull. Seism. Soc. Am. 90, 977-992.

Neri, G., Barberi, G., Oliva, G. Orecchio, B., 2004. Tectonic stress ans seismogenic faulting in the area of the 1908 Messina earthquake, south Italy. Geoph. Res. Lett., 31, L10602-1-L10602-5.

Neri, G., Barberi, G., Oliva, G., Orecchio, B., 2005. Spatial variations of seismogenic stress orientation in Sicily, south Italy. Phys. Earth Planet. Int., 148, 175-191.

Neri, G., Barberi, G., Orecchio, B., Aloisi, M., 2002. Seismotomography of the crust in the transition zone between the southern Tyrrhenian and Sicilian tectonic domains, Geophys. Res. Lett. 29, 23, 2135.

Neri, G., Barberi, G., Orecchio, B., Mostaccio, A., 2003. Seismic starin and seismogenic stress regimes in the crust of the southern Tyrrenian region, Earth Planet. Sci. Lett., 213, 97-112.

Neri, G, Marotta A.M., Orecchio B., Presti D., Totaro C., Barzaghi R., Borghi A.; 2010: How lithospheric subduction changes along the calabrian arc in southern Italy: geophysical evidences, submitted to Geophys. J. Int.

Neri, G., Orecchio, B., Presti, D., 2008. Sismicità attuale, campo di sforzo e dinamiche litosferiche nell'area dello Stretto di Messina. In: Bertolaso G., Boschi E., Guidoboni E., Valensise G. (Editors). Il terremoto e il maremoto del 28 dicembre 1908, INGV-SGA, 461-474.

Neri, G., Orecchio, B., Totaro, C., Falcone, G., Presti, D., 2009. Subduction beneath southern Italy close the ending: results from seismic tomography. Seim. Res. Lett., 80, 63-70.

Nocquet, J.-M., and Calais, E., 2004. Geodetic measurements of crustal deformation in the Western Mediterranean and Europe. Pure Appl. Geophys., 161, 661-681.

Ortega, R., Herrmann, R. B., Quintanar L., 2003. Earthquake ground-motion scaling in Central Mexico between 0.7 and 7 Hz, Bull. Seism. Soc. Am. 93, 397–413.

Peterschmitt, E,, 1956. Quelques Donnes Nouvelles sur les Seismics Profonds de la Mer Tyrrhenienne. Ann. Geofis.. 9:305 334.

Pino, N. A., Malagnini, L., Akinci, A., Scognamiglio, L., Herrmann, R. B., Stavrakakis, G., Chouliaras, G., 2001. Ground motion scaling relationships for mainland Greece and Crete, Seism. Res. Lett. 72, 258.

Pino, N.A., Piatanesi, A., Valensise, G., Boschi, E., 2009. The 28 December 1908 Messina Straits Earthquake (Mw 7.1): A Great Earthquake throughout a Century of Seismology, Seism. Res. Lett., 80, 243-259.

Pondrelli, S., Salimbeni, S., Ekström, G., Morelli, A., Gasperini, P., Vannucci, G.; 2006: The Italian CMT dataset from 1977 to the present, Phys. Earth Planet. Int., 159, 286-303, doi:10.1016/j.pepi.2006.07.008

Pontevivo, A, and Panza, G.F., 2006 The Lithosphere-Asthenosphere System in the Calabrian Arc and Surrounding Seas – Southern Italy, Pure Appl. Geophys., 163 1617–1659, doi 10.1007/s00024-006-0093-3.

Raoof, M., Herrmann, R. B., Malagnini, L., 1999. Attenuation and excitation of three-component ground motion in southern California, Bull. Seism. Soc. Am. 89, 888–902.

Rapolla, A., Akinci, A., Bruno, P. P., D'Amico, S., Di Fiore, V., Malagnini, L., Maschio, L., Paoletti, V., Secomandi, M., Vietri, A., 2008. La pericolosità sismica: dalla classificazione sismica alla microzonazione dei territori comunali, alla risposta sismica del sito. Liguori Editore

Ritsema J., and Lay T.,; 1993: Rapid source mechanism determination of large earthquakes in the western United States, Geophys. Res. Lett., 20, 1611 –1614.

Romanowicz, B., Dreger, D., Pasyanos, M., Uhrhammer, R.; 1993: Monitoring of strain release in central and northern California, Geophys. Res. Lett., 20, 1643– 1646.

Rosenbaum, G., et al. 2002, Reconstruction of the tectonic evolution of the western Mediterranean since the Oligocene, J. Virtual Explorer, 8, 107– 130

Sabetta, F., and Pugliese A., 1987. Attenuation of peak horizontal acceleration and velocity from Italian strong-motion records, Bull. Seism. Soc. Am. 77, 1491–1511.

Sabetta, F., and Pugliese A. 1996. Estimation of response spectra and simulation of nonstationary earthquake ground motion, Bull. Seism. Soc. Am. 86, 337–352.

Sadigh, K., 1997. Attenuation Relation ships for Shallow Crustal Earthquakes Based on California Strong Motion Data, Seism., Res. Lett., 68 (1), 180-189.

Scherbaum, F., Schmedes, J., Cotton, F., 2004. On the Conversion of Source-to-Site Distance Measures for Extended Earthquake Source Models, Bull. Seismol. Soc. Am., 94, 1053–1069.

Scognamiglio, L., Malagnini, L., Akinci, A., 2005. Ground motion scaling in eastern Sicily, Italy. Bull. Seism. Soc. Am. 95, 568-578.

Scognamiglio, L., Tinti, E., Michelini, A.; 2009: Real-Time Determination of Seismic Moment Tensor for the Italian Region, Bull. Seism. Soc. Amer., 99, 2223 – 2242.

Serpelloni, E., Vannucci, G., Pondrelli, S., Argnani, A., Casula, G., Anzidei, M., Baldi, P., Gasperini P., 2007. Kinematics of the Western Africa-Eurasia plate boundary from focal mechanism and GPS data. Geophys. J. Int., doi:10.1111/j.1365-246X.2007.03367.x.

Somerville, P. G., Smith, N. F., Graves, R. W., Abrahamson, N. A., 1997. Modification of empirical strong motion attenuation relations to include the amplitude and duration effects of rupture directivity. Seism., Res. Lett., 68, 199-222.

Spakman, W., Wortel R., 2004. A tomographic view on Western Mediterranean Geodynamics, in: The Transmed Atlas, 31-52, Springer, New York.

Stiedl, J.H., Tumarkin, A. G., Archuleta, R. L., 1996. What is a reference site, Bull. Seism. Soc. Am. 86, 1733-1748.

Tan, Y., Zhu, L., Helmberger D., Saikia, C.; 2006: Locating and modeling regional earthquakes with two stations. J. Geophys. Res., 111, B01306.

Thio, H.-K., and Kanamori H., 1995: Moment-tensor inversions for local earthquakes using surface waves recorded at TERRAscope, Bull. Seismol. Soc. Am., 85, 1021–1038.

Toro, G. R. and McGuire, R. K., 1987. An Investigation into Earthquake Ground Motion Characteristics in Eastern North America, Bull. Seism. Soc. Am., 77, 468-489.

Wald, D., Worden, B., Quitoriano, V., Pankow, K. L., 2005. Shake Map manual: technical manual, user's guide, and software guide. U.S. Geological Survey Techiniques and Methods, book 12, section A, 132 pp.

Weisberg, S., 1980. Applied Linear Regression, Wiley, New York, 282 pp.

Wells, D. L., and Coppersmith K. J., 1994. New empirical relationships among magnitude, rupture length, rupture width, rupture area, and surface displacement, Bull. Seism. Soc. Am. 84, 974–1002.

Valensise, G., Pantosti, D., 1992. A 125 Kyr-long geological record of seismic source repeatability: the Messina Straits (southern Italy) and the 1908 earthquake (MS 71⁄2). Terra Nova, 4, 472–483.

Vannucci, G., Gasperini, P., 2004. The new release for Earthquake mechanisms of the Mediterranean Area (EMMA Version 2), Ann. Geophys., 47 Supp. N. 1, 307-334.

Yazd, M. R. S. 1993. Ground motion studies in the Southern Great Basin of Nevada and California, Ph.D. Thesis, Saint Louis University

Zhu, L., Akyol, N., Mitchell, B., Sozbiliz, H.; 2006: Seismotectonics of western Turkey from high resolution and moment tensor determinations. Geophys. Res. Lett., 33, 16.

Zhu, L., and Helmberger, D.; 1996: Advancement in source estimation technique using broadband regional seismograms, Bull. Seism. Soc. Amer. 86, 1634-1641.

Zhu, L., and Helmberger, D.; 1997: Regional waveform calibration in the Pamir-Hindu Kush region, J. Geophys. Res., 102, 22799-22813.

Zhu, L., and Rivera, L.A.; 2002: A note on the dynamic and static displacement from a point source in multi-layered media; Geophys. J. Int., 148, 619-627.

Zhao, L.S., Helmberger, D., 1994. Source estimation from broad-band regional seismograms, Bull. Seism. Soc. Am., 85, 590-605.

Zoback, M.L., 1992. First- and second-order patterns of stress in the lithosphere: The World Stress Map project. J. Geophys. Res., 97, 11, 703-11, 728.

Vita Auctoris

Sebastiano D'Amico was born in Messina (Italy) on 7 June 1979. He finished his elementary education in Tortorici and the secondary education in Messina. He was enrolled in the Physics program of the University of Messina where he was awarded the tile of "Dottore in Fisica".

In 2005 he moved to Rome where he jointed the working group directed by Dr. Luca Malagnini and Dr. Aybige Akinci at the Istituto Nazionale di Geofisica e Vulcanologia (INGV).

In 2007 he married Rosarianna and together with his wife he moved to the U.S., to join the Saint Louis University, Earth and Atmospheric Sciences Department.